DIVING BEHAVIOR, HABITAT ASSOCIATIONS, AND SENSORY MODALITIES FOR PREY DETECTION IN ELEPHANT SEALS

A Dissertation

by

KRISTEN ANN MCGOVERN

Submitted to the Office of Graduate and Professional Studies of
Texas A&M University
in partial fulfillment of the requirements for the degree of

DOCTOR OF PHILOSOPHY

Chair of Committee,	Randall Davis
Committee Members,	Christopher Marshall
	Gilbert Rowe
	Bernd Würsig
Head of Department,	David Caldwell

May 2018

Major Subject: Wildlife and Fisheries Sciences

ABSTRACT

I used video and movement data obtained from animal-borne video and data recorders (VDRs) and histological data obtained from vibrissal pads of elephant seals to address the questions: When, where, how, and on what prey do female southern elephant seals forage? Although the annual cycle of southern elephant seals for breeding, molting, and foraging is well known, there is little information about their foraging strategies, hunting tactics, habitat-associations and sensory biology at sea. I deployed VDRs and satellite telemeters on eight female southern elephant seals from Península Valdés, Argentina, during their two-month post-breeding migration. I identified three distinct dive types and their functions (foraging, resting and transiting) in the deep waters of the Patagonian continental slope and Argentine Basin. Compared to resting and transit dives, foraging dives were deeper and less linear with bursts of speed, steeper descent and ascent angles, longer two-dimensional and three-dimensional dive paths, and greater variation in speed, descent angle, and vertical head movements. The primary prey identified on video included herring smelt (*Argentinidae*) and myctophids (*Myctophidae*). Seals foraged at a mean maximum depth of 469 m with a mean water temperature of 3.7°C and mean salinity of 33.8 psu associated with Sub-Antarctic Mode Water, Antarctic Intermediate Water and Upper Circumpolar Deep Water. These habitat associations were similar to those for elephant seals from other colonies. Compared to foraging and transit dives, resting dives were longer in duration with shorter two-dimensional dive paths, lower stroking rates and speeds, and greater variation in pitch and roll angle during descent. Transit dives were shallower and more linear with higher swim speeds and stroking rates, shorter durations, shallower ascent angles, and farthest straight-line distances traveled. I provide evidence that elephant seal vibrissae have similar microstructure and innervation to other seals, adding to the growing body of evidence

that species in the family Phocidae, and perhaps all pinnipeds, possess highly sensitive vibrissae that form a sensory system for prey detection and capture.

In summary, female southern elephant seals from Península Valdés immediately depart the coast after breeding and travel to the continental slope while making shallow transit dives with little variation in easterly heading. Once beyond the continental shelf, they begin making deep foraging dives along the continental slope and Argentine Basin in cold water that arises from southern polar regions. While at sea for 75 days, they travel an average horizontal distance of 6,080 km and make 2,815 foraging dives. Their primary prey are small fish, some of which are bioluminescent, that they detect and capture in total darkness using vision and the tactile sensory system in their vibrissae. Between bouts of foraging dives, they make transit dives to new foraging areas or rest and probably sleep at an average maximum depth of 375 m. Of the 26 species of seals in the family Phocidae, southern elephant seals are the deepest diving and most pelagic, spending 10 months per year at sea and 89% of their time submerged while transiting, hunting and resting at depth.

ACKNOWLEDGEMENTS

I thank my committee chair, Dr. Randall Davis, and other committee members, Dr. Christopher Marshall, Dr. Gilbert Rowe, and Dr. Bernd Würsig, for their guidance throughout the course of completing my dissertation. I am immensely grateful to Dr. Randall Davis for his mentorship and for affording me opportunities to participate in myriad research projects. I have learned many skills and techniques from my experiences that I can draw upon as a researcher. I am thankful to Dr. Christopher Marshall for taking me under his wing at the beginning of my program and (with great patience) teaching me histological techniques. I am much obliged to Dr. Bernd Würsig for his encouragement and guidance in the process of writing my dissertation and for his reminders to look at the bigger picture and make connections between the diverse parts of my research. I thank Dr. Davis, Dr. Marshall, and Dr. Würsig for supporting me with research and/or teaching assistantships over the course of my tenure as a graduate student. I am thankful to Dr. Gilbert Rowe for his assistance in framing the oceanographic component of my research. I am also thankful to Dr. Douglas Biggs for his assistance in learning about biological oceanographic processes.

I thank Bill Hagey of Pisces Design for his role in designing, producing, and calibrating the video-data recorders, and for his sincerity and optimism. I thank Willem Buitendyk and Erin Frolli for their advice on instrument calibrations and calculating the three-dimensional coordinates. I thank Dr. Lee Fuiman and Dr. Terrie Williams for their mentorship during my three years as a research assistant in McMurdo Station, Antarctica. Although the experience was distinct from my dissertation research, I gained a great deal of knowledge about carrying out a research project, problem-solving and collaborating in the field. I thank the staff of the Marine

Biology Department on the Galveston campus and in the Wildlife and Fisheries Science Department on the College Station campus for all of their assistance and support over the years.

There are many people to thank for providing support in the field in Argentina. I thank Dr. Diego Rodríguez for the immense effort he put into planning and assisting with travel, documentation, permitting, and logistics, and for his insight and feedback during data analysis. I am grateful to Dr. Mirtha Lewis for leading the research team, serving as lead veterinarian, and preparing and arranging support and logistics for both the deployment and recovery of the instruments. I am thankful to many individuals that assisted with data collection, especially Elena "Lorna" Eder and Julieta Campagna, who were indispensable throughout the instrument recovery process. I am also grateful to Ricardo "Bebo" Vera, navigator extraordinaire. I thank Eduardo Mateos and Marcela Uhart for offering their veterinarian services when Dr. Lewis was unable to attend. I thank Dr. Claudio Campagna for sharing his time with us when he was in Argentina and for sharing portions of his immense knowledge of southern elephant seal biology with me. I also thank Mariela Dassis, Georgina Davis, Gisela Giardino, Nathan Reed, and Fred Weltz for their assistance in the field. I thank Kelly Rozas and Hannah Preischel for their assistance in processing histological specimens in Galveston.

To Zach, I am indebted to you for starting me on this journey. To my family and to my friends here in TX and elsewhere, I am grateful for your support and love. To my friends who have gone through this PhD process with me, thank you for the bottomless cups of coffee, encouragement, and understanding ears. To Jennifer, thank you for keeping me (reasonably) sane and for your wholehearted loving support.

CONTRIBUTORS AND FUNDING SOURCES

Contributors

This work was supervised by a dissertation committee consisting of Dr. Randall Davis, Dr. Christopher Marshall, and Dr. Bernd Würsig of the Departments of Wildlife and Fisheries Sciences and Marine Biology, Dr. Gilbert Rowe of the Departments of Oceanography and Marine Biology, and Dr. Douglas Biggs of the Department of Oceanography.

Data collection for Sections 2 and 3 was conducted in part by Dr. Randall Davis and Nathan Reed of the Department of Marine Biology; researchers from the Universidad Nacional de Mar del Plata in Mar del Plata, Argentina: Dr. Diego Rodríguez, Dr. Mariela Dassis, and Dr. Gisela Giardino; researchers and support staff from Centro Nacional Patagónico in Puerto Madryn, Argentina: Dr. Mirtha Lewis, Dr. Elena Lorna Eder, Dr. Claudio Campagna, Julieta Campagna, and Ricardo Vera; two independent veterinarians: Dr. Eduardo Mateos of Mar del Plata, Argentina, and Dr. Marcela Uhart of Puerto Madryn, Argentina; and Georgina Davis and Fred Weltz. Data was collected under written permits to Dr. Diego Rodríguez and Dr. Mirtha Lewis. Calibrations of the video-data recorder sensors were conducted by William Hagey of Pisces Design. The analyses depicted in Sections 2 and 3 were supervised by Dr. Randall Davis of the Department of Marine Biology and completed by the student independently. Dara Orbach provided comments to strengthen the manuscript for Section 2.

Data collection for Section 4 was conducted in part by Dr. Christopher Marshall, Kelly Rozas and Hannah Preischel of the Department of Marine Biology. Biological samples were provided by Lauren Rust of the Marine Mammal Center in Sausalito, CA under a written permit to Dr. Christopher Marshall from the National Marine Fisheries Service Southeast Regional Office. The

analyses depicted in Section 4 were supervised by Dr. Christopher Marshall of the Department of Marine Biology and completed by the student independently.

Funding sources

Graduate study was supported by a first-year fellowship, research assistantships, and teaching assistantships from Texas A&M University and a three year pre-doctoral fellowship from the National Science Foundation (grant number 1252521).

This work was made possible in part by Texas A&M University at Galveston Marine Biology Mini-Grants, Erma Lee and Luke Mooney Travel Grants, Texas A&M University at Galveston Research Advisory Grants, the Prince Bernhard Naturefund, and the National Science Foundation under grant numbers 1063198 and 1455546. Its contents are solely the responsibility of the author and do not necessarily represent the official views of the funding sources.

NOMENCLATURE

2D	two-dimensional
3D	three-dimensional
AAIW	Antarctic Intermediate Water
AR1	auto-correlated model of order 1
AUC	area under the curve
AVISO	Archivage, Validation et Interprétation des données des Satellites Océanographiques
Basin	Argentine Basin
Chl-α	Chlorophyll-α
Cluster	cluster analysis
cm	centimeters
CNES	Centre National d'Etudes Spatiales
DC	dermal capsule
DVN	deep vibrissal nerve
ESA	European Space Agency
FPT	first-passage time
F-SC	follicle-sinus complex
g	grams
GAM	generalized additive model
GB	gigabyte
GEBCO	Generalized Bathymetric Chart of the Oceans

GM	glassy membrane
GMT	Greenwich Mean Time
GPS	global positioning system
hr	hours
HS	hair shaft
Hz	hertz
ICB	inner conical body
IRS	inner root sheath
kg	kilograms
kHz	kilohertz
km	kilometers
LCDW	Lower Circumpolar Deep Water
LCS	lower cavernous sinus
LDA	linear discriminant analysis
LED	light-emitting diode
m	meters
mg	milligrams
ml	milliliters
mm	millimeters
MNC	Merkel-cell neurite complex
MODIS	Modern Resolution Imaging Spectroradiometer
MS	mesenchymal sheath
n	number

NADW	North Atlantic Deep Water
NASA	National Aeronautics and Space Administration
NOAA	National Oceanic and Atmospheric Administration
NODC	National Oceanographic Data Center
ORS	outer root sheath
PO.DAAC	Physical Oceanography Distributed Active Archive Center
psu	practical salinity units
QDA	quadratic discriminant analysis
RF	random forest analysis
ROC	receiver operating characteristic
RS	ring sinus
SD	standard deviation
sec	seconds
shelf	Patagonian continental shelf
slope	Patagonian continental slope
SMOS	Soil Moisture and Ocean Salinity
SSHA	sea surface height anomaly
SSS	sea surface salinity
SST	sea surface temperature
SAMW	Subantarctic Mode Water
STMW	Subtropical Mode Water
SW	Surface Water
UCDW	Upper Circumpolar Deep Water

UCS	upper cavernous sinus
WSDW	Weddell Sea Deep Water
VDR	video-data recorder
VHF	very high frequency

TABLE OF CONTENTS

LIST OF FIGURES

LIST OF TABLES

1. INTRODUCTION

1.1 Distribution and brief history of southern elephant seals

Southern elephant seals (*Mirounga leonina)*, the largest of the phocid seals, have a circumpolar distribution in the southern hemisphere (Fig. 1.1) (Hall et al., 2006). Breeding colonies occur from approximately 40°S to 62°S (Carrick and Ingham, 1962). There is one well-established mainland colony, however, the majority of breeding occurs on numerous sub-Antarctic islands (Hall et al., 2006; Hoelzel et al., 2001). There are four main genetic stocks of southern elephant seals located at Macquarie Island in the South Pacific Ocean, Kerguelen and Heard Islands in the South Indian Ocean, South Georgia in the South Atlantic Ocean, and Península Valdés, Argentina in the South Atlantic Ocean (Slade et al., 1998).

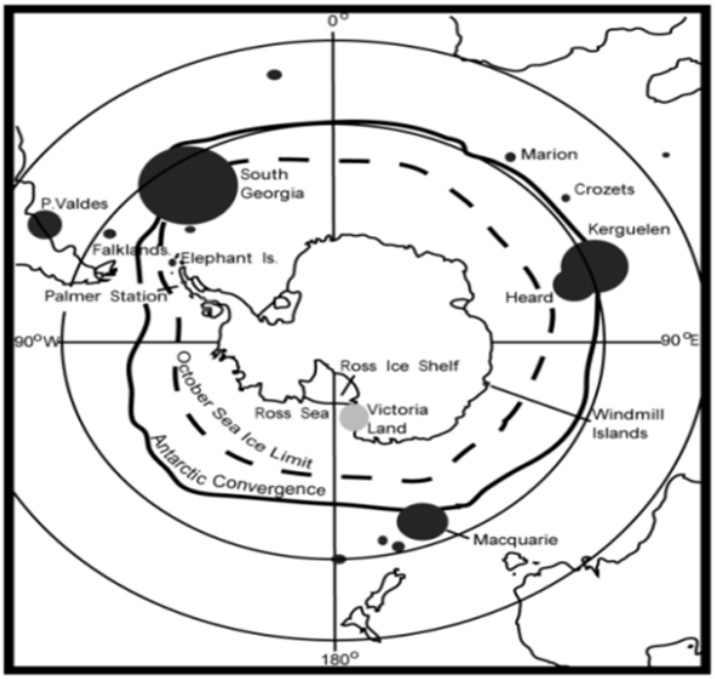

Figure 1.1. Distribution of southern elephant seals reprinted from De Bruyn et al. (2009), under CC-BY license.

According to studies of population genetics, the Península Valdés population, the only large mainland colony, shared a common ancestor with the Macquarie Island population ca. 600,000 years ago. The remaining populations diverged ca. 200,000-300,000 years ago, except for the populations at South Georgia and Heard Islands, which may have diverged as recently as 20,000 years ago (Slade et al., 1998). The population at Península Valdés has low mitochondrial DNA (mtDNA) diversity; only three haplotypes are present in the population, two of which could be derived from the third with a single mutation. This suggests that the Península Valdés population derived from a single matriline, indicating a single founder event 600,000-700,000 years ago (Corrigan et al., 2016; Hoelzel et al., 2001; Slade et al., 1998). However, there is evidence for limited male dispersal, especially between South Georgia and Península Valdés (Hoelzel et al., 2001).

Although the global population of southern elephant seals largely declined from the 1950s-1990s, recent reports indicate that it has stabilized in recent years (Hindell et al., 2016; McMahon et al., 2005). The population at Kerguelen Island, which historically had been decreasing, has now stabilized. The population at South Georgia has remained stable and the population at Península Valdés has been increasing since the 1970s. The population at Macquarie Island, however, has been decreasing steadily since the 1950s (Hindell and Perrin, 2008; Hindell et al., 2016; McMahon et al., 2005).

1.2 Southern elephant seals at Península Valdés

The southern elephant seal population at Península Valdés is the only well-established mainland colony, the northernmost sizeable colony, and the only colony that has been consistently increasing over recent decades (Campagna et al., 1995; Campagna and Lewis, 1992; Hindell et al., 2016; Hoelzel et al., 2001).

1.2.1 Annual cycle

The annual cycle of southern elephant seals from all colonies is similar, regardless of population size or colony latitude, although the breeding and molting seasons at Península Valdés commence approximately two weeks earlier than other colonies (Lewis et al., 2004). Southern elephant seals haul out on land for weeks at a time during the breeding and molting seasons, during which they fast (Carrick et al., 1962; Matthews, 1929). Female seals haul out for approximately one month during the breeding season, depart on a foraging trip of ca. two months in duration, haul out for approximately one month to molt, and then depart on a foraging trip of ca. eight months in duration prior to the following breeding season. Adult males follow a similar annual schedule, but haul out for longer durations (2-3 months) during the breeding season (Campagna et al., 1993; Le Boeuf and Laws, 1994).

Southern elephant seals undergo a cataclysmic molt, during which the fur and upper epidermis are cast and replaced (Carrick et al., 1962). This type of molt is unique to the elephant seal species and the Hawaiian monk seal, and is not known to occur in any other mammal, aquatic or terrestrial (Kenyon and Rice, 1959). At Península Valdés, adult females molt in December and January and adult males molt between late February and April. Juveniles do not follow the same annual schedule as adults; the maximum number of juveniles molting on shore occurs in mid-November (Lewis et al., 2004).

Southern elephant seals are a polygynous species, and males establish harems on the beaches during the breeding season. Females give birth to a single pup annually (Campagna et al., 1993; Le Boeuf and Laws, 1994). At Península Valdés, reproductive males begin arriving in late August and harems are formed by alpha males by the second week of September. Females begin arriving in September and the adult female population peaks during the first week of October.

Females give birth within a week of coming ashore, and wean their pups approximately 22 days later. Females copulate ca. 20 days after parturition, mostly with alpha males. Female presence begins declining after the second week of October, and most alpha males are gone by mid-November (Campagna et al., 1993). Seals at other colonies follow a similar schedule, albeit delayed by approximately two weeks (Carrick et al., 1962; Lewis et al., 2004).

1.2.2 Marine habitat

The Patagonian continental shelf, along which Península Valdés is located, encompasses an area greater than 1,000,000 km^2 (Sánchez and Ciechomski, 1995). It is one of the most productive shelves in the world and extends 300-400 km east from Península Valdés (Campagna et al., 1999). Near-shore vertical mixing creates tidal fronts, (Campagna et al., 2007), which in this location are associated with increased densities of copepods, euphausiids, cephalopods, and commercial fish larvae, and are the spawning grounds of the Argentine short-fin squid (Acha et al., 2004). At the edge of the shelf, along the continental shelf break, the cold water of the Malvinas Current flows northward along the 1,000 m isobath and meets the warmer shelf waters (Fig. 1.2). The shelf break front located here is an area of increased primary productivity as measured by satellite and in-situ chlorophyll concentrations (Campagna et al., 2007; Campagna et al., 2000; Piola and Matano, 2001), and is thought to be caused by upwelling created by the interaction of the Malvinas Current with the high gradient of the continental slope in this area (Romero et al., 2006a). The shelf-break front is a known hatchery for Argentine hake and is important for the migration of anchovies and Argentine hake. Argentine short-fin squid and myctophid fish are found here in great quantities (Acha et al., 2004).

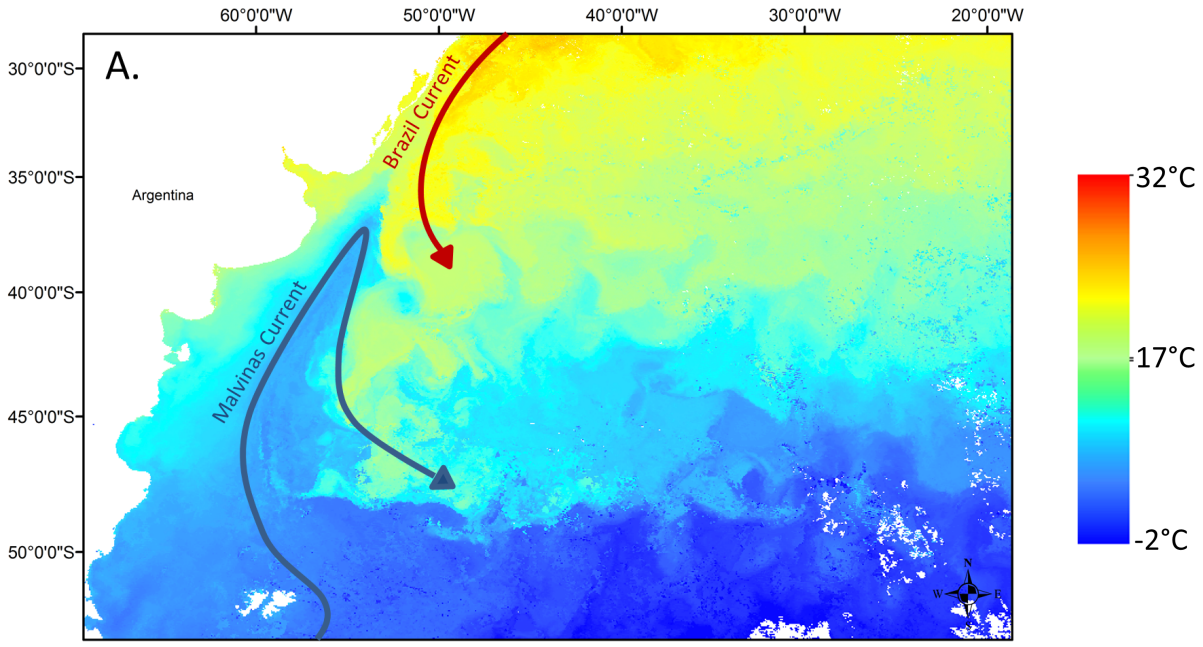

Figure 1.2. The Brazil-Malvinas Confluence. Simplified map depicting the cold water of the Malvinas Current flowing north colliding with the warm water of the Brazil Current flowing south. Sea Surface Temperature data from NASA's Earth Observations website and obtained from the Moderate Resolution Imaging Spectroradiometer (MODIS) instrument aboard NASA's Aqua and Terra satellites.

The Malvinas Current is a branch of the Antarctic Circumpolar Current, which transports deep and intermediate waters between the three major oceans (Atlantic, Pacific, and Indian) (Stewart, 2008). The Antarctic Circumpolar Current is majorly constricted in the narrow Drake Passage, and as it leaves, it hugs the boundary of South America as the Malvinas Current and carries sub-Antarctic waters up to ca. 39°S. This is the northernmost excursion of the Antarctic Circumpolar Current (Fig. 1.2) (Talley, 2011).

North of the Antarctic Circumpolar Current, strong southward currents are found near the western boundary of each ocean. In the South Atlantic, this boundary current is called the Brazil Current, which carries warm, subtropical water southward (Fig. 1.2). The eastward extension of each of these currents forms the southern branch of the respective subtropical gyres. The transition between subantarctic waters and subtropical waters occurs in each of the oceans

between the Antarctic Circumpolar Current and the southern branch of the subtropical gyre (Orsi et al., 1995; Saraceno et al., 2004). In the South Atlantic, this transition zone is known as the Brazil-Malvinas Confluence, a frontal zone created by the collision of the Brazil and Malvinas Currents (Piola and Matano, 2001; Wainer et al., 2000). After colliding with the Brazil Current, the Malvinas Current takes a sharp turn to the south and then east. The Brazil Current splits into two branches, with one forming a recirculation cell and the other flowing east as the South Atlantic Current (the southern limb of the subtropical gyre) (Saraceno et al., 2004). The Brazil-Malvinas Confluence is characterized by a sharp horizontal temperature gradient and is a region of intense mesoscale eddy activity (Campagna et al., 2000; Piola and Matano, 2001). The confluence is home to the hatchery grounds of at least two stocks of Argentine short-fin squid (Acha et al., 2004).

1.2.3 Potential prey

Little is known about the diet of southern elephant seals due to the difficulty of observing foraging behavior at sea. Stomach lavage samples taken on shore cannot be expected to accurately characterize prey consumed while foraging hundreds of kilometers away from rookeries (McMahon et al., 2005; Slip, 1995). In addition, cephalopod beaks are not digested as readily as fish bones and can amass in the stomach, biasing estimates of the relative contribution of individual prey to the diet (Cherel et al., 2008; Rodhouse et al., 1992; Whitehead et al., 2003).

Most of the information available on diet is based on studies of southern elephant seals from subantarctic islands and suggests that southern elephant seals are wide-ranging, generalist predators that exhibit intraspecific variation and plasticity in both foraging habitat and prey preference (Biuw et al., 2010; Bradshaw et al., 2003; Campagna et al., 2007; Daneri et al., 2000; Ducatez et al., 2008; Eder et al., 2010; Field et al., 2007; Field et al., 2005; Hindell et al., 1991;

Lewis et al., 2006; Newland et al., 2009; Piatkowski et al., 2002). They feed in deep waters on dielly migrating meso-pelagic prey, as well as in neritic habitats on demersal and benthic prey (Boyd and Arnbom, 1991; Campagna et al., 1998; Eder et al., 2010; Field et al., 2001; Hindell et al., 1991; Hückstädt et al., 2011; McIntyre et al., 2011). Stable isotope analyses indicate that individual seals occupy trophic levels over a wide range of values (Cherel et al., 2008; Eder and Lewis, 2005). Stable isotope and fatty acid analyses, as well as stomach lavage studies, indicate a diet composed primarily of cephalopods and fish. Known prey identified from stomach lavage includes 28 cephalopod species (24 squid and 4 octopus) and 22 fish species (mainly nototheniid and myctophid species) (Appendix A: Tables A.1, A.2) (Bradshaw et al., 2003; Brown et al., 1999; Burton and van den Hoff, 2002; Clarke and MacLeod, 1982; Daneri et al., 2000; Eder et al., 2010; Field et al., 2007; Green and Burton, 1993; Laws, 1956; Murphy, 1914; Piatkowski and Vergani, 2000; Rodhouse et al., 1992; Slip, 1995; van den Hoff, 2004; van den Hoff et al., 2003). Benthic mollusks, ascidians, and crustaceans, including euphausiids, copepods, amphipods, mysids, and isopods have been found in stomach contents, although with the exception of euphausiids, it is unknown whether ingestion occurred primarily or secondarily (Burton and van den Hoff, 2002; Field et al., 2004; Green and Burton, 1993; Laws, 1956; Piatkowski and Vergani, 2000; Rodhouse et al., 1992; Slip, 1995; van den Hoff et al., 2003).

1.2.4 Foraging behavior

It is known that adult southern elephant seals from Península Valdés and some other colonies display intersexual differences in foraging locations (Campagna et al., 1999; Campagna et al., 2007; Hindell et al., 1991). Males forage predominantly over the continental shelf and slope. Females transit the shelf in a matter of days to forage over the continental slope and deep waters of the Argentine Basin, diving to depths at times >1000 m (Campagna et al., 1999; Campagna et

al., 1995; Campagna et al., 2007; Campagna et al., 1998). There is evidence that this sexual segregation in foraging habitat begins to emerge early in development (Campagna et al., 2006). According to stable isotope studies, it appears that individual males of this population are specialists, split between several strategies. Stable isotope values for females are more homogenous, indicating that females forage on similar prey (Lewis et al., 2006).

1.3 Sensory modalities for tracking and capturing prey

Many deep-diving marine carnivores, including elephant seals, have adapted pigments that increase sensitivity to the blue-green wavelengths of light that persist at depth (Hanke et al., 2009; Levenson et al., 2006; Levenson and Schusterman, 1999). However, seals forage in the aphotic zone and at night when light levels are greatly diminished (Vacquié-Garcia et al., 2015). Although there is evidence that seals forage on bioluminescent prey such as myctophids, which may be located and tracked visually, seals also forage on meso-pelagic prey that are not bioluminescent and thus must be located and tracked using other sensory means during periods of or at depths with little to no ambient light (Field et al., 2007; Green and Burton, 1993; Slip, 1995). Studies of other pinniped species, i.e. harbor seals and California sea lions, indicate that they can sense and track hydrodynamic trails in the water using their vibrissae (Dehnhardt et al., 2001; Gläser et al., 2011; Schulte-Pelkum et al., 2007) and readily use mystacial whiskers during feeding events (Grant et al., 2013; Marshall et al., 2008; Marshall et al., 2015; Marshall et al., 2014b). Most phocid species have hair shafts with a distinct beaded profile (Ginter et al., 2012; Ginter et al., 2010; Hanke et al., 2013; Hyvärinen, 1995; Hyvärinen et al., 2009; Ling, 1966; Yablokov and Klezeval, 1969), with the known exceptions of monk seals (*Monachus* sp.), bearded seals, Ross seals, and leopard seals (*Hydrurga leptonyx*) (Berta et al., 2006; Ginter et al., 2012; Ginter et al., 2010; Ling, 1972; Marshall et al., 2006). Otariids and terrestrial mammals

have smooth hair shafts (Ginter et al., 2012; Hanke et al., 2013; Hyvärinen et al., 2009). This has functional significance, as the beaded profile of harbor seal vibrissae suppresses vortex shedding while the vibrissae are moving through water, resulting in a higher signal-to-noise ratio than that experienced by smooth vibrissae (Hanke et al., 2013; Hanke et al., 2010). Histological studies of pinniped vibrissae indicate that each mystacial vibrissal follicle is innervated by 5-10 times more axons than those of terrestrial mammals (Dehnhardt et al., 1999; Hyvärinen and Katajisto, 1984; Hyvärinen et al., 2009; Marshall et al., 2006; Mattson and Marshall, 2016; Sprowls, 2017). It is clear that vibrissae serve as sensory structures for prey capture and detection in a wide range of pinniped species, including southern elephant seals.

1.4 Northern elephant seal vibrissae as a proxy for southern elephant seal vibrissae

Southern and northern elephant seals (*Mirounga angustirostris*) diverged ca. 800,000 years ago, and the Península Valdés population shared its last common ancestor with other southern elephant seal populations ca. 600,000 years ago (Slade et al., 1998). Northern elephant seals and southern elephant seals from Península Valdés share many similarities, including comparable annual cycles and intersexual differences in foraging habitat, with females foraging in deeper waters (Le Boeuf and Laws, 1994; Le Boeuf et al., 2000; Lewis et al., 2006). There is a positive relationship between innervation (sensitivity) of vibrissae and aquatic specialization (Dehnhardt et al., 1999; Hyvärinen et al., 2009; Marshall et al., 2014a). Southern and northern elephant seals diverged recently in geologic time and share the same degree of aquatic specialization; it is likely that the function and structure of their vibrissae are similar, if not identical.

1.5 Research objectives

The purpose of this dissertation was to examine the diving and foraging behavior as well as foraging habitat of female southern elephant seals from Península Valdés, Argentina during their

post-breeding foraging trip using animal-borne instruments that recorded video of prey encounters and other behaviors, oceanographic data, and movement data that allowed me to calculate three-dimensional dive paths for each dive. In addition, I investigated the potential for the use of the vibrissae as a sensory structure for prey detection and capture using vibrissae obtained from stranded northern elephant seals as an analog for the vibrissae of southern elephant seals.

In Chapter 2, data from dives with associated video recordings were used to develop a model to assign functions (foraging, resting, transit) to dives without associated video and an algorithm to identify individual prey encounters within each foraging dive. I hypothesized that seals from the Península Valdés colony forage on similar prey as seals from other geographic areas, and that seals forage primarily over the continental slope and Argentine Basin at depths below 400 m. In Chapter 3, the association for foraging dives with location, bathymetry, oceanographic features, individual water masses, productivity, and hydrographic variables were examined. I hypothesized that seals forage in association with cyclonic eddies shed from the Malvinas Current in the Brazil-Malvinas Confluence Zone, and in association with frontal zones as indicated by high chlorophyll-α concentrations, temperature, or salinity gradients. In Chapter 4, the innervation of individual mystacial vibrissal follicles was quantified, using northern elephant seal vibrissae as a proxy, and the potential role for prey detection and capture was assessed. I hypothesized that elephant seal mystacial vibrissae were similar in microstructure to that of other pinnipeds, and that each follicle-sinus complex would be innervated by $\geq$ 1000 axons.

2. DIVING BEHAVIOR OF POST-BREEDING FEMALE SOUTHERN ELEPHANT SEALS (*Mirounga leonina*)

2.1 Introduction

Southern elephant seals spend the majority of the year in the deep waters of the Southern Ocean and the southern regions of the Atlantic, Pacific and Indian Oceans. Adult females spend ten months at sea, divided into a two-month post-breeding foraging trip and an eight-month post-molt foraging trip. In between these two periods at sea, they haul out on land for approximately one month each during the breeding and molting seasons, respectively (Le Boeuf and Laws, 1994). The peak period for pupping and breeding at Península Valdés, Argentina occurs during the first week of October, and the peak period for molting occurs during December and early January (Lewis et al., 2004).

Southern elephant seals from Península Valdés display intersexual differences in foraging behavior. Males forage in shallower waters along the continental shelf or slope, while females cross the 300-400 km wide continental shelf during the first few days of their foraging trip on their way to deeper waters in the Argentine Basin (Campagna et al., 1999; Campagna et al., 2007; Lewis et al., 2006). They exhibit diurnal diving behavior, indicating that they forage on prey in the deep scattering layer (Campagna et al., 1998; Hindell et al., 2016; McIntyre et al., 2011; McIntyre et al., 2010; Vacquié-Garcia et al., 2015). Little is known about the common prey items of southern elephant seals during their extended foraging trips (Burns et al., 2006). Stomach lavage, stable isotope, and fatty acid signature analyses indicate a diet comprised of fish and cephalopods (Green and Burton, 1993; Lewis et al., 2006; Newland et al., 2009). However, stomach content analyses may not accurately represent common prey items of seals that forage kilometers away from rookeries (McMahon et al., 2005; Slip, 1995).

Previous studies of pinniped foraging behavior have focused on the geographical location and depth of foraging using animal-borne instruments. Geographical locations (latitude and longitude) of southern elephant seals foraging behavior have been inferred based on increased residence time using surface tracks derived from satellite transmitters or geolocation tags (Bailleul et al., 2007; Hindell et al., 2016; Muelbert et al., 2013; O'Toole et al., 2014). Foraging behavior has also been inferred based on the shape of time-depth profiles (Campagna et al., 1995; McIntyre et al., 2011; Schreer and Testa, 1996), bottom time (McIntyre et al., 2011; Mcintyre et al., 2012), or variation in accelerometry, depth, or speed (Hassrick et al., 2007).

Recent advances in technology led to the development of various animal-borne instruments with high-resolution recording capability that are able to detect individual prey encounters in various pinniped species using video (Davis et al., 2003; Volpov et al., 2016), stomach temperature sensors (Horsburgh et al., 2008; Kuhn and Costa, 2006; Skinner et al., 2014) and jaw-motion accelerometers (Naito et al., 2013; Naito et al., 2017; Viviant et al., 2010). There have also been a number of studies that infer prey encounters based on rapid head movements detected by animal-borne accelerometers attached to the head (Gallon et al., 2013; Jouma'a et al., 2016; Vacquié-Garcia et al., 2015). Gallon et al. (2013) suggested that video-recorded validation is required to confirm the function of these rapid head movements.

The objective of this study was to assign functions (foraging, resting, or transit) to the dives of post-breeding female southern elephant seals using animal-borne instruments that recorded video of prey encounters and other behaviors, three-dimensional dive path, and locomotory performance. We used video recordings of prey capture to develop a model to identify foraging dives and an algorithm to identify prey encounters for dives without video. We hypothesized that

Seals from the Península Valdés colony forage on similar prey as seals from other geographic areas, and that seals forage primarily over slope and Argentine Basin at depths below 400 m.

2.2 Methods

2.2.1 Animals and Instrumentation

Miniature video-data recorders (VDRs, Pisces Design, La Jolla, CA; Fig. 2.1) were attached to the heads of 12 adult female southern elephant seals (standard length 260 ± 16.4 s.d. cm, curvilinear length 273 ± 15.5 s.d. cm, axillary girth 173 ± 9.7 s.d. cm) prior to their post-breeding foraging trip at a rookery (42.573851 S, 63.590378 W) 21 km north of Punta Delgada, *Península Valdés*, Argentina in October and November of 2012, 2013, and 2015. Females with pups that appeared healthy and close to weaning (silver pelage after molting their black, natal pelage) were selected to minimize the length of time they would remain on the rookery after instrumentation. Females were approached from behind while resting on the beach and sedated with an intramuscular injection of Telazol (0.5 mg kg^{-1}).

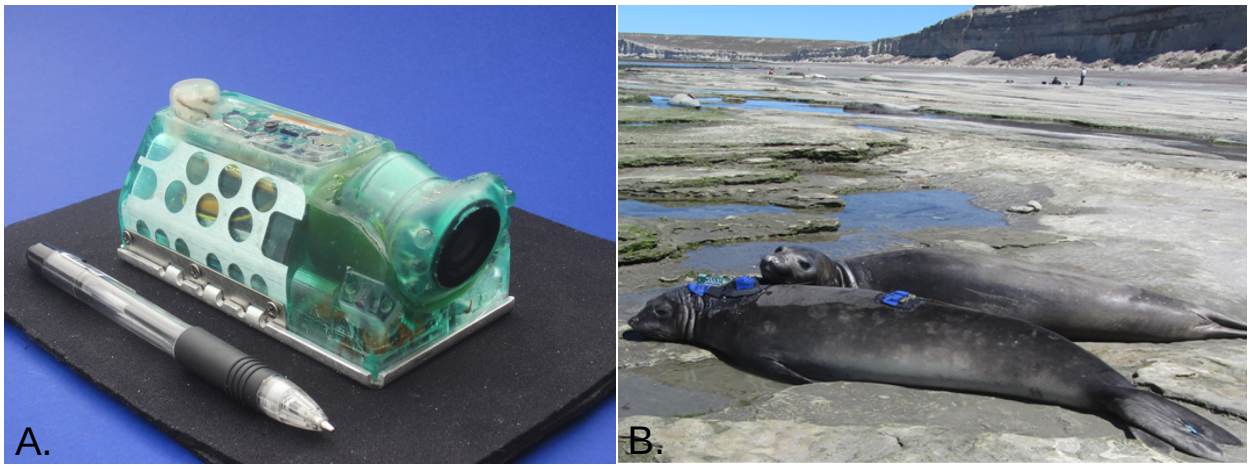

Figure 2.1. A.Video-data recorder (VDR). B. VDR, satellite transmitters, and VHF radio transmitters attached to a southern elephant seal female. The VDR contains a VisionMOS mDVR2 monochrome digital video recorder, an STMicroelectronics LIS3DH three-axis accelerometer, three-axis magnetometer, and sensors for depth, speed, light level, dissolved oxygen, conductivity, temperature, and sound (50 Hz - 16 KHz).

The VDR (12 cm long, 5.7 cm wide and 4.6 cm high; weight in water is ca. 60 g) is encased in polyurethane and depth rated to 2,000 m (Fig. 2.1). It has a Vision MOS mDVR2 monochrome digital video recorder and six near-infrared Light Emitting Diodes (LEDs) as a light source. The near-infrared LEDs allow imaging in total darkness without disturbing the animal's behavior (near-infrared light is invisible to marine vertebrates; Levenson et al., 2006). Compressed video (MPEG4) is stored on a digital video recorder with 32 GB of memory, and data are stored on 8 GB Flash memory. Sensor data are recorded at 1 Hz except speed (4 Hz) and the 3-axis accelerometer (16 Hz). Some instruments have a fast acquisition Global Positioning System (GPS) that records geolocation while the seal is at the surface. Power is provided by two lithium-ion batteries (10 cm long, 3 cm wide, 3 cm tall; mass = 270 g in water each). The battery pack enables 28 hours of programmable video recording and data recording for up to nine months. All sensors were calibrated prior to deployment.

The VDR was mounted on the head and the auxiliary battery pack behind the head. The seals were also instrumented with two VHF radio transmitters (Advanced Telemetry System, Isanti, MN) and two satellite transmitters (Spot 5 or 6, Wildlife Computers, Redmond, WA). One of each was placed on the head and back and enabled us to track the seals at sea and when they returned to shore. After cleaning the fur with acetone, all instruments were mounted on custom fitted, nylon-backed neoprene rubber and affixed to the fur with neoprene cement.

In 2012 and 2013, the video was programmed to begin recording when the seal exceeded a depth of 250 m, which indicated that it had finished traversing the shelf and was beginning to dive over the continental slope. In 2015, the video was programmed to commence recording 10 (n=2) or 20 (n=2) days after leaving the rookery and once it exceeded a depth of 250 m. This was done to improve the chance of recording foraging activity in deeper water, as the majority of the

prey encounters recorded during the first two field seasons were located over the continental slope.

Each seal was tracked at sea using satellite telemetry for the duration of the post-breeding foraging trip (75 $\pm$ 9 s.d. days). After returning to shore, the seals were relocated using satellite and radio telemetry, then sedated with an intramuscular injection of Telazol (0.5 mg kg^{-1}) to remove the instruments. The neoprene rubber molted off within one week after the seals returned to the rookery.

2.2.2 Video and Data Analysis

Video and data were downloaded and archived after instrument recovery. The video for each seal was viewed at the original recording speed and frame-by-frame to identify foraging events, prey species, and other behaviors. Dives with video were divided into three categories: foraging, transit, and resting. Foraging dives were defined as those in which prey were visible in the video and ingestion of prey was either viewed on the video or heard (crunching sound) on the audio. Dives in which foraging behavior was suspected but not confirmed (e.g., crunching sound but no visual of prey, prey visible on camera but no indication of consumption, etc.) were not included in the analysis. Transit dives were defined as those in which no resting or prey encounters were observed. Resting dives were defined as those during which the seal either drifted in the water column (drift dives) or rested on the ocean floor. A total of 269 video-recorded dives were analyzed and identified as foraging, resting, or transit.

The beginning and end of individual dives were determined using the VDR's saltwater switch, which indicated when the seal was at the surface. This surface indicator was also used to correct any drift that occurred in the depth sensor over the course of the deployment. The beginning and end of descent and ascent for each dive was determined based on changes in

depth. Descent began when the change in depth was negative for at least 5 consecutive seconds and ended when depth change was equal to zero for more than 10 seconds or became positive for more than 5 seconds. Ascent beginning and end was determined similarly. Bottom time comprised the time between descent and ascent. Stroking rate was calculated from the smoothed y-axis accelerometer record using the findPeaks function in the quantmod package in R ((R Core Team, 2013; Ryan, 2013). One stroke was defined as one full stroke cycle.

The uncorrected, three-dimensional dive paths (course steered) for each dive were calculated using the AnimalTrack package in R (Farrell and Fuiman, 2013), which used depth, speed, and bearing (based on magnetometer and accelerometer data) to determine X, Y, and Z coordinates at a resolution of 1 Hz. The course steered was corrected for set and drift using filtered ARGOS locations to determine the actual dive path (course made good). ARGOS locations were filtered in a multi-step process. All class Z locations were removed. Locations of classes A and B that were not located within 5 km and 2 hr of another location were eliminated. The remaining locations were filtered with the vmask function in the argosfilter package in R (Freitas, 2010), which applies the McConnell et al. (1992) algorithm, with a speed threshold of 2 m sec^{-1}. A subsequent filter removed locations occurring within 12 hr of another location. This increased the minimum time lag between successive correction points for the three-dimensional coordinates to 12 hr. When the ARGOS locations were closer in time, even a small location error created a large drift correction for a small subset of the data.

Four VDRs recorded both data and video. Two VDRs were not recovered, and two VDRs malfunctioned and did not record data or video. One VDR recorded for the entire trip (82 days), while the remaining seven VDRs recorded from 2 - 59 days. The four VDRs deployed during the 2015 season recorded data but not video. In total, 14,834 dives were recorded by eight seals

among the years 2012-16. Of these, 1,037 dives were excluded from the analysis for various reasons including inaccurate speed sensor and depth readings. The remaining 13,797 dives were analyzed. In total, 235 variables were calculated for each dive (broken down into ascent, bottom, descent, first half, second half, and the entire dive; Table A2.1) and used to create a model with the video-recorded dives (known class) that could be used to determine dive types for the remaining dives (unknown class) without video. Several classification models were tested to identify the one with the highest predictive accuracy.

Variables for all dives were combined into a single matrix in R. Each variable was standardized (rescaled to mean of 0 and standard deviation of 1), and data corresponding to video-recorded dives was extracted. Overall, 213 of the 269 dives with video were suitable for inclusion in the analysis. Dives with video were divided into subsets by random assignment using stratified sampling based on class: 70% for developing the models and 30% for testing the models. Supervised models included linear discriminant analysis (LDA), quadratic discriminant analysis (QDA), and random forest analysis (RF). Kmeans cluster analysis (Cluster), an unsupervised machine learning algorithm, was also performed. More information on individual model development can be found in Appendix B.

Models were compared and the best was chosen based on accuracy, area under the curve (AUC), and the Kappa statistic. Accuracy and the Kappa statistic were computed using each classifier's predicted dive types for the test dataset with the confusionMatrix function in the caret package in R (Kuhn et al., 2014). Statistics for the Kmeans cluster assignments were computed using all dives with video. Receiver Operating Characteristic (ROC) curves, which plot sensitivity as a function of specificity across a range of cut-off values (Florkowski, 2008; Lee and Fujita, 2007) were computed for each class (one class *vs* all others) with the roc function in

the pROC package in R (Robin et al., 2011) for the LDA, QDA, and RF classifiers and with the algorithm described by Lee and Fujita (2007) for the Cluster classifier. Area under the curve (AUC), a proxy for overall classifier accuracy (Florkowski, 2008) was computed for each ROC curve using the auc function in the flux package in R (Jurasinski et al., 2014).

Dive types were predicted using the final model (RF). To ascertain where and when the seals were foraging, transiting, or resting, the relative proportions of dive types by location and time of day were analyzed. The maptools and rgeos packages in R (Bivand and Lewin-Koh, 2013; Bivand and Rundel, 2013) were used to create a new time-of-day variable, which labeled each dive as occurring during dawn, day, dusk, or night based on date, location, and time of day. Astronomical dawn and dusk were used (sun at 18° below horizon). Bathymetry (obtained from the General Bathymetric Chart for the Oceans) for each dive was extracted using the raster package in R (Hijmans and van Etten, 2014) and used to determine whether each dive took place on the continental shelf (defined as <200 m[38]), slope (200-3,500 m,), or in deep water (>3,500 m) (Dogliotti et al., 2014; Violante et al., 2010). The hourly distribution of dive types by dive location was also examined.

A prey encounter event algorithm was developed as an indicator of foraging success using the video dive data. A new variable was created which was coded as “yes” during verified prey encounters (prey pursuit visible on camera and prey capture either seen on camera or heard on audio), “maybe” during likely prey encounters (e.g., prey seen on camera but no evident capture, suspected foraging based on audio or movement of seal’s head, but no visual confirmation of prey encounter, etc.), or “no” during periods of no suspected prey encounters. Prey encounters verified with video were 32.5 $\pm$ 30 s.d. seconds in duration and represent one or more prey captures. Because prey capture could often not be seen on the video because the snout overhangs

the mouth, the total number of prey captures per prey encounter event could not be verified. However, there was a characteristic head movement evident in the Z-axis (vertical axis) of the accelerometer that occurred during prey capture and a crunching sound on the audio recording. In total, 1,183 detection algorithms with varying input variables and detection threshold combinations were developed and compared. If all input variables for a specific algorithm were over threshold within two seconds of each other, a prey encounter event was detected. Detections within five seconds of each other were combined into a single prey encounter event. The best prey encounter algorithm was selected based on sensitivity (true positive rate) and specificity (true negative rate).

First-passage time analysis (Fauchald and Tveraa, 2003) was conducted using the beginning coordinates of each dive to determine the spatial scale at which seals searched for prey on the order of kilometers over the course of the foraging trip. Spherical first-passage time analysis (Adachi et al., 2017; Bailleul et al., 2008) was conducted using the three-dimensional locations at a resolution of 1 Hz to determine the spatial scale at which seals searched for and pursued prey on the order of meters over the course of a dive.

2.3 Results

2.3.1 Model Comparison and Selection

Models to identify dive type were compared based on accuracy, the Kappa statistic, and area under the curve (AUC) (for a detailed comparison, see Appendix C). Accuracy scores for all models were better than the no information rate (0.591) at a 0.01 significance level. Random forest analysis (RF) had the highest overall accuracy (0.909), Kappa statistic (0.842), mean sensitivity (0.92), mean specificity (0.96), and balanced accuracy averaged across classes

(0.936) and for each individual class (0.936, 0.938, and 0.936 for foraging, resting, and transit dives, respectively) (Tables 2.1, 2.2, and 2.3).

	Accuracy (95% CI)	Kappa statistic
LDA	0.803 (0.687, 0.891)*	0.638
QDA	0.864 (0.757, 0.936)*	0.755
RF	0.909 (0.813, 0.966)*	0.842
Cluster	0.812 (0.753, 0.862)*	0.667

Table 2.1. Accuracy and Kappa statistic for each model (* indicates that the accuracy was significantly better than the no information rate at a significance level of <0.01).

	Cluster	LDA	QDA	RF
Sensitivity	0.75	0.74	0.85	0.92
Specificity	0.90	0.88	0.92	0.96
Pos Pred Value	0.86	0.79	0.83	0.92
Neg Pred Value	0.89	0.88	0.92	0.94
Balanced Accuracy	0.83	0.81	0.88	0.94

Table 2.2. Predictive model measures averaged across the three classes for each model.

	Foraging				**Resting**				**Transit**			
	Cluster	LDA	QDA	RF	Cluster	LDA	QDA	RF	Cluster	LDA	QDA	RF
Sensitivity	0.811	0.872	0.923	0.872	0.480	0.625	0.875	0.875	0.951	0.737	0.737	1.000
Specificity	0.930	0.778	0.889	1.000	1.000	0.983	0.966	1.000	0.776	0.872	0.915	0.872
Pos Pred Value	0.945	0.850	0.923	1.000	1.000	0.833	0.778	1.000	0.630	0.700	0.778	0.760
Neg Pred Value	0.769	0.808	0.889	0.844	0.935	0.950	0.983	0.983	0.975	0.891	0.896	1.000
Balanced Accuracy	0.871	0.825	0.906	0.936	0.740	0.804	0.920	0.938	0.864	0.805	0.826	0.936

Table 2.3. Predictive model measures by class.

Receiver operating characteristic (ROC) curve plots and AUC calculations showed that RF performed better than all other models for foraging (AUC = 0.978, Fig. 2.2A), transit (AUC = 0.975, Fig. 2.2B), and resting (AUC = 0.998, Fig. 2.2C) dive classes individually and when averaged across dive classes for each model (AUC = 0.984; Table 2.4). As RF performed better than the other models according to all metrics, it was selected as the final model for classifying the 13,797 dives (9,453 foraging, 1,405 resting, 3,039 transit; Fig. 2.3).

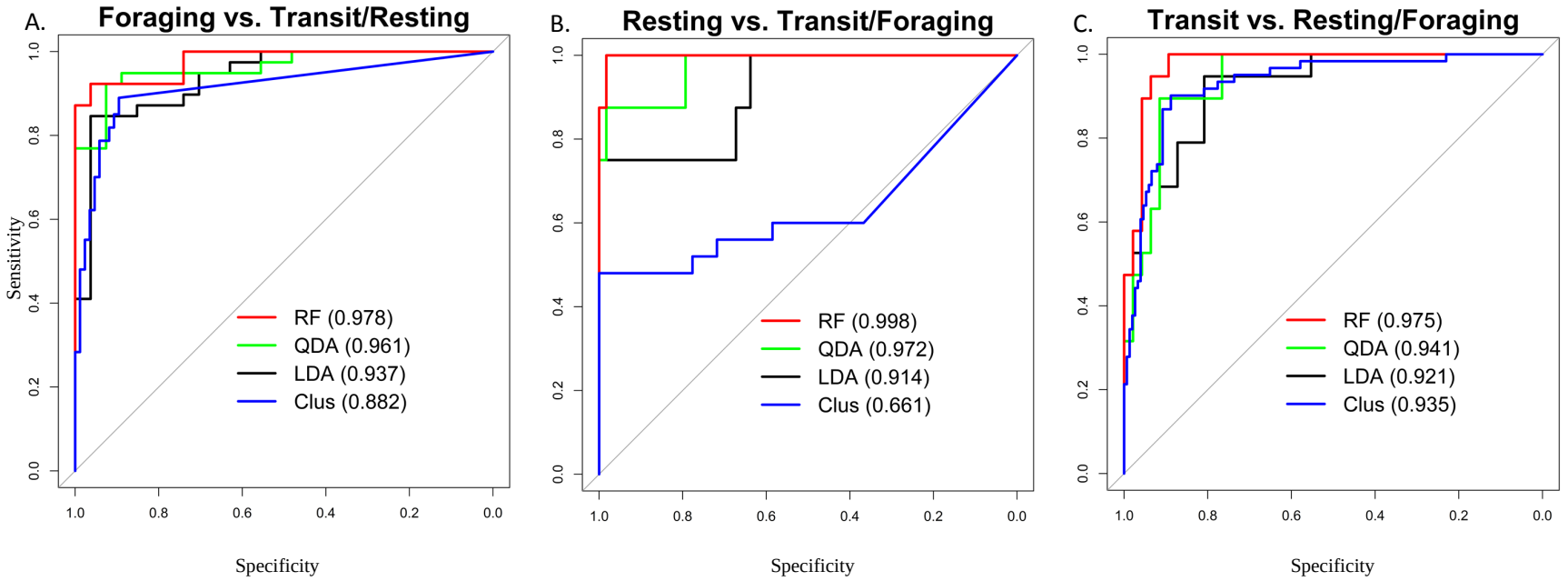

Figure 2.2. ROC curves (sensitivity by specificity plots) for one class vs. all other classes for all models (AUC in parentheses). Gray line indicates "line of no discrimination". A. Foraging vs. all other classes. B. Transit vs. all other classes. C. Resting vs. all other classes.

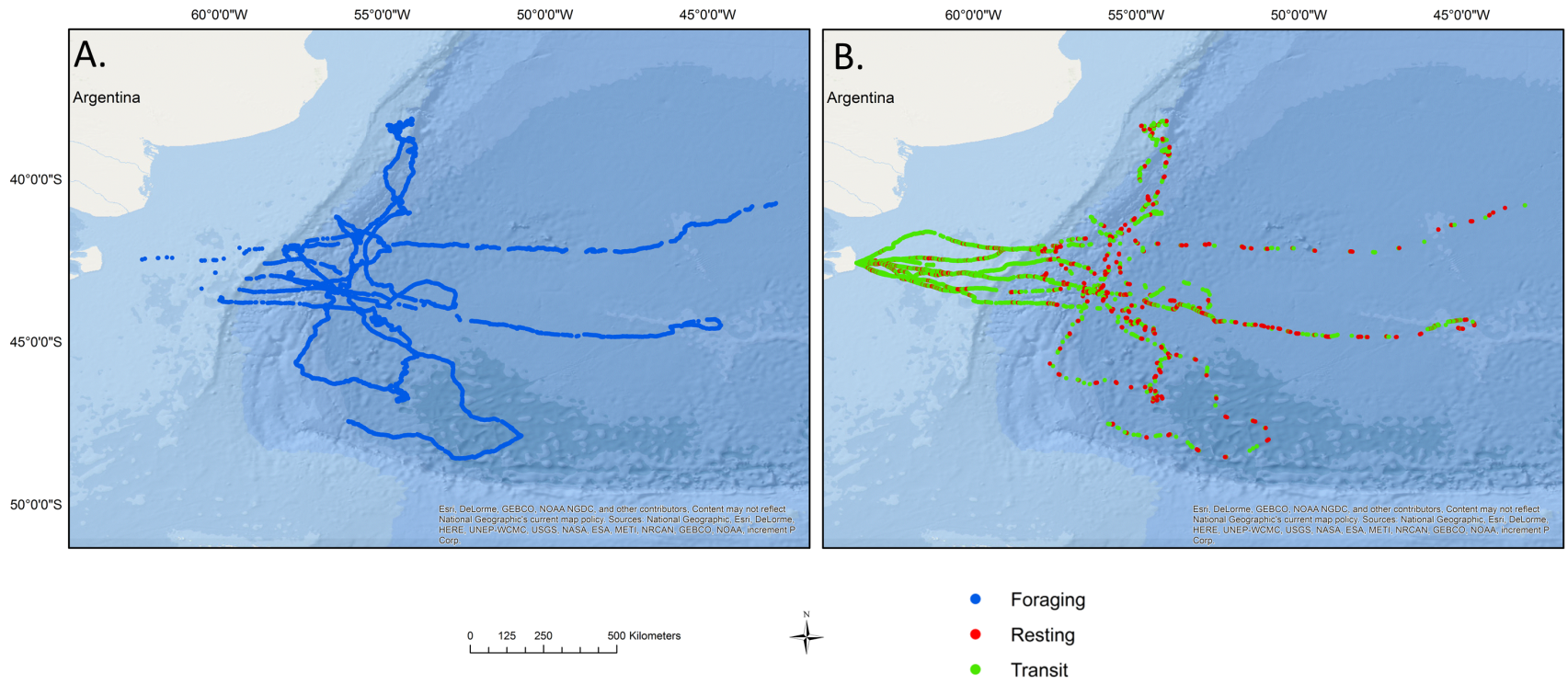

Figure 2.3. Seal dive locations colored by dive type (classified using random forest). A. Foraging dives. B. Resting and transit dives.

	Foraging	Transit	Resting	Mean
RF	0.978	0.975	0.998	0.984
QDA	0.961	0.941	0.972	0.958
LDA	0.937	0.921	0.914	0.924
Cluster	0.882	0.935	0.661	0.826

Table 2.4. AUC calculations by class for all models.

2.3.2 Daily behavior and proportion of dives types over the shelf, slope and deep water

The females crossed the continental shelf in 3.7 ± 0.3 s.d. days, and the post-breeding trip lasted 75 ± 9 s.d. days. Upon leaving the rookery, the seals all swam perpendicular to the coast on an easterly (~100°) bearing, making 87.8 ± 27.8 s.d. (range 57-158) dives per day over the shelf, of which 71 ± 28.4 s.d. (range 42-140) were transit dives, 15.1 ± 8.6 s.d. (range 0-31) were resting dives, and 1.7 ± 3.8 s.d. (range 0-13) were foraging dives. Most dives were transit dives (mean number of consecutive dives: 10.8 ± 12.7 s.d.), with resting dives occurring singly and in bouts of 2-9 dives (mean number of consecutive dives: 1.85 ± 0.6 s.d.). Foraging dives were rare. Dive type over the shelf was not influenced by time of day (Fisher's exact test, p-value = 0.8). The first 5-10 dives were generally of short duration (5-10 min), and the mean transit dive duration over the shelf was 13.4 ± 4.4 min. Most of the dives were square-bottomed and appeared to closely follow the bathymetry of the shelf, although some had vertical excursions of 5-20 meters. Speed did not vary during these vertical excursions, and it is possible that the seals were simply following the bathymetry. Video was recorded for 19 dives over the shelf by one seal. The sea floor was visible during the majority of the dives, but for some dives the sea floor was not visible or only visible for a short period of time. Over the continental shelf, transit dives represented 85-89% of daily dives, resting dives ranged from 9-13% and foraging dives ranged from 0-2%.

Over deeper water, seals made 59.9 ± 9.8 s.d. (range 43-92) dives per day, of which 48.2 ± 10.3 s.d. (range 2-75) were foraging, 5.9 ± 5.2 s.d. (range 0-37) were resting, and 5.8 ± 7.8 s.d. (range 0-46) were transit. Foraging occurred almost exclusively in bouts (98% of foraging dives preceded and/or followed another foraging dive). The average foraging bout consisted of 14 ± 8.4 s.d. dives with a maximum of 51. Transit dives occurred singly and in bouts of up to 18 consecutive dives (mean consecutive number of dives: 1.5 ± 0.6 s.d.). Resting dives occurred mostly in bouts with a maximum of 30 (mean consecutive number of dives: 4.2 ± 3.1); 85% of resting dives preceded and/or followed another resting dive.

A diurnal pattern was present in dives over the continental slope and Argentine Basin for all three dive types (Fig. 2.4). Kruskal Wallis tests indicated significant differences in dive depth by time of day for foraging (χ^2 statistic 3035.9, p-value <0.0001), resting (χ^2 statistic 64.059, p value <0.0001), and transit (χ^2 statistic113.57, p value <0.0001) dives. Post-hoc pairwise comparisons were made using the Mann-Whitney Wilcoxon test to determine which time of day categories (dawn, day, dusk, night) differed from each other. P-values were adjusted with a Bonferroni correction. The pattern was most obvious for foraging dives, which had a mean maximum depth of 689 ± 213 s.d. m during the day and 391 ± 219 s.d. m at night (adjusted p-value <0.0001). Mean maximum depth for resting dives was 382 ± 110 and 261 ± 132 s.d. m during day and night, respectively (adjusted p-value <0.0001). Mean maximum depth for transit dives was 360 ± 192 s.d. m for daytime dives and 255 ± 131 s.d. m for nighttime dives (adjusted p-value <0.0001).

Over the slope, the proportion of foraging dives was not significantly different among dawn, day, dusk, and night (Fisher's exact test Bonferroni-adjusted p-value 0.42, Table 2.5). Although Fisher's exact test detected a significant difference in transit dives by time of day over the slope

(Bonferroni-adjusted p-value 0.04), subsequent pairwise comparisons were insignificant after adjusting p-values with a Bonferroni correction. Fisher's exact test detected a significant difference in resting dives by time of day over the slope (Fisher's exact test adjusted p-value <0.0001, Table 2.5). Subsequent pairwise comparisons indicated that resting dives constituted a significantly higher percentage of day dives (15%) than during dawn, dusk, or night (all 2%).

Over the deep water of the Argentine Basin, Fisher's exact test detected a significant difference in foraging dives by time of day (adjusted p-value <0.001). Subsequent pairwise comparisons indicated that foraging dives made up a significantly lower percentage of dives during the day (75%) than during dawn and dusk (92% and 95%), but was not significantly different between day and night after applying a Bonferroni correction (Table 2.5). The percentage of transit dives was not significantly different among time periods (Fisher's exact test unadjusted p-value 0.71). Fisher's exact test detected a significant difference in resting dives by time of day (p-value <0.0001, Table 2.5). Resting dives made up 1% of the dives during dawn, dusk, and night, but comprised a significantly greater percentage (17%) of dives occurring during daytime hours (Table 2.5).

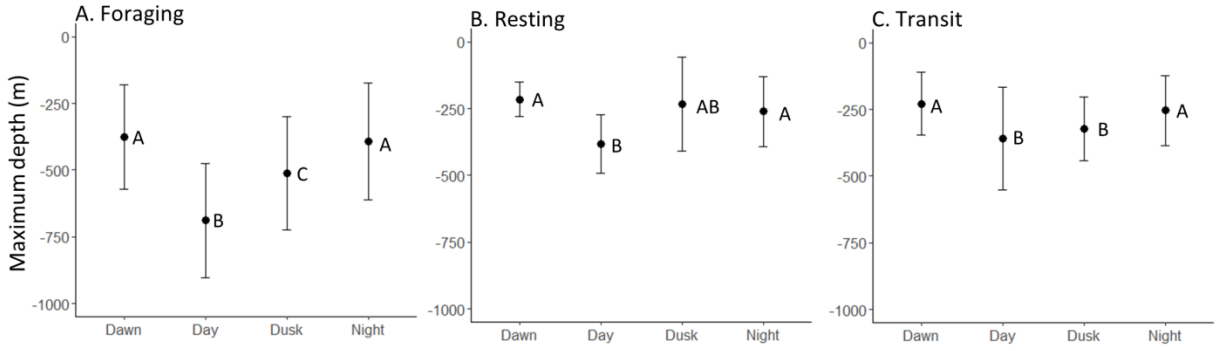

Figure 2.4. Maximum dive depth (m, s.d. bars) by time of day for all dives over the continental slope and Argentine Basin. A. Foraging dives. B. Resting dives. C. Transit dives. For each plot, means with different letters are significantly different at the $\alpha = 0.05$ level (Kruskal Wallis test, post hoc Mann-Whitney Wilcoxon pairwise tests with Bonferroni correction).

		Dawn	Day	Dusk	Night
Shelf	Foraging	0.02	0.02	0.02	0
	Resting	0.11	0.13	0.09	0.13
	Transit	0.87	0.85	0.89	0.87
Slope*	Foraging	0.81	0.71	0.72	0.67
	Resting*	0.02^{A}	0.15^{B}	0.02^{A}	0.02^{A}
	Transit	0.17	0.14	0.26	0.31
DW*	Foraging*	0.92^{A}	0.75^{B}	0.95^{A}	0.9^{AB}
	Resting*	0.01^{A}	0.17^{B}	0.01^{A}	0.01^{A}
	Transit	0.07	0.08	0.05	0.09

Table 2.5. Percent dive type by time of day over the continental shelf, continental slope, and over deep water. Asterisks indicate significant p-values (α=0.05) for Fisher's exact test. Significantly different pairwise values by row are denoted by different superscripts. P-values for post-hoc comparisons were adjusted with a Bonferroni correction.

Circular histograms and line plots with percentage of dive type by hour provided more detail on the distribution of dives relative to time of day. Dives were binned by hour (0-23). Over the shelf, no clear pattern for dive type distribution by hour was evident. Foraging dives accounted for 0-7% of dives per hour (small sample size of only 32 foraging dives over shelf). Resting dives accounted for 4-19% of dives per hour, and transit dives accounted for 79-96% of dives per hour (Figs. 2.5, 2.6). Resting and transit dive distribution by hour over the shelf were not significantly different from uniform distribution (Rayleigh's z-test, p-values 0.51 and 0.66, respectively). Foraging dive distribution by hour over the shelf was not tested due to the small sample size. Over the slope, dive distribution for each dive type by hour was significantly different from uniform (Rayleigh's z-test, p-value 0.02, <0.0001, and <0.0001 for foraging, resting, and transit, respectively). Foraging dives accounted for 42-90% of dives per hour and occurred at greater than average frequency during the hours of 0200, 0400, 0600-0900 and 1700-2300 GMT. Resting dives accounted for 0-35% of dives per hour and occurred at a greater than average frequency between 1000-1600 GMT. Transit dives accounted for 5-41% of dives per hour and occurred at greater than average frequency between 2300-0600 and 1200-1300 GMT

(Figs. 2.5, 2.7). Over deep water, dive distributions for foraging and resting dives by hour were significantly different from uniform (Rayleigh's z-test, adjusted p-value <0.0001 for both foraging and resting). Dive distribution for transit dives by hour was not significantly different from uniform distribution (p-value 0.07). Foraging dives accounted for 56-95% of dives per hour and occurred at a greater than average frequency from 1700-0800 GMT. Transit dives accounted for 3-11% of dives per hour. Resting dives accounted for 0-35% of dives per hour and occurred at greater than average frequency between 0900 and 1600 GMT (Figs. 2.5, 2.8).

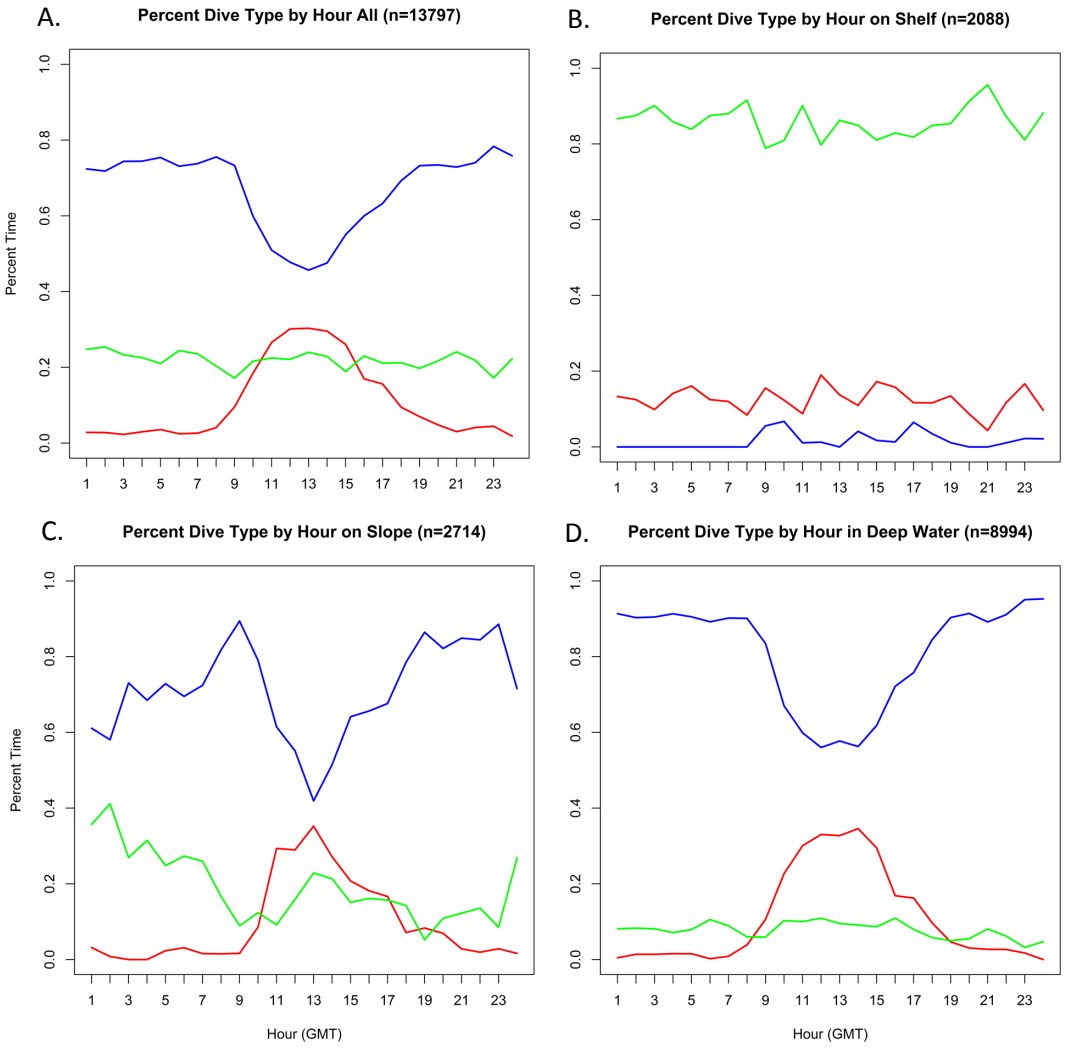

Figure 2.5. Percentage of dive type by hour for A. all dives, B. dives over the continental shelf, C. dives over the continental slope, and D. deep water dives.

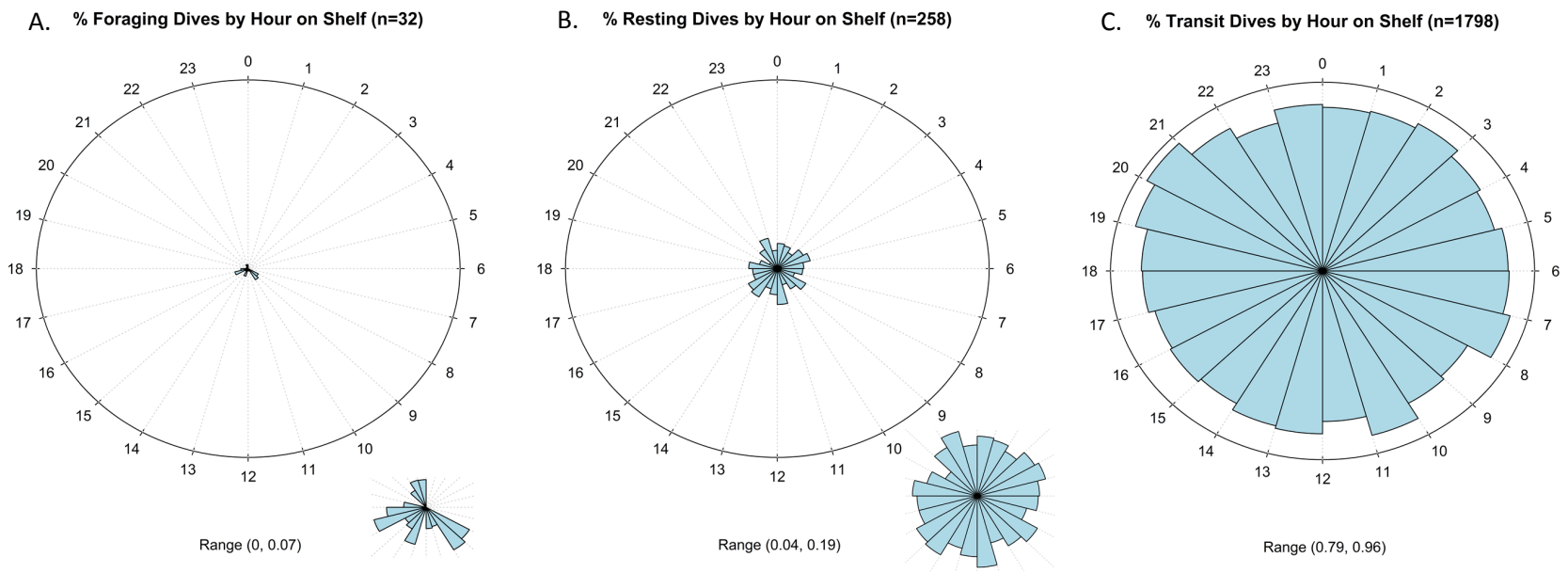

Figure 2.6. Distribution of percentage of dive type by hour for dives occurring over the continental shelf (insets are square root plots to magnify the distribution for easier viewing). A. Foraging dives. B. Resting dives. C. Transit dives.

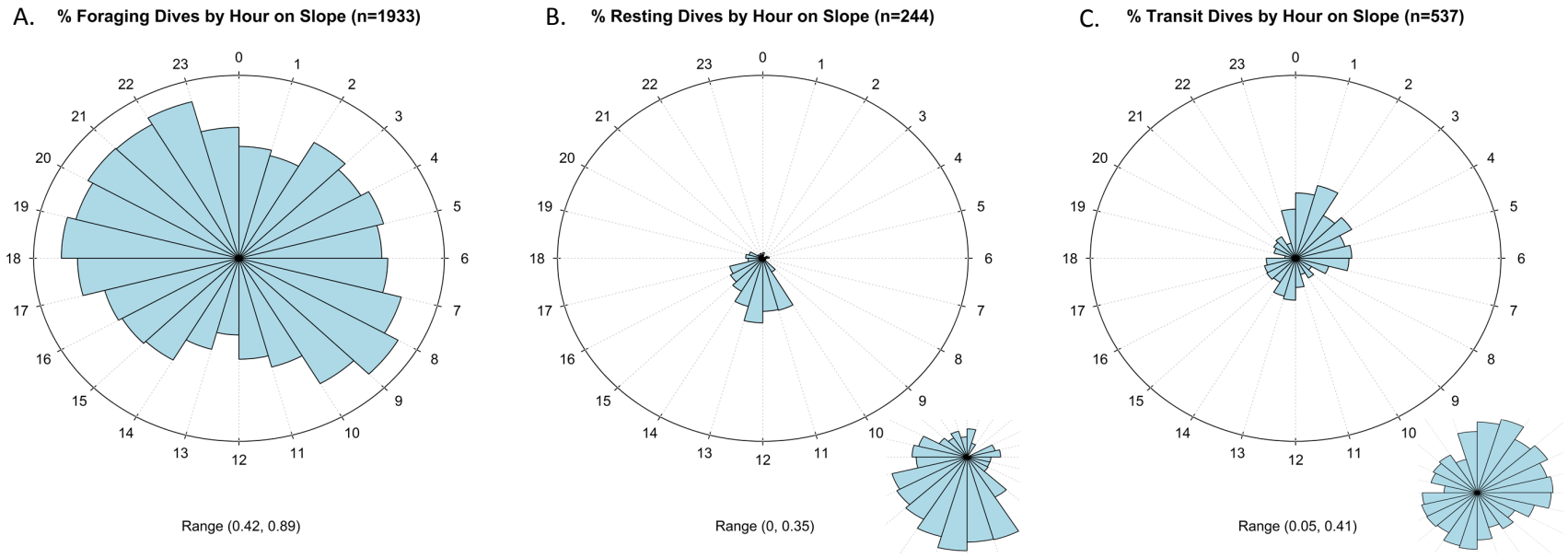

Figure 2.7. Distribution of percentage of dive type by hour for dives occurring over the continental slope (insets are square root plots to magnify the distribution for easier viewing). A. Foraging dives. B. Resting dives. C. Transit dives.

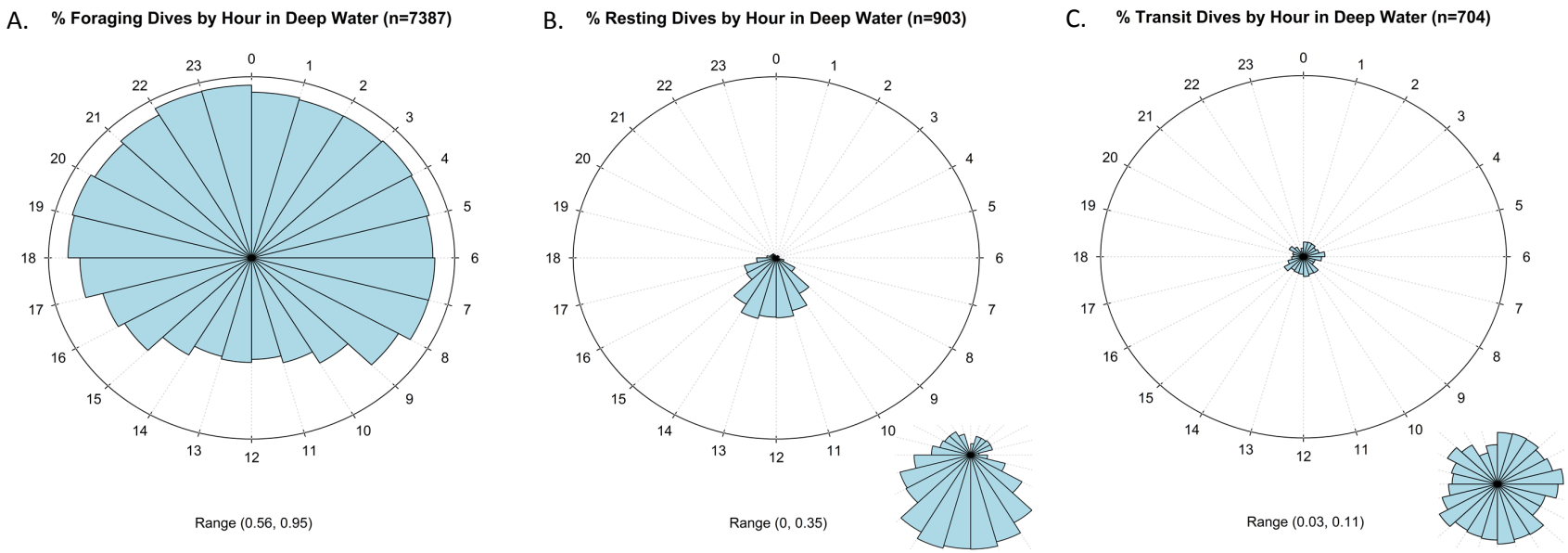

Figure 2.8. Distribution of percentage of dive type by hour for dives occurring over the deep water of the Argentine basin (insets are square root plots to magnify the distribution for easier viewing). A. Foraging dives. B. Resting dives. C. Transit dives.

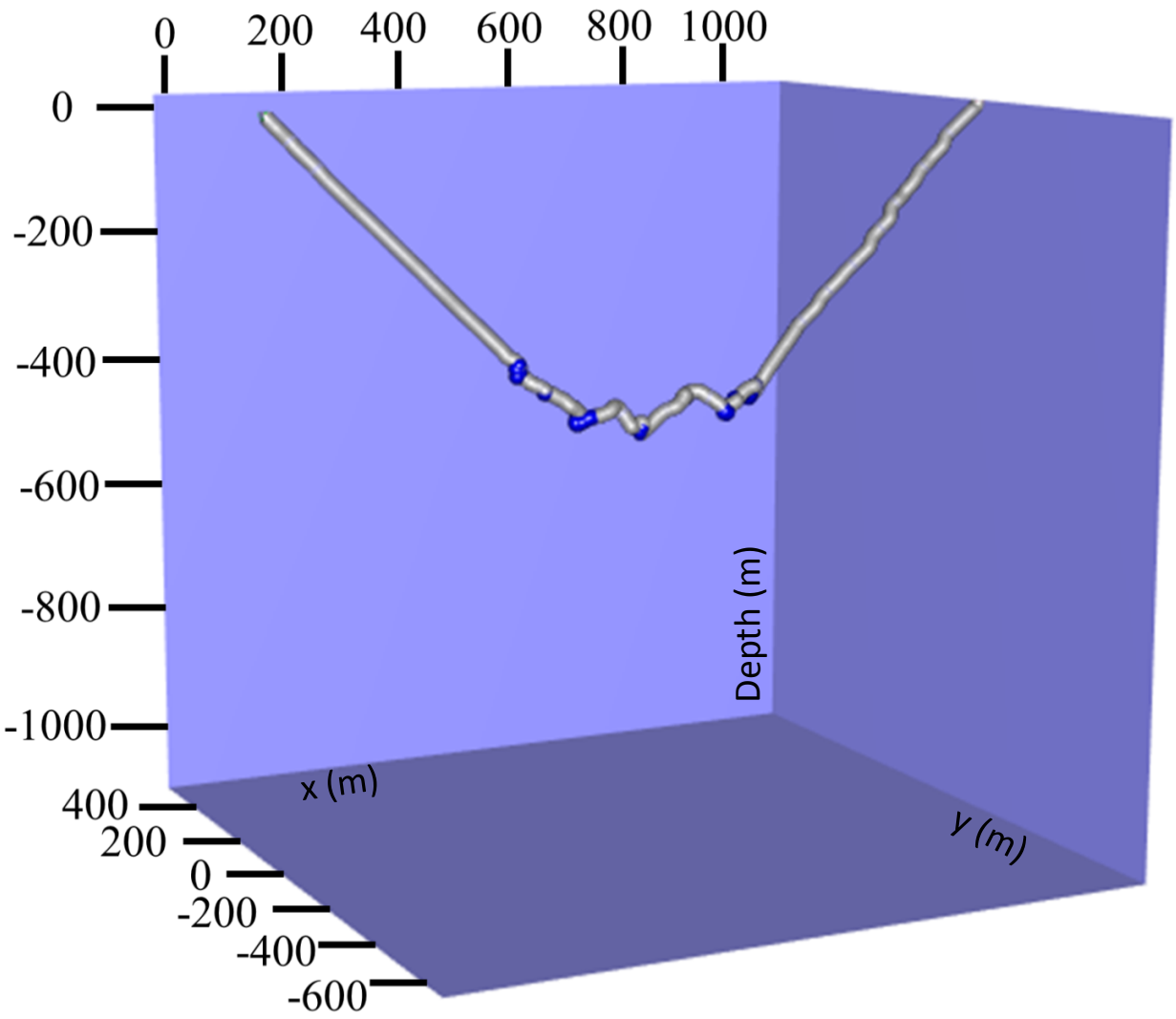

Figure 2.9. Square 3D plot of representative foraging dive, with prey encounters viewed on video highlighted in blue.

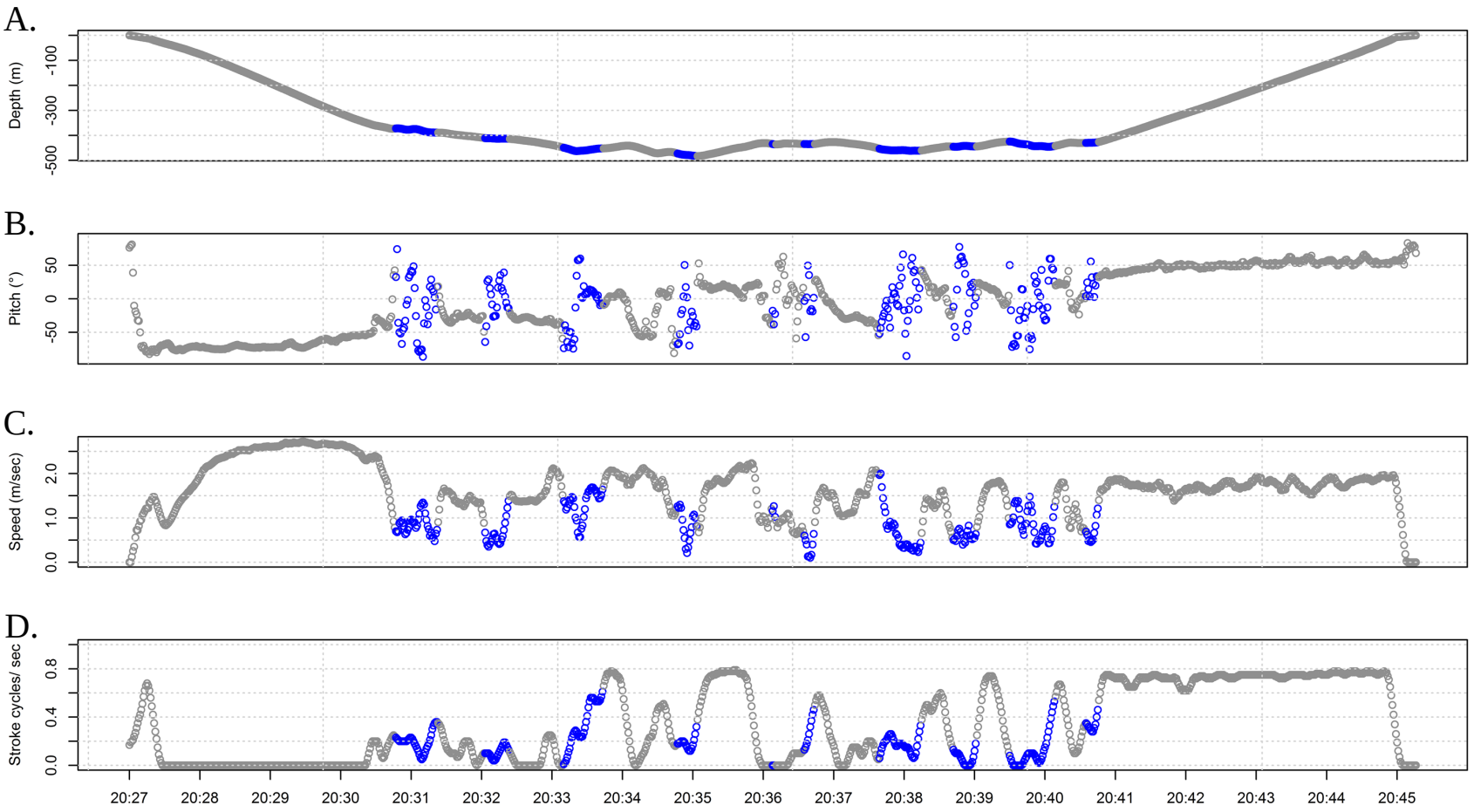

Figure 2.10. A-D. Time series plots of representative foraging dive, with prey encounters viewed on video highlighted in blue.: A. Depth (m), B. Pitch (°), C. Speed (m sec-1), D. Stroking rate (stroke cycles sec-1).

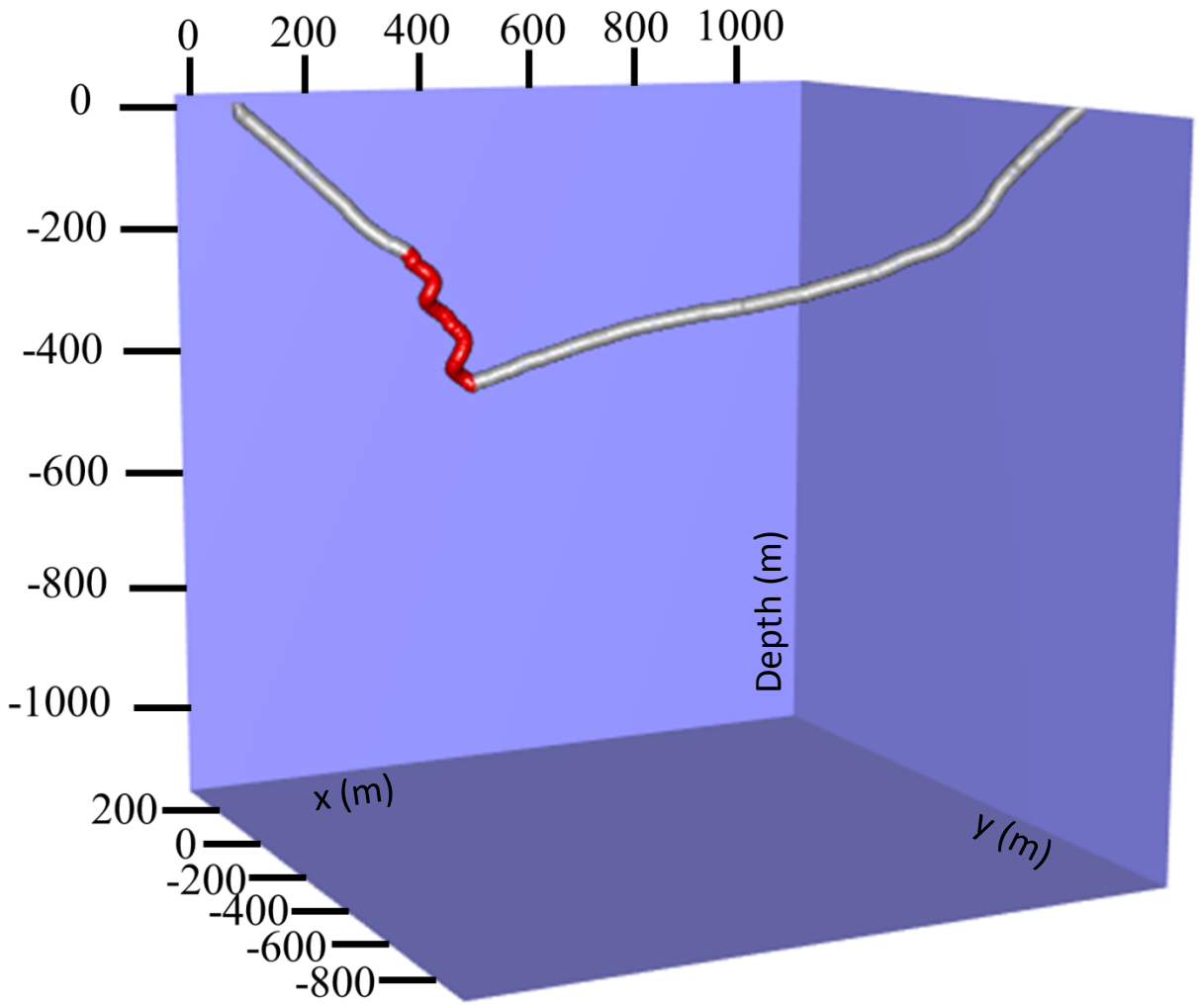

Figure 2.11. Square 3D plot of representative resting dive, with drift phase highlighted in red.

.

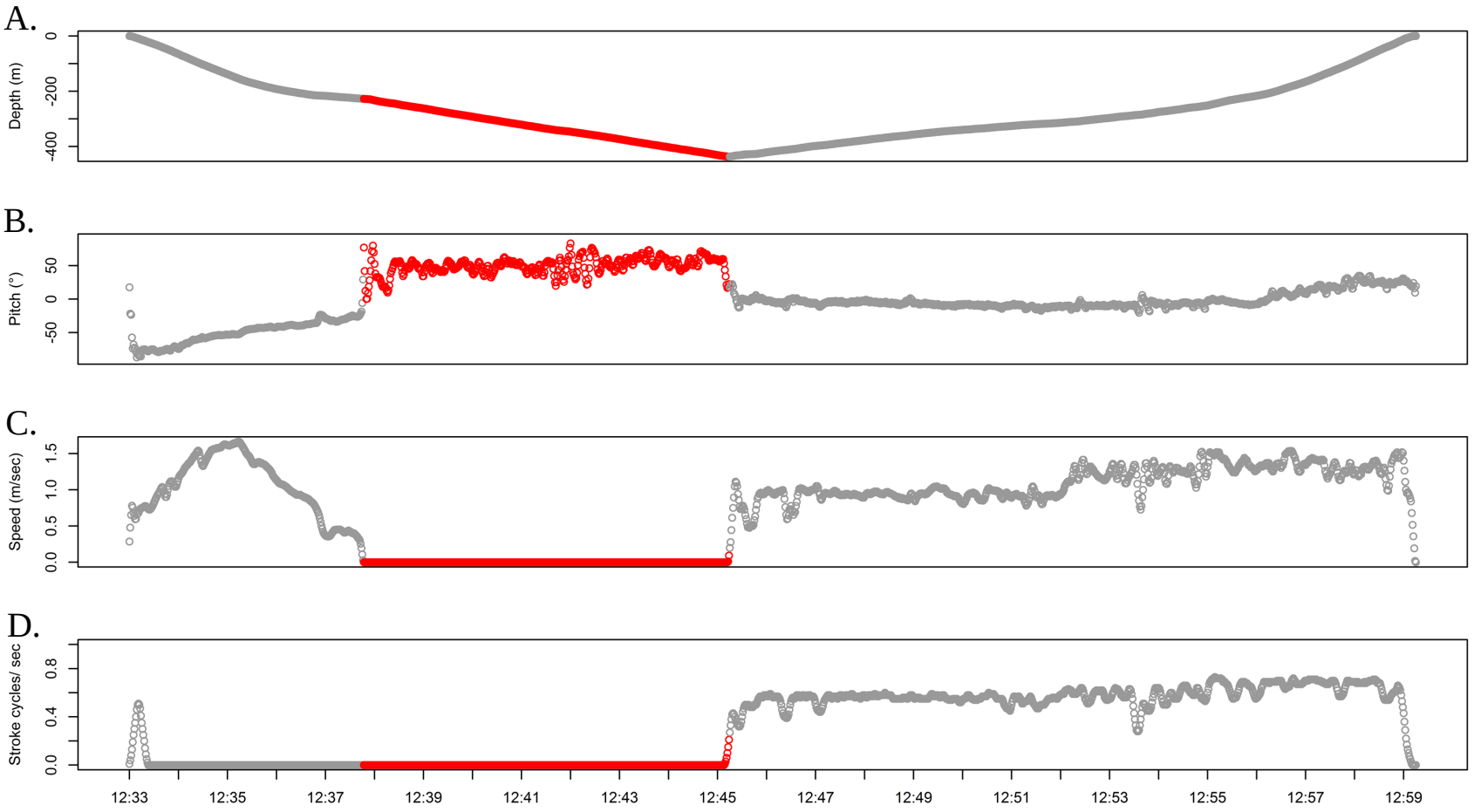

Figure 2.12. A-D. Time series plots of representative resting dive, with drift phase highlighted in red.: A. Depth (m), B. Pitch (°), C. Speed (m sec-1), D. Stroking rate (stroke cycles sec-1).

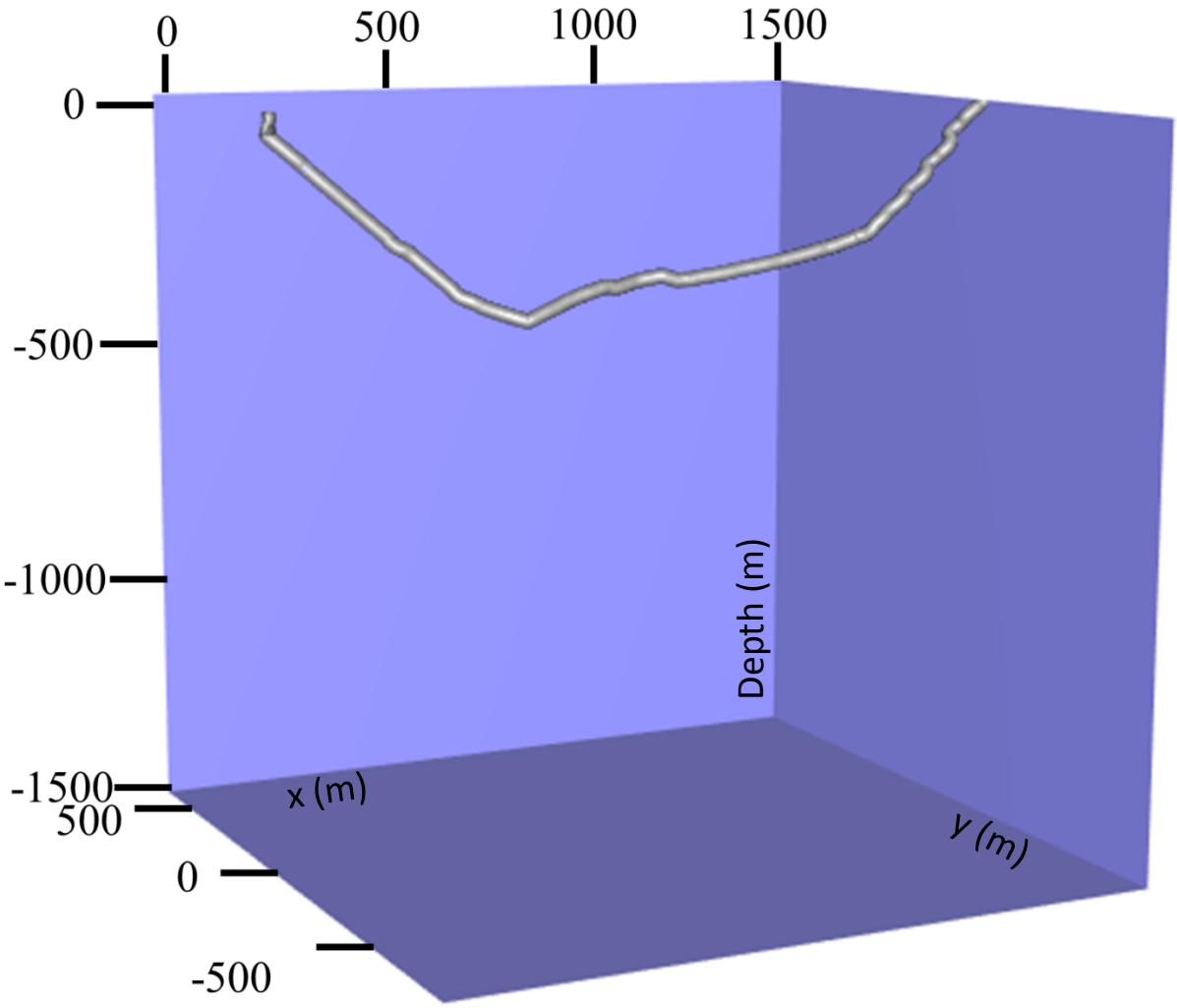

Figure 2.13. Square 3D plot of representative transit dive.

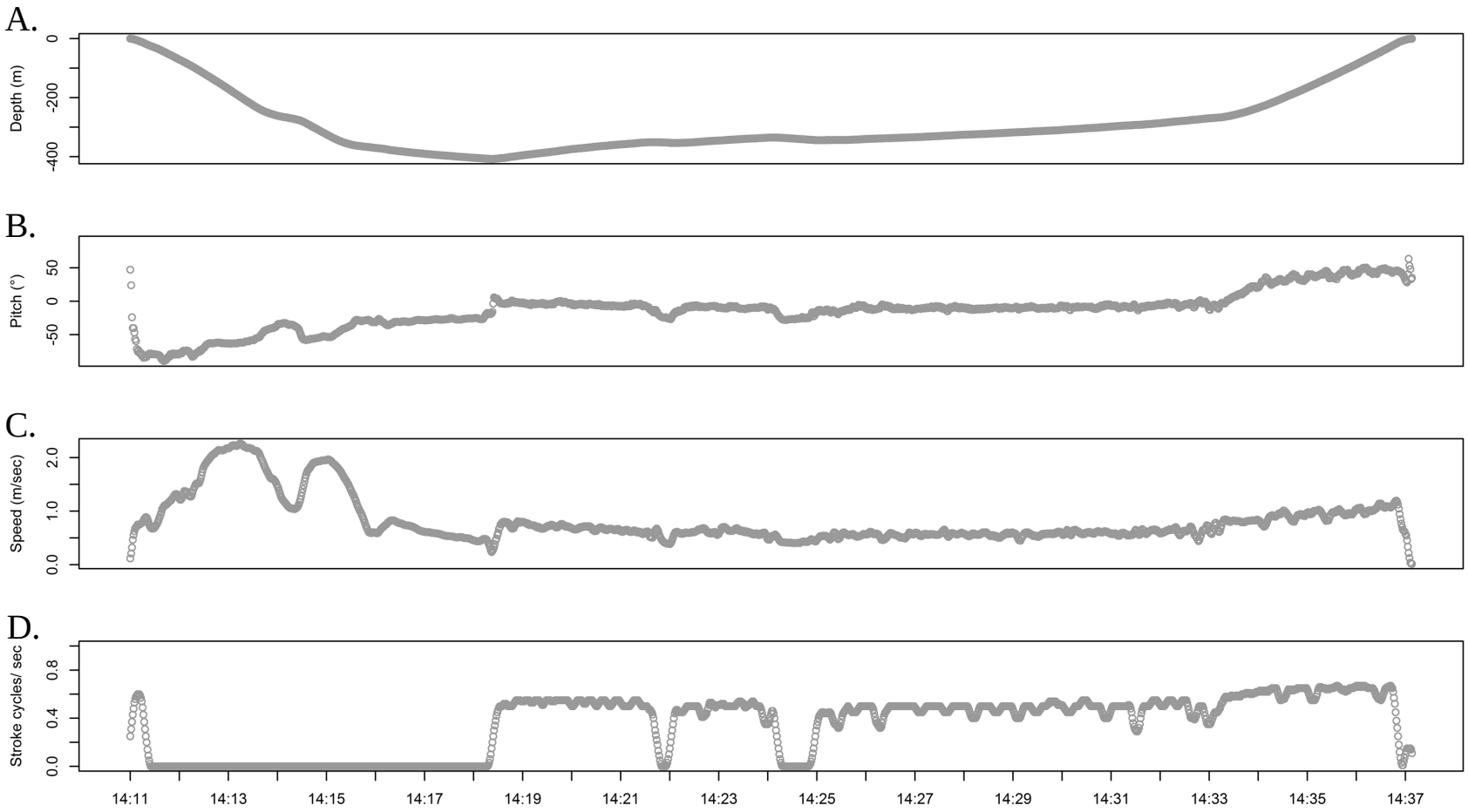

Figure 2.14. A-D. Time series plots of representative transit dive. A. Depth (m), B. Pitch (°), C. Speed (m sec^{-1}), D. Stroking rate (stroke cycles sec^{-1}).

	Foraging		Resting		Transit	
	Mean	SD	Mean	SD	Mean	SD
Maximum depth shelf (m)	96^{A}	8	88^{B}	19	75^{C}	29
Maximum depth slope/ Argentine Basin (m)	553^{A}	258	375^{B}	114	307^{C}	171
Dive duration shelf (min)	13.8^{A}	2.1	17.9^{B}	5.7	13.4^{A}	4.4
Dive duration slope/ Argentine Basin (min)	21.5^{A}	5.8	22.6^{B}	6.2	19.9^{C}	6.6
Total corrected 3D distance (m)	1955^{A}	671	1262^{B}	409	1292^{B}	472
Total corrected horizontal distance (m)	1419^{A}	498	997^{B}	355	1154^{C}	417
Corrected straight line horizontal distance (m)	949^{A}	462	756^{B}	375	1069^{C}	402
Mean Speed (m sec^{-1})	1.19^{A}	0.33	0.62^{B}	0.26	1.25^{C}	0.35
Max Speed (m sec^{-1})	2.57^{A}	0.54	2.02^{B}	0.71	2.11^{C}	0.49
Mean stroking rate bottom (stroke cycles sec^{-1})	0.25^{A}	0.12	0.2^{B}	0.15	0.36^{C}	0.18
Mean stroking rate ascent (stroke cycles sec^{-1})*	0.52^{A}	0.1	0.5^{B}	0.1	0.54^{C}	0.11
Path linearity	0.48^{A}	0.15	0.6^{B}	0.22	0.84^{C}	0.16
Horizontal path linearity	0.65^{A}	0.18	0.74^{B}	0.21	0.92^{C}	0.11
Mean pitch angle descent (°)*	-49.6^{A}	8.8	-11.6^{B}	28.4	-37^{C}	7.5
Mean pitch angle ascent (°)*	43.8^{A}	11.4	29.2^{B}	15.5	22^{C}	16.3
Mean descent speed (m sec^{-1})*	1.38^{A}	0.42	0.66^{B}	0.43	1.16^{C}	0.29
Mean ascent speed (m sec^{-1})*	1.19^{A}	0.26	0.98^{B}	0.29	1.32^{C}	0.33
Mean vertical speed (depth change) descent (m sec^{-1})*	1.28^{A}	0.34	0.67^{B}	0.26	0.76^{C}	0.24
Mean vertical speed (depth change) ascent (m sec^{-1})*	1.27^{A}	0.2	0.84^{B}	0.22	0.75^{C}	0.24
Speed variance	0.24^{A}	0.11	0.26^{B}	0.1	0.13^{C}	0.07
Mean horizontal speed (m sec^{-1})	1.1^{A}	0.27	0.67^{B}	0.18	1.1^{A}	0.33
Horizontal speed variance	0.25^{A}	0.07	0.18^{B}	0.09	0.15^{C}	0.07
Rate of change in z-axis accelerometer	0.05^{A}	0.02	0.03^{B}	0.01	0.02^{C}	0.01
Mean vector length	0.66^{A}	0.14	0.64^{B}	0.2	0.92^{C}	0.09
Pitch angle variance during descent*	461^{A}	251	1243^{B}	883	244^{C}	200

Table 2.6. Descriptive statistics by dive type for all 13797 dives (9453 foraging, 1405 resting, 3039 transit). Mean values with different superscripts are significantly different (Kruskal-Wallis test, post-hoc Mann-Whitney-Wilcoxon pairwise tests with Bonferroni correction).

* Statistics for descent and ascent variables were computed with dives > 5 m in depth; shallower dives were not included.

2.3.3 Comparison of dive types

Almost all dives recorded, regardless of bathymetry or dive type, began with a few strokes proximal to the surface followed by a gliding descent (Figs. 2.9-2.14). No gliding ascents from depth were observed, but data from the final days of the foraging trip was limited to one seal. Seals did glide the final 10-20 m while ascending.

2.3.3.1 Foraging dives

Compared with transit and resting dives, foraging dives (Figs. 2.9, 2.10) were deep and meandering with bursts of speed and rapid changes in pitch and direction associated with prey encounters. The mean maximum dive depth over the slope and Argentine Basin (553 $\pm$ 258 s.d. m) was significantly deeper than resting and transit dives (Table 2.6), with a maximum depth of 1,850 m. The mean dive duration over the slope and Argentine Basin (21.5 $\pm$ 5.8 s.d. min) was significantly longer than transit but not resting dives. When foraging, seals traveled the farthest total and horizontal distances (1,955 $\pm$ 671 s.d. and 1,419 $\pm$ 498 s.d. m, respectively), and their dive paths were less linear with frequent changes in compass bearing. Mean speed (1.2 $\pm$ 0.33 s.d. m sec^{-1}), stroking rate on ascent (0.52 $\pm$ 0.1 s.d. strokes sec^{-1}) and straight-line horizontal distance (949 $\pm$ 462 s.d. m) were all significantly greater than for resting dives but slightly less than for transit dives. Compared to resting and transit dives, foraging dives had greater variation in speed, the highest maximum speed (2.6 $\pm$ 0.54 s.d. m sec^{-1}), the highest mean descent speed (1.38 $\pm$ 0.42 s.d. m sec^{-1}), the steepest descent and ascent angles (-49.6 $\pm$ 8.8 s.d. and 43.8 $\pm$ 11.4 s.d. °, respectively), and greater variation in descent angle and vertical head movements (higher rate-of-change in the z-axis accelerometer) associated with prey pursuit and capture. Due to the steeper descent and ascent angles, foraging dives had the highest mean vertical speed during descent and ascent (1.28 $\pm$ 0.34 s.d. and 1.27 $\pm$ 0.2 s.d. m sec^{-1}, respectively).

A typical foraging dive over deeper water began with the seal descending to a mean maximum depth of 689 meters during the day and 391 meters at night with a steeper descent angle (~50°) than for resting or transit dives. During some foraging dives, the seal glided to the maximum dive depth. During other foraging dives, the seal glided approximately halfway to the maximum dive depth and then continued via stroking and gliding. The descent heading was initially linear, but as the seal began to pursue prey, there were large variations in heading, roll, and pitch accompanied by bursts of speed associated with prey pursuit and capture. Prey encounters were typically associated with torturous paths composed of many twists and turns. The seal typically made short ascents and descents of 10-50 m in the water column between prey encounters.

2.3.3.2 Resting dives

Resting dives (Figs. 2.11, 2.12) included drift dives and dives in which the seals rested on the ocean floor over the continental shelf and slope for prolonged periods. However, during some resting dives, the seals rested intermittently on the order of seconds throughout the dive. Compared to foraging and transit dives, resting dives were longer in duration and had more variation in pitch and roll angle during descent, but distance traveled, swim speed and flipper stroke rate were significantly less than both foraging and transit dives (Table 2.6). The mean maximum depth (375 $\pm$ 114 s.d. m over the slope and Argentine Basin) was deeper than transit dives but shallower than foraging dives. The mean dive duration over the shelf (17.9 $\pm$ 5.7 s.d. min) and in deeper water (22.6 $\pm$ 6.2 s.d. min) was significantly longer than both foraging and transit dives. During resting dives, seals traveled the shortest straight line and total horizontal distances (997 $\pm$ 355 s.d. and 756 $\pm$ 375 s.d. m, respectively), and their dive paths were less linear with more variation in compass bearing than transit dives. Mean descent angle (-11.6 $\pm$

28.4 s.d. °) was less steep than both foraging and transit dives. Mean speed (0.62 ± 0.26 s.d. m sec^{-1}), mean maximum speed (2.02 ± 0.71 s.d. m sec^{-1}), mean descent and ascent speeds (0.66 ± 0.43 s.d. and 0.98 ± 0.29 s.d. m sec^{-1}), and mean vertical speed during descent (0.67 ± 0.26 s.d. m sec^{-1}) were significantly less than for foraging and transit dives.

A typical resting dive over the shelf involved gliding to the ocean floor and resting for approximately six minutes. The seal began the descent with a few strokes. During most resting dives, the seal was stationary for an extended period, but there were some dives in which the seal rested intermittently for 10-120 sec at a time over the course of the dive. In resting dives over the deeper water of the slope and Argentine Basin, seals typically glided to 100-200 m with a pitch angle of -48.2 ± 15.9 s.d. ° before beginning the drift portion of the dive. As they drifted, the roll angle increased to 150-180°, indicating that the seal was drifting belly-up and vertically downward. Under these conditions, the speed sensors recorded zero speed because the downward drift was perpendicular to the sensor. The average amount of time per resting dive where speed was equal to zero was 6.7 ± 4.5 s.d. min. There were a few resting dives recorded over the slope (depth < 500 m) in which the seal glided to the ocean floor and rested on the bottom instead of drifting, similar to how the seals rested on the shelf.

2.3.3.3 Transit dives

Compared to foraging and resting dives, transit (Figs. 2.13, 2.14) dives were shallow, shorter in duration and very linear with little change in compass bearing. Seals glided to maximum depth and then either stroked continuously or used a stroke-and-glide mode of locomotion. Because the continental shelf along Península Valdés is less than 120 m deep, the depth of transit dives over the shelf were shallow (mean depth 75 ± 29 s.d. m). One seal had approximately 150 shallow dives of only a few meters in depth (mean 2 m, mean 5.9 min duration). With those dives

removed, mean transit dive duration was 14.6 ± 4.4 s.d. min and mean transit dive depth was 82.3 ± 20.5 s.d. m over the shelf.

Transit dives that occurred over the slope and in the Argentine basin were deeper (mean maximum depth 307 ± 171 s.d. m) than transit dives over the shelf but shallower than deep water foraging and resting dives. Transit dives had a more linear path (mean vector length of 0.87 where 1 = highly directional, 0=not directional) than foraging (0.66) and resting (0.59) dives, but were slightly less directional than transit dives over the shelf (0.94). Seals glided to maximum depth and then either began to ascend or continued to swim at depth using stroke-and-glide locomotion before ascending using continuous stroking. The mean speed of transit dives over deep water was not as fast as those over the shelf (0.98 m sec^{-1} and 1.42 m sec^{-1}, respectively) and also not as fast as foraging dives over deep water (1.19 m sec^{-1}), but faster than resting dives (0.57 m sec^{-1}). Some transit dives were deeper than average and had a time-depth profile with some vertical excursions (10-50 meters) that may have been associated with searching behavior. The mean duration of these dives (19.9 ± 6.6 s.d. min) was shorter than both resting and foraging dives, in part because of a higher mean speed (1.25 ± 0.35 s.d.. m $sec^{-}1$) and mean flipper stroke rate during both bottom swimming and ascent (0.36 ± 0.18 and 0.54 ± 0.11 s.d. strokes sec^{-1}, respectively; Table 2.6) which depletes body oxygen stores more quickly and reduces the aerobic dive limit. However, the longest dive recorded (70.1 min in duration) was a transit dive which had a mean speed of 0.44 m sec^{-1} with a mean stroke frequency of 0.15 strokes sec^{-1} at the bottom of the dive. Transit dives were the most linear with little variation in compass bearing, speed, and roll and pitch angles. Mean descent angle (-37 ± 7.5 s.d. °) was less steep than for foraging dives, and mean ascent angle (22 ± 16.3 s.d. °) was less steep than both resting and foraging dives. As a result, transit dives had lower mean vertical speed during descent and ascent

(0.76 ± 0.24 s.d. and 0.75 ± 0.24 s.d. m sec^{-1}). In addition, because they were shorter in duration than foraging dives, total (1,292 ± 472 s.d. m) and horizontal distances (1,154 ± 417 s.d. m) traveled were less, but straight line distance (1,069 ± 402 s.d. m) was the highest due to their linearity.

2.3.4 Identification of foraging events

The final prey encounter algorithm used two variables: the rate of change in the z-axis accelerometer (calculated in 16 Hz, subsampled to 1 Hz) and the rate of change in heading (in 1 Hz), both smoothed with a running 10-point average. The cutoff values were 0.035 and 0.16, respectively. This algorithm was chosen because it had a sensitivity of 95% (detected 95% of video-recorded prey encounters; 5% of video-recorded events were not detected by the algorithm) and a specificity of 94% (94% of detected events occurred during a definite or probable video-recorded prey encounter; 6% of detected events were false positives). In total, 32,367 prey encounters were identified. Of these, 31,552 (97.5%) occurred during foraging dives, 268 (0.8%) occurred during resting dives, and 547 (1.7%) occurred during transit dives. Prey encounters were detected during 9,503 dives. At least one encounter was detected in 96.4% of all foraging dives (9,013 of 9,353 dives), 8.8% of resting dives (123 of 1,405 dives), and 12% of transit dives (373 of 3,039 dives).

The mean number of prey encounters for foraging dives was 3.4 ± 2.1 s.d. (range 0-19), and the mean duration of an encounter was 28 ± 19.3 s.d. sec (range 1-207 sec). The combined duration of all prey encounters for foraging dives (an index of foraging success) was 97 ± 65 s.d. sec over the slope (range 0-465 sec) and 95 ± 59 s.d. sec over deep water (range 0-344 sec, Fig. 2.15). Using this index for foraging success, which did not consider dive duration, day dives were significantly more successful than night dives and dusk dives were significantly more

successful than day dives over the slope. Over deep water, this index indicated that both dusk and night dives were significantly more successful than day dives (Table 2.7). When dive duration was taken into consideration (dividing the cumulative duration of prey encounters by dive duration), foraging dives during dawn, dusk, and night were significantly more successful (more prey encounters per unit time) than foraging dives during the day over both the slope and deep water (all adjusted p-values <0.01) (Table 2.8).

		Mean	SD	SE	CI (95%)	Min	Max	Median
Slope	All	97	65	1.5	2.9	0	465	86
	Dawn	96^{AB}	58	4.0	7.9	0	267	88
	Day	99^{A}	69	2.1	4.1	0	465	87
	Dusk	102^{B}	64	6.7	13.2	0	286	94
	Night	92^{B}	58	2.5	4.9	0	296	83
Deep water	All	95	59	0.7	1.3	0	344	87
	Dawn	98^{AB}	61	2.0	3.9	0	312	90
	Day	93^{A}	57	0.9	1.8	0	336	85
	Dusk	101^{B}	55	2.8	5.6	0	342	95
	Night	98^{B}	60	1.3	2.5	0	344	90

Table 2.7. Raw foraging success. Cumulative prey encounter duration in seconds for foraging dives over the continental slope and in deep water. Different subscripts indicate significantly different mean values (Kruskal-Wallis test, post-hoc Wilcoxon-Mann Whitney with Bonferonni correction).

		Mean	SD	SE	CI (95%)	Min	Max	Median
Slope	All	0.131	0.098	0.002	0.004	0.000	1.000	0.114
	Dawn	0.155^{A}	0.103	0.007	0.014	0.000	0.564	0.126
	Day	0.122^{B}	0.099	0.003	0.006	0.000	1.000	0.106
	Dusk	0.155^{A}	0.102	0.011	0.021	0.000	0.489	0.131
	Night	0.136^{A}	0.092	0.004	0.008	0.000	0.473	0.122
Deep water	All	0.14	0.09	0.00	0.00	0.00	0.71	0.12
	Dawn	0.17^{A}	0.11	0.00	0.01	0.00	0.68	0.15
	Day	0.12^{B}	0.07	0.00	0.00	0.00	0.51	0.10
	Dusk	0.16^{A}	0.09	0.00	0.01	0.00	0.56	0.15
	Night	0.17^{A}	0.11	0.00	0.00	0.00	0.71	0.15

Table 2.8. Adjusted foraging success. Cumulative prey encounter duration divided by dive duration in foraging dives over the continental slope and in deep water (normalized to range 0-1). Different subscripts indicate significantly different mean values (Kruskal-Wallis test, post-hoc Wilcoxon-Mann Whitney with Bonferonni correction).

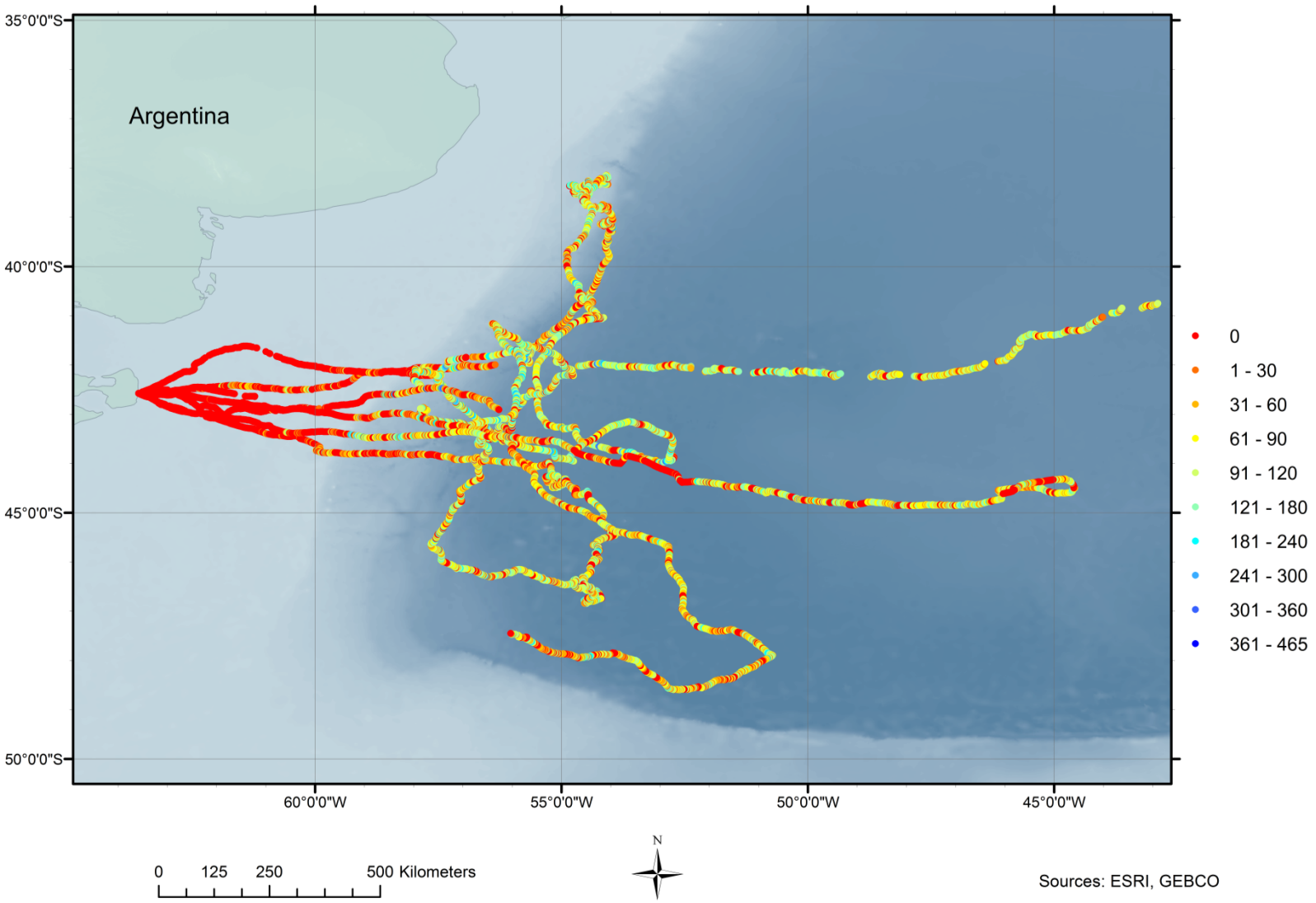

Figure 2.15. Corrected seal locations colored by number of cumulative prey encounter seconds.

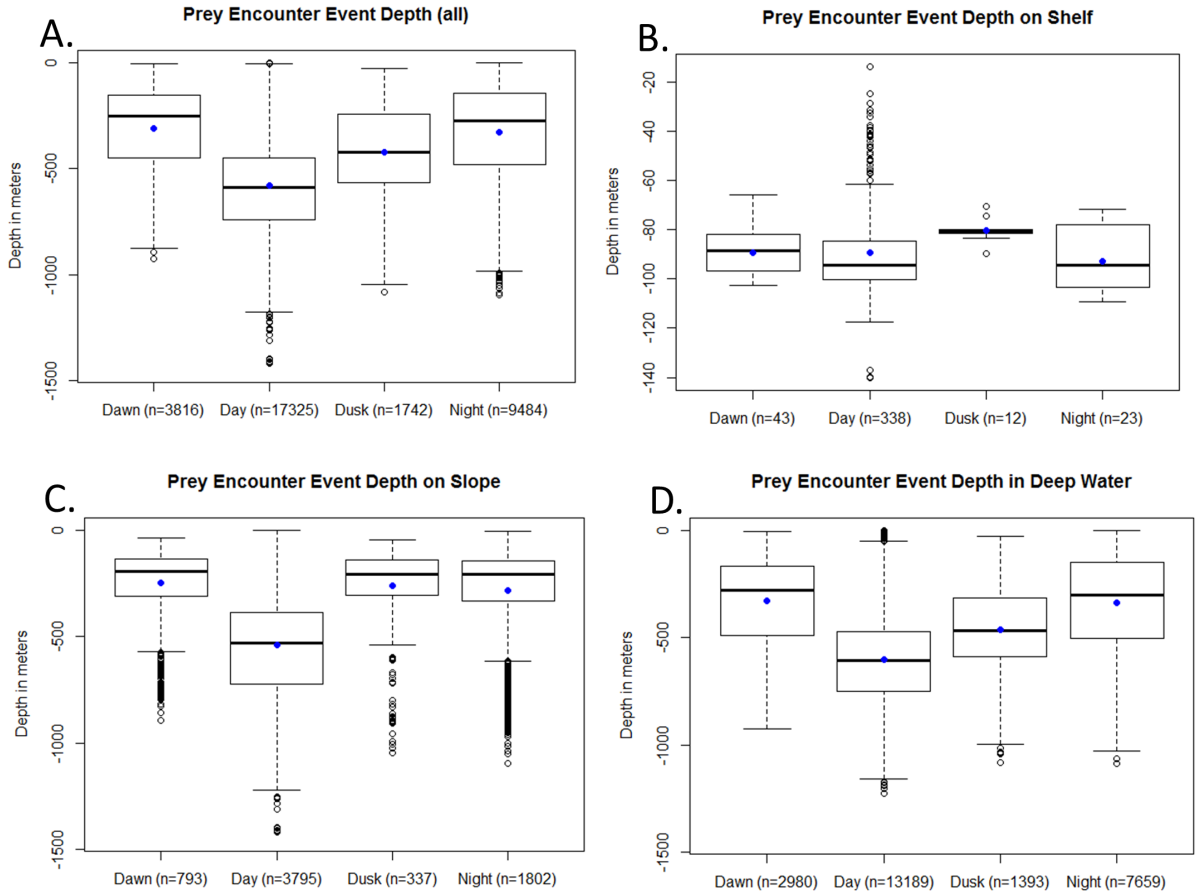

Figure 2.16. Boxplots of mean depth of detected prey encounters in foraging dives by time of day for A. all dives, B. dives over the continental shelf, C. dives over the continental slope, and D. deep water dives. Mean values are displayed in blue.

		Mean	SD	SE	CI (95%)	Min	Max	Median
Slope	All	431	258	3.2	6.3	1	1419	403
	Dawn	249^{A}	177	6.3	12.4	33	892	192
	Day	539^{B}	232	3.8	7.4	1	1419	528
	Dusk	262^{AC}	196	10.7	21.0	46	1045	205
	Night	285^{C}	220	5.2	10.2	2	1096	207
Deep water	All	483	244	1.5	3.0	0	1227	497
	Dawn	327^{A}	201	3.7	7.2	4	925	276
	Day	603^{B}	202	1.8	3.4	1	1227	607
	Dusk	462^{C}	193	5.2	10.1	28	1082	466
	Night	336^{A}	217	2.5	4.9	0	1088	300

Table 2.9. Mean depth (m) for prey encounters over the continental slope and in deep water by time of day. Significantly different means are denoted by different superscripts (Kruskal-Wallis test, post-hoc Mann-Whitney-Wilcoxon pairwise tests with Bonferroni correction).

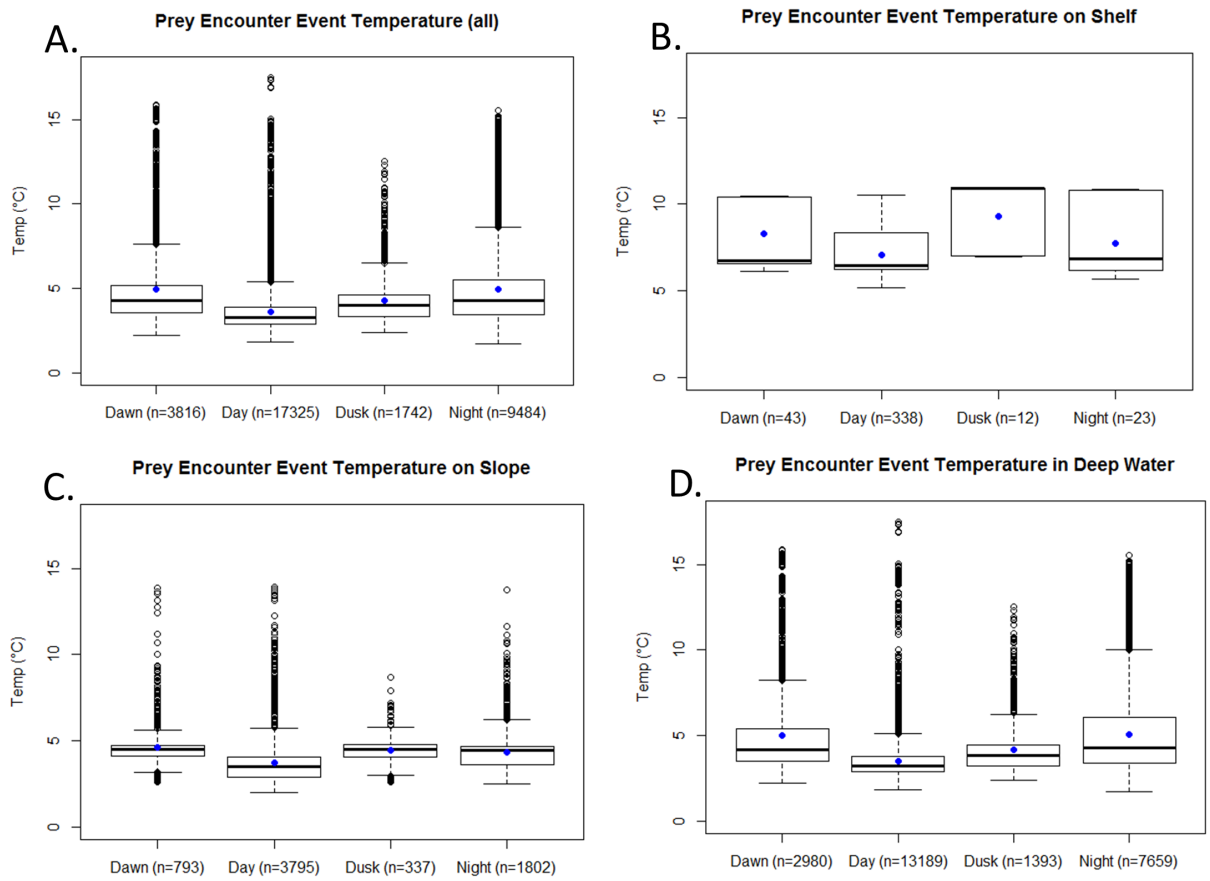

Figure 2.17. Boxplots of mean temperature of detected prey encounters in foraging dives by time of day for A. all dives, B. dives over the continental shelf, C. dives over the continental slope, and D. deep water dives. Mean values are displayed in blue.

		Mean	SD	SE	CI (95%)	Min	Max	Median
Slope	All	4.0	1.3	0.02	0.03	2.0	13.9	3.8
	Dawn	4.6	1.5	0.05	0.11	2.6	13.9	4.5
	Day	3.7	1.3	0.02	0.04	2.0	13.9	3.5
	Dusk	4.4	0.9	0.05	0.09	2.6	8.7	4.5
	Night	4.3	1.2	0.03	0.06	2.5	13.8	4.4
Deep water	All	4.2	1.9	0.01	0.02	1.7	17.5	3.6
	Dawn	5.0	2.5	0.05	0.09	2.2	15.9	4.1
	Day	3.5	1.1	0.01	0.02	1.8	17.5	3.2
	Dusk	4.2	1.5	0.04	0.08	2.4	12.5	3.9
	Night	5.1	2.4	0.03	0.05	1.7	15.6	4.3

Table 2.10. Mean temperature (° C) for prey encounters over the continental slope and in deep water by time of day.

The mean prey encounter depths over the slope and Argentine Basin were 431 ± 258 s.d. m and 483 ± 244 s.d. m, respectively. Kruskal Wallis tests indicated that there were significant differences in mean depth of prey encounters by time of day over both the slope and deep water (p-value <0.0001 for both). Post-hoc comparisons were made with the Mann-Whitney-Wilcoxon test with a Bonferroni correction. Over the slope, mean prey encounter depth was significantly deeper during the day (539 ± 232 s.d. m) than during dusk, night, and dawn (262 ± 196 s.d. m, 285 ± 220 s.d. m, and 249 ± 177 s.d., m respectively). Mean prey encounter depth at dawn was significantly shallower than at dusk (Fig. 2.16, Table 2.9). Over the deep water of the Argentine basin, mean prey encounter depth was significantly shallower during dusk, night, and dawn (462 ± 193 s.d. m, 336 ± 217 s.d. m, and 327 ± 201 s.d. m, respectively) than during day (603 ± 202 s.d. m). Mean prey encounter depth was significantly deeper at dusk than dawn or night (Fig. 2.16, Table 2.9). Mean prey encounter temperature was 4 ± 1.3 s.d. °C (range 2-13.9°C) over the slope and 4.2 ± 1.9 s.d. °C in deep water (range 1.7-17.5°C) (Fig. 2.17, Table 2.10).

2.3.5 First-passage time analysis

Dive locations for two VDRs that recorded for the majority of the foraging trip were used to conduct first-passage time analysis. Peak variance occurred at a radius of 45 kilometers, indicating that two-dimensional movement patterns occurred on a scale of approximately 45 km over the course of the foraging trip (Fig. 2.18). Spherical first-time passage analysis was conducted using the corrected three-dimensional locations at a resolution of 1 Hz from all seals. Mean peak variance occurred at a radius of 10 meters, indicating that movement patterns in the three-dimensional trajectory of individual dives occurred on a scale of approximately 10 m (Fig. 2.19).

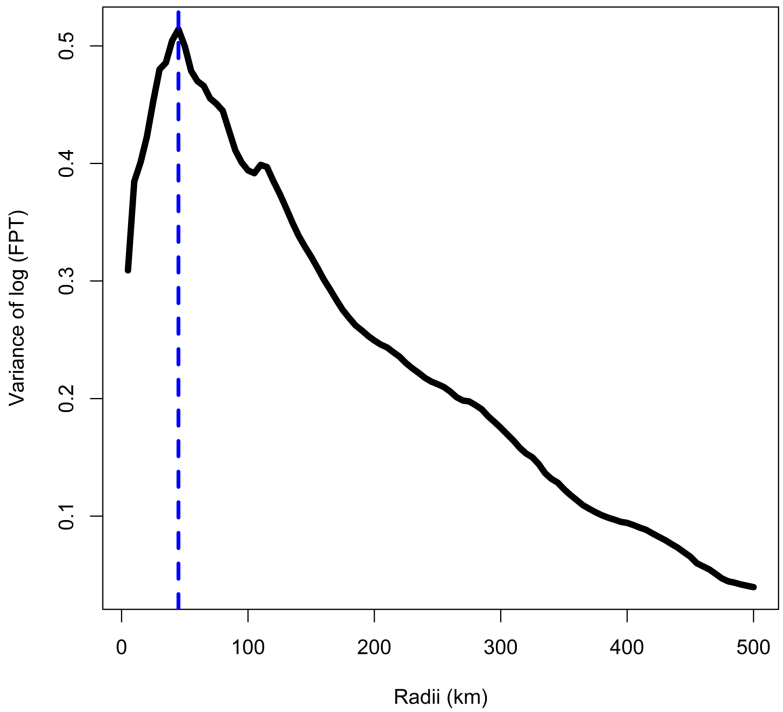

Figure 2.18. First passage time (horizontal, 2D) averaged for two seals for which data recorded for the majority of the migration.

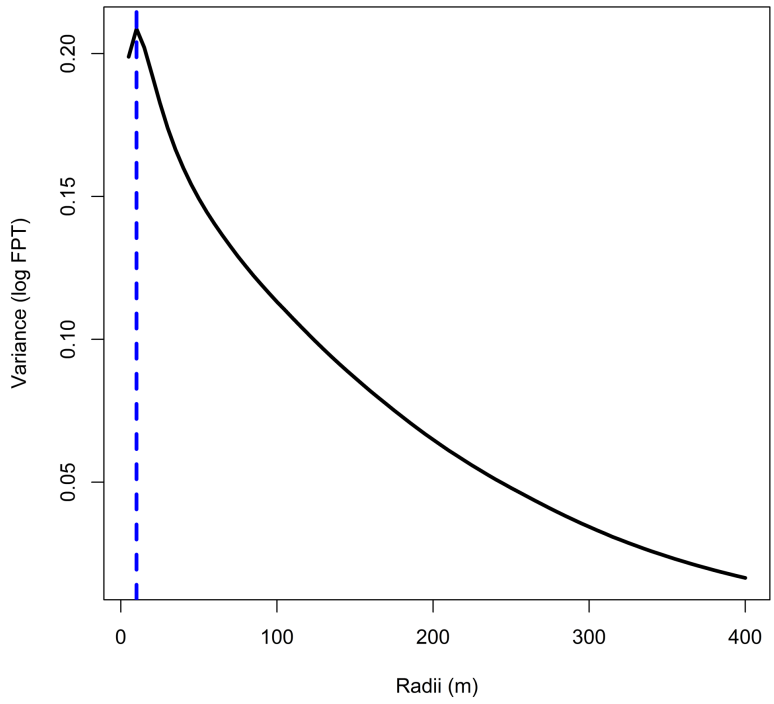

Figure 2.19. Mean spherical first passage time averaged for all 8 seals.

2.4 Discussion

This study reports herring smelt as a prey item of southern elephant seals. Herring smelt are generally known to occur further north, but there are reports of larval Argentinidae occurring near Islas Malvinas (Falkland Islands) (Ehrlich et al., 1999; Richards, 2005). Myctophids have previously been reported as prey using stomach lavage on Macquarie Island (Field et al., 2007; Green and Burton, 1993; Slip, 1995), as well as for northern elephant seals based on still images obtained with animal-borne cameras (Naito et al., 2013). Although southern elephant seals may feed on both fish and squid, only fish were observed in the video during this study. Rodhouse et al. (1992) noted that cephalopod beaks are less digestible than fish bones and may accrue in the stomach, biasing diet composition estimation. It is therefore possible that cephalopods do not comprise as great a proportion of the diet of the southern elephant seal as assumed, at least in the Península Valdés population. Although confirmed prey species of southern elephant seals also include members of Families Bathylagidae, Centrolophidae, Channichthyidae, Gempylidae, Nototheniidae, Paralepididae, and Phosichthyidae (Field et al., 2007; Green and Burton, 1993; Laws, 1956; Slip, 1995), no representatives from these families were identified on the video records. However, species identification was not possible for many of the prey encounters. Another limiting factor was that much of the video of prey encounters was obtained over the continental slope and not over the deeper water of the Argentine Basin where the majority of foraging dives occurred. Hence, further research is warranted.

Previous studies of female elephant seals from Península Valdés reported no resting dives over the continental shelf (Campagna et al., 1995). In this study, all resting dives observed over the shelf involved gliding to the seafloor and then remaining stationary. Because previous research relied on time-depth recorders, which do not record speed or accelerometry (Campagna

et al., 1995; Campagna et al., 1998; Campagna et al., 2000), this resting behavior may not have been detected or confused with swimming along the seafloor (i.e., a typical, square-bottomed transit dive). This study described resting on the seafloor by southern elephant seals. It is unknown why they do not commence resting at the surface, but avoiding predators such as killer whales, which are in this area, may be an explanation.

Our observation of little to no foraging on the shelf is consistent with previous reports for females from this colony and with reports for post-breeding females from the Kerguelen Islands, Macquarie Island, and South Georgia (Campagna et al., 1995; Hindell et al., 2016; Labrousse et al., 2015). This is in contrast to post-breeding females from the Antarctic Peninsula that mainly forage on the continental shelf.

The time to cross the shelf was consistent with previous reports for post-breeding females from Península Valdés (Campagna et al., 1998). Over the continental shelf, dive durations for all dive types were shorter than over deep water, consistent with previous reports (Campagna et al., 1995; Campagna et al., 1998). The majority of dives over the shelf were transit dives, which in this study had faster mean speeds and higher mean stroke rates. Crocker et al. (1994) hypothesized that northern elephant seals may maximize travel velocity to the detriment of dive duration to avoid predation by white sharks in shallower waters. Previous studies of females from Península Valdés indicated a mean dive duration of 12.7 min over the shelf and 23.4 minutes over deep water (Campagna et al., 1995). These are similar to the overall mean dive durations observed in this study: 14 $\pm$ 4.8 s.d. min over the shelf and 21.4 $\pm$ 6 s.d. min over deep water.

Once off the continental shelf and over the continental slope, some seals began to engage in foraging dives, while other seals continued to transit for a day or two (foraging sporadically)

before beginning to intensely forage. Some exhibited clear, area-restricted searching from the satellite tracks at the surface. However, other seals foraged just as intensively while continuing to move away from the rookery with no apparent area-restricted search behavior.

A diel pattern was present in dives over the continental slope and Argentine Basin, consistent with known information about southern elephant seals diving in deep water (Campagna et al., 1998; Hindell et al., 2016; McIntyre et al., 2011; McIntyre et al., 2010; Vacquié-Garcia et al., 2015). Although this pattern is consistent with feeding on the deep scattering layer, its presence during transit and resting dives was unexpected and may be associated with predator avoidance.

The steeper descent angle and deeper depth during foraging dives suggests that the seals were preparing for a specific depth and/or a specific dive type as soon as they began descending. There was a moderate correlation between maximum dive depth and descent angle (Pearson's correlation coefficient = 0.53, p-value <0.0001). In a study of free-range dives of Weddell seals (*Leptonychotes weddellii*), foraging dives were also deeper, covered the longest distance, and had steeper ascent and descent angles (Davis et al., 2013), consistent with deep-living prey.

The seals glided during descent for all dive types. A model of the energetic cost of transit and foraging dives in northern elephant seals indicated that gliding to depth in deep foraging dives is cost-effective and saves energy. This model also indicated that an ascent speed of 1.2 m sec^{-1} was the optimal speed for both deep and flat-bottom foraging dives (~ 400 m in depth) in which a gliding descent is performed. For deep foraging dives, this speed is the best compromise between minimizing the cost of ascent and maximizing dive duration. For flat-bottomed foraging dives, this ascent speed combined with a gliding descent increases the aerobic dive limit by up to 1.8 minutes when compared to continuous stroking. This estimate of 1.2 m sec^{-1} is an exact

match for the mean speed of foraging dives over deep water in this study (Davis and Weihs, 2007).

The shallower ascent angle during transit dives (22°) was consistent with optimal ascent angle estimates from Davis and Weih's (2007) model. The model indicated that maximum horizontal displacement occurs at ascent angles of 20-30°. The model also plotted maximum depth of transit dives as a function of ascent angle, and projected a maximum dive depth of ~275-350 m for transit dives with ascent angles of 20-30°. Mean maximum depth of deep-water transit dives in this study was 307 m, falling within the projected range. The speed chosen for modeling the transit dives (1.2 m sec^{-1}) was similar to the 1.25 m sec^{-1} mean for transit dives in this study. One interesting thing the model determined was that there is little savings in energetic cost compared to subsurface swimming if the primary purpose of the dive is transit. This suggests that there may be other factors at play here (e.g., predator avoidance).

Previous studies indicated that Marion Island females dive deeper than southern elephant seal females from other colonies (McIntyre et al., 2011). The mean maximum depths for the Península Valdés population included dives over the shelf. Marion Island is surrounded by deep water (Mcintyre et al., 2012), and thus this may not be a realistic comparison. Dive depths of Península Valdés females that occurred solely over the slope and deep water overlap with those of Marion Island females. During the daytime, dive depths of Marion Island and Península Valdés females were 517.8 $\pm$ 162.9 s.d. m and 608 $\pm$ 240 s.d., respectively. At night, dive depths were very similar for the two populations, with Marion Island females diving to 359 $\pm$ 142.5 s.d. m and Península Valdés females diving to 370 $\pm$ 213 s.d. m. These values were also similar to Kerguelen post-breeding females when only dives in water >1000 m are considered: daytime dive depth of 519.2 $\pm$ 208.3 s.d. m and nighttime dive depth of 384.4 $\pm$ 199.2 s.d. m (Guinet et

al., 2014). These data indicate that these females are all foraging on prey in the deep scattering layer, which appears to occur at similar depths across the foraging ranges of these seals.

Over the deeper waters of the continental slope and Argentine Basin, females showed a temporal pattern in dive type, with resting dives occurring more frequently during daylight hours. According to optimal foraging theory, marine mammals should minimize the cost of transport to their foraging locations (Crocker et al., 2001). Horizontally, the southern elephant seal females travel thousands of kilometers during their foraging trips. However, they may reduce the cost of transport vertically by saving energy during peak daytime hours, when prey are the deepest, using that time to rest, then increase foraging frequency when prey moves closer to the surface. An index for foraging success, the fraction of each dive associated with prey encounters, indicated that foraging dives during the day were significantly less successful than during dusk, night, and dawn over both the continental slope and the Argentine Basin. Research on the foraging behavior of Kerguelen Island females indicates that they forage more efficiently at night versus during the day; however, the authors did not suggest that the seals fed preferentially at night (Guinet et al., 2014). A large proportion of southern elephant seal tagging studies have used satellite-relay data loggers (SRDLs). The resolution of the data uplinked by these tags may be insufficient to reliably identify drift dives (McIntyre et al., 2011), and therefore it is unknown whether any temporal pattern that was present would have been detected.

The spherical first-time passage analysis indicated that three-dimensional movements occur on a scale of approximately 10 m. This is very similar to the only other known application of spherical first-time passage analysis based on data from northern elephant seals. That analysis found the highest variance at 8 m and a second smaller peak at 17 m (Adachi et al., 2017).

In summary, this study both confirmed some previously known information and provided some new insights into the post-breeding foraging trips of female southern elephant seals from the Península Valdés colony. Females from this colony rapidly transit the continental shelf to forage over the continental slope and Argentine Basin, and once in deep water, they exhibit a diurnal diving pattern. The diel pattern applies not only to foraging dives, but to resting and transit dives as well, suggesting that another factor besides feeding on the deep scattering layer may be at play, such as predator avoidance. The seals conserve energy through varied means during their foraging trip. Their mean ascent swim speed of 1.2 m sec^{-1} during foraging dives is the optimal speed identified for energy savings in a northern elephant seal model. Their mean ascent angle of 22° for transit dives falls into the optimal range of 20-30° identified as covering the most distance for the least cost. Seals minimize the cost of transport to foraging grounds vertically by resting more during the day, when prey are further from the surface and when foraging dives are significantly less successful. By combining video and movement data, this study was able to categorize dives without video and identify prey encounters with 95% success using data from two sensors, the magnetometer and accelerometer. More research is needed to determine whether further refinement of dive type classification is possible, i.e. separating transit dives from searching dives, and to determine prey preference over deep water.

3. HABITAT ASSOCIATIONS OF FEMALE SOUTHERN ELEPHANT SEALS (*Mirounga leonina*) FROM PENÍNSULA VALDÉS, ARGENTINA

3.1 Introduction

Southern elephant seals (*Mirounga leonina*) are wide-ranging predators that make a post-breeding foraging trip of two months and a post-molt foraging trip of seven months (Campagna et al., 1999; Hindell et al., 2016; Lewis et al., 2006) While at sea, the distribution of southern elephant seals, like many apex marine predators, is often associated with oceanographic features (Campagna et al., 2006; Campagna et al., 2000; Cotté et al., 2015). This is thought to be a consequence of the enhanced productivity that is often linked with these features, which results in an accumulation of primary, secondary, and tertiary consumers through a trophic food web (Ballance et al., 2006; Simmons et al., 2007).

Female southern elephant seals from the Península Valdés, Argentina colony are known to forage along the Patagonian continental shelf break and in the Argentine Basin (Fig. 3.1) (Campagna et al., 1995; Campagna et al., 1998). At the shelf-break, the Malvinas Current, carrying cold sub-Antarctic water north from the Antarctic Circumpolar Current, meets the low-salinity shelf water, which is freshened by discharges from the Magellan Strait to the south (Charo and Martinez, 2000; Jullion et al., 2010; Matano et al., 2010; Palma et al., 2008). This front is associated with temperature and salinity gradients and increased primary productivity (Campagna et al., 2000; Romero et al., 2006a). In the Argentine Basin, cold, relatively fresh water from the Malvinas Current and warm, salty subtropical water from the Brazil Current collide to produce the Brazil-Malvinas Confluence (Fig. 1.2), one of the most energetic regions of the world ocean. The Brazil-Malvinas Confluence is characterized by increased primary

productivity, large temperature gradients, and intense mesoscale eddy activity (Acha et al., 2004; Jullion et al., 2010; Legeckis and Gordon, 1982; Piola and Matano, 2001).

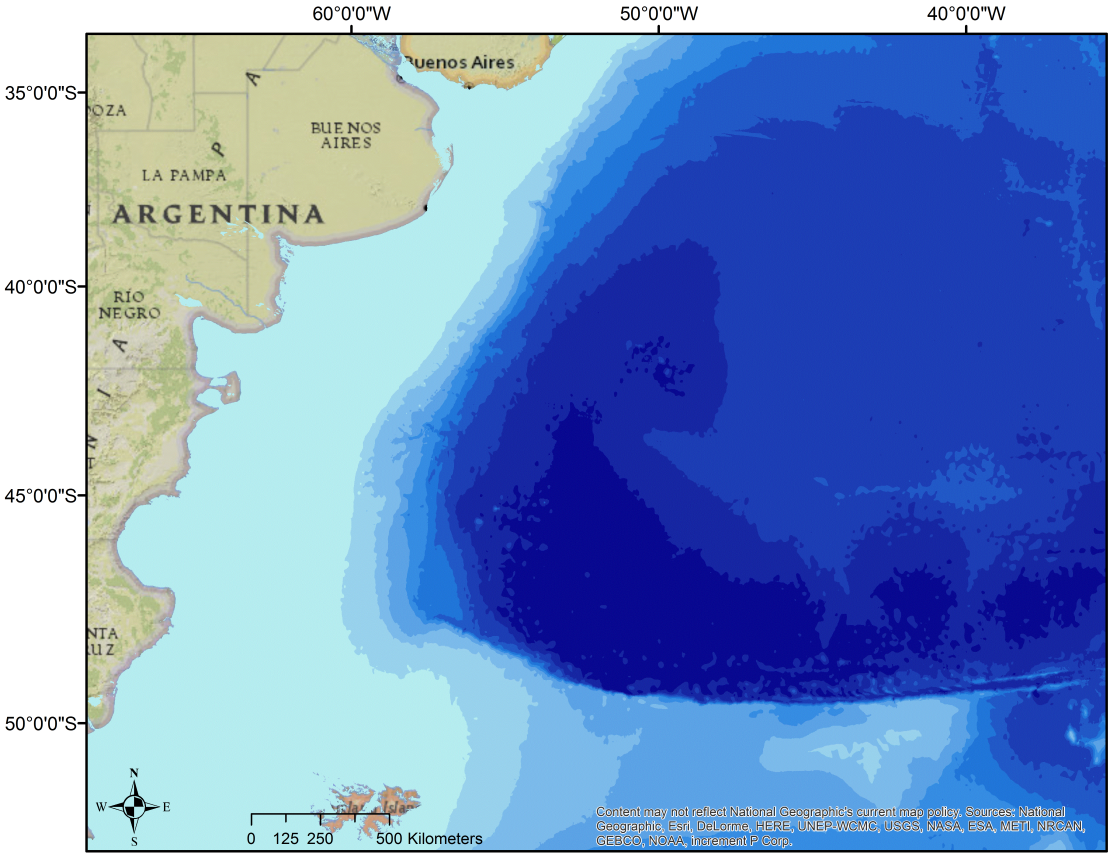

Figure 3.1. Map depicting the Patagonian continental shelf, slope, and Argentine Basin. The shelf, which is <200 m in depth, extends 300-400 km east from Peninsula Valdés. The continental slope drops steeply to the Argentine Basin, which has depths of 5000-6000 m. Males forage over the continental shelf and slope, while females forage over the continental slope and Argentine Basin. Map data from ArcGIS and GEBCO.

The primary purpose of the current study was to assess the association for foraging dives with location, bathymetry, productivity (chlorophyll-α), hydrographic variables (e.g., temperature, salinity, sea surface height), oceanographic features (e.g., eddies and confluence zones) and distinctive water masses during the post-breeding foraging trip of female southern elephant seals from Península Valdés, Argentina. Our hypothesis was that seals forage in association with cyclonic eddies generated by the collision of the Brazil and Malvinas Currents and in association with frontal zones as indicated by high surface temperature and salinity gradients and/or high chlorophyll concentration.

3.2 Methods

3.2.1 Animals, Instrumentation, and Data Processing

Miniature video-data recorders (VDRs, Pisces Design, La Jolla, CA) were attached to the heads of 12 adult female southern elephant seals 21 km north of Punta Delgada, Península Valdés, Argentina in October and November of 2012, 2013, and 2015 prior to their post-breeding foraging trip. Females were sedated with an intramuscular injection of Telazol (0.5 mg kg^{-1}).

The VDR (12 x 5.7 x 4.6 cm, weigh = 60 g in water) is enclosed in polyurethane and depth rated to 2,000 m. Six near-infrared Light Emitting Diodes serve as a light source for the Vision MOS mDVR2 monochrome digital video recorder. Compressed video is stored as MPEG4 files on a digital video recorder with 32 GB of memory, and data are stored on an 8 GB flash drive. All sensor data are recorded at 1 Hz, with the exception of speed (4 Hz) and the 3-axis accelerometer (16 Hz). Some instruments are equipped with a fast-acquisition Global Positioning System (GPS) that records geolocation at the surface. Power is supplied by two lithium ion

batteries (10 x 3 x 3 cm, mass = 270 g in water each). All sensors were calibrated prior to deployment.

The VDR was mounted on the head and the battery pack behind the head. The seals were also instrumented with two satellite transmitters (Spot 5 or 6, Wildlife Computers, Redmond, WA) and two VHF radio transmitters (Advanced Telemetry System, Isanti, MN). One of each was placed on the head and back to facilitate tracking of the animals at sea and when they returned to the rookery. All instruments were mounted on nylon-backed neoprene rubber and glued to the fur with neoprene cement after the fur had been cleaned with acetone.

In 2012 and 2013, the video was programmed to commence recording once the seal had exceeded a depth of 250 m, which indicated that it had reached the continental slope. In 2015, the video was programmed to begin recording 10 (n=2) or 20 (n=2) days after departing the rookery and once it had exceeded a depth of 250 m. Each seal was tracked at sea using satellite telemetry for the duration of the foraging trip. After returning to the rookery, seals were relocated using satellite and radio telemetry and sedated with an intramuscular injection of Telazol (0.5 mg kg^{-1}) so that the instruments could be retrieved.

Video and data were downloaded and archived. The beginning and end of individual dives were determined based on the VDR's saltwater switch, which indicated when the VDR was at the surface. Three-dimensional dive paths (course steered) for each dive were calculated using the AnimalTrack package in R (Farrel and Fuiman, 2013), which used speed, depth, and bearing to determine X, Y, and Z coordinates in 1 Hz. Course steered was corrected for set and drift using filtered ARGOS locations to establish the dive path (course made good). ARGOS locations were filtered by removing all Z class locations and all A|B locations that were not located within 5 km and 2 hours of another location. The vmask function in the argosfilter package in R was

used to filter the remaining locations using a speed threshold of 2 m sec^{-1} (Freitas, 2010, McConnell et al., 1992). All locations occurring within 12 hours of another location were removed to increase the minimum time lag between correction points for set and drift. When the correction points were closer in time, even minute location errors created large drift corrections for a small subset of the data.

Four VDRs functioned fully with audio and video. Two VDRs were lost, two VDRs malfunctioned, and four VDRs recorded data but not video. VDRs recorded for 2-82 days. 14,834 dives were recorded by eight seals among 2012-2016. 1037 were excluded due to various reasons including inaccurate speed and depth sensor readings. The remaining 13,797 dives were designated as foraging, resting, or transit by applying a random forest classification based on 22 summary variables calculated for each dive (Appendix C: Figure C.6).

3.2.2 Environmental Data Acquisition

Bathymetry data were obtained from The General Bathymetric Chart of the Oceans (GEBCO) (IOC, 2003). Chlorophyll-α (Chl-α, mg ml^{-3}) data were accessed from NASA's Earth Observations website and obtained from the Moderate Resolution Imaging Spectroradiometer (MODIS) instrument aboard NASA's Aqua and Terra satellites, consisting of 8-day composites at a 0.1° spatial resolution. Sea surface temperature data (SST, °C) were obtained from the same dataset at an 8-day temporal and 0.041° spatial resolution (NASA Goddard Space Flight Center, 2014). Current speed (m sec^{-1}) and direction (°) were calculated using data from NASA's Physical Oceanography Distributed Active Archive Center's (PO.DAAC) Ocean Surface Current Analysis Real-time (OSCAR) dataset, available in 5-day temporal and 0.33° spatial resolution (ESR, 2009). Sea surface height anomaly (m) data were obtained from NASA's PO.DAAC website, and consisted of gridded data from TOPEX/Poseidon, Jason-1, Jason-2 and Jason-3

satellites at a 5-day temporal and 0.17° spatial resolution (Zlotnicki, 2016). Sea surface salinity (SSS) data, measured in practical salinity units (psu), were downloaded from NOAA's National Oceanographic Data Center (NODC) and obtained from the European Space Agency's (ESA) Soil Moisture and Ocean Salinity (SMOS) satellite at a 7-day temporal and 0.25° spatial resolution (Zhang, 2016). Sea surface temperature gradient and sea surface salinity gradient were calculated using the Spatial Analyst toolbox in ArcGIS. All oceanographic datasets were converted into raster images using either ArcGIS or R. Global eddy track data were processed by Centre National d'Etudes Spatiales (CNES) and downloaded from Archivage, Validation et Interprétation des données des Satellites Océanographiques (AVISO, 2017). Only eddies that persisted for a minimum of four weeks were retained in the dataset. The data for each eddy track included daily coordinates for the eddy centroid, eddy type (cyclonic or anticyclonic) and radius. Eddies matching the spatial and temporal extent of the study were extracted and daily raster images were created using the raster package in R. All individual raster images for each dataset were stacked using the raster package in R and coded by date. Values for each variable were extracted for all seal locations. Temperature (°C) for the upper 5 m of each dive (surface temperature) was extracted from the VDR data for each dive, providing higher-resolution information than the SST data. Maximum dive depth (m), as well as temperature (°C) and salinity (psu) at maximum depth were also extracted from the VDR data.

3.2.3 Data Analysis

Generalized additive models (GAM) were used to determine the influence of environmental variables and time of day on presence/ absence of foraging during female southern elephant seal dives over the post-breeding foraging migration; binomial GAMs with a logit link and cubic spline smoothing functions were fit using the mgcv package in R. Of the 13,797 dives available

for analysis, 1,762 dives were eliminated due to missing environmental data. The remaining 12,035 dives (8,206 of which were foraging) were used in the GAMs. Dives that were classified as foraging (see Chapter 2) were coded "1" for presence, while dives that were classified as resting or transit (non-foraging) were coded "0" for absence (Fig. 3.2). Initial variables included in the models included time of day (Hour in decimal form), bathymetry (m), sea surface salinity (psu), chlorophyll-α concentration (mg ml^{-3}), surface temperature (°C, VDR data), sea surface temperature (°C, satellite data), sea surface height anomaly (m), vertical temperature gradient of the upper 50 m (°C m^{-1}, calculated with VDR data), current speed (m sec^{-1}), current direction (°), location (longitude and latitude), sea surface salinity gradient, sea surface temperature gradient, and sea surface height anomaly gradient. Seal ID number was added as a random effect. An autoregressive model of order 1 (AR1) was fitted to the model residuals with Seal ID number as a grouping variable due to the high autocorrelation between successive dives for each seal. Before fitting the models, variables were tested for concurvity using the mgcv package in R, which assesses to what degree each covariate can be modeled as a function of each of the remaining covariates (Wood, 2008). Variables were also tested for collinearity using the Spearman Rank Correlation Coefficient. If two variables exhibited concurvity or collinearity (>0.6), they were individually fit to a GAM with the remainder of the variables and the GAM with the lowest Akaike's Information Criterion (AIC) was chosen as the starting GAM for the backward selection process. Once all variables exhibiting collinearity and/or concurvity were eliminated from the model, the least significant (lowest p-value) variable was removed from the GAM. This process was repeated as a stepwise procedure, removing the least significant variable until either all variables were significant (p-values <0.05) or there was an increase in the AIC of >1%. Model residuals were checked for temporal autocorrelation via partial autocorrelation

plots, spatial autocorrelation via variograms, and model fit via binning and plotting the residuals by the fitted values.

Summary statistics for foraging dives were computed for all variables. Boxplots were created to view univariate data distribution. Two-dimensional (2D) binned histograms for each pair of variables were created using the hexbin package in R to illustrate bivariate data distribution. Summary statistics and boxplots for salinity and temperature (VDR data) at the maximum depth of foraging dives were computed to ascertain depth, temperature and salinity ranges of prey. Conductivity sensors were not present on every instrument; salinity data were available for 3,995 foraging dives recorded by three seals.

Neutral density (γ^n) of the water mass at the bottom of each foraging dive for which salinity values were present (n = 3,995) was estimated using latitude, longitude, temperature, salinity, and pressure (decibars) in conjunction with Matlab code provided by the Intergovernmental Oceanographic Commission (Jackett and McDougall, 1997). Neutral density is a continuous analog of potential density surfaces, which were previously the gold standard for fitting isopycnals to hydrographic data (Jackett and McDougall, 1997). Water mass was then identified based on neutral density (γ^n) values using water mass definitions for the Brazil-Malvinas Confluence area published by Jullion et al. (2010) (Fig. 3.3, Table 3.1).

Water mass	Neutral density (γ^n)
Surface Water (SW)	< 26
Subtropical Mode Water (STMW)	< 26.5
Subantarctic Mode Water (SAMW)	< 27.2
Antarctic Intermediate Water (AAIW)	< 27.55
Upper Circumpolar Deep Water (UCDW)	< 27.92
North Atlantic Deep Water (NADW)	< 28.11
Lower Circumpolar Deep Water (LCDW)	< 28.26
Weddell Sea Deep Water (WSDW)	>= 28.26

Table 3.1. Water mass definitions (Jullion et al., 2010). Surface water includes low salinity shelf waters.

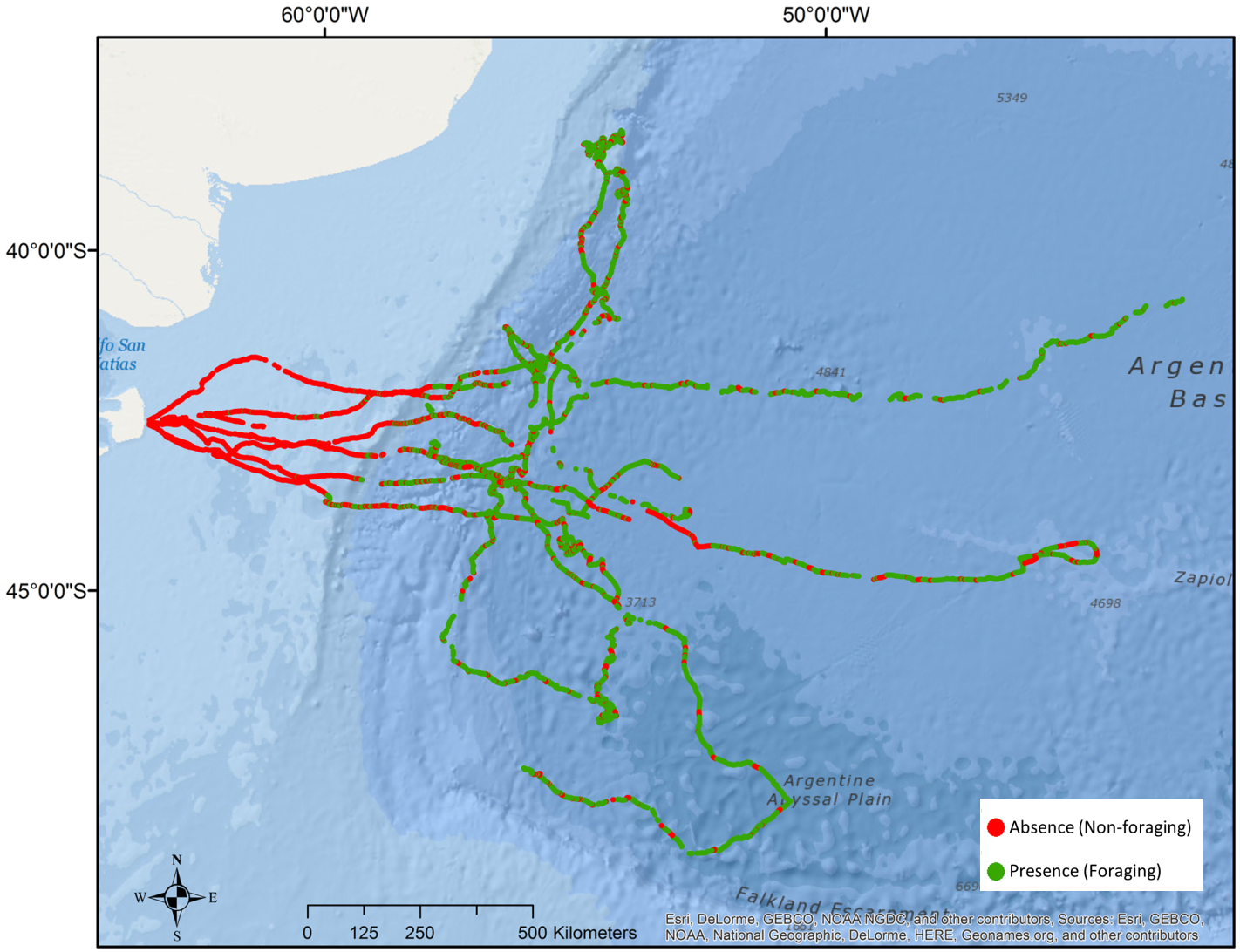

Figure 3.2. Map depicting seal locations over the Argentine shelf, slope, and Basin from 2012-2016 used in the binomial GAM. Red indicates absence of foraging, while green indicates presence of foraging.

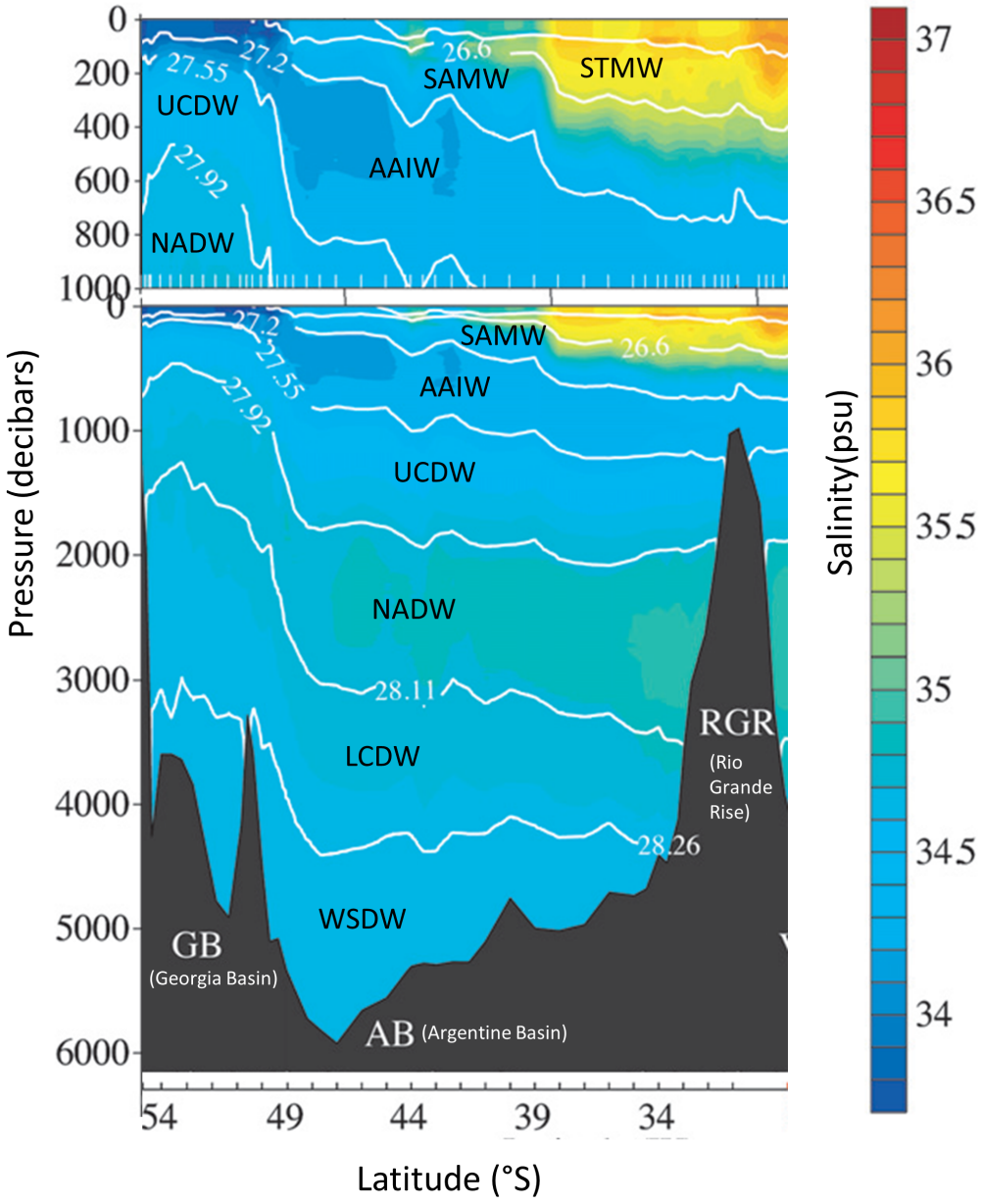

Figure 3.3. Depth ranges for water masses across latitudes 29-54°S, encompassing Georgia Basin, Argentine Basin, and Rio Grande Rise. Figure adapted from Jullion et al. (2010). ©American Meteorological Society. Used with permission.

3.3 Results

3.3.1 GAM Results

Bathymetry, location (longitude and latitude), and sea surface salinity all exhibited pairwise concurvity. Surface temperature (measured by the VDR) was collinear with sea surface temperature (satellite-derived), and bathymetry was collinear with sea surface height anomaly gradient. GAMs including bathymetry and surface temperature resulted in the lowest AIC values, so sea surface height anomaly gradient, location, and sea surface salinity were excluded from the initial model before the backward selection process began. The final model AIC was 5,203 and % deviance explained was 40.6%. Variables retained in the final model were all significant (p-value <0.05) and included time of day, bathymetry, sea surface height anomaly, chlorophyll-α concentration, and surface temperature. Additive effects plots indicated that bathymetries deeper than 3000 m, the period from dusk to dawn (1650-0739 GMT), chlorophyll-α concentration (>5.8 mg ml^{-3}), lower sea surface height anomaly (<0.06 m), and surface temperatures of 11.7-15.5°C were all associated with presence of foraging. Higher sea surface height anomaly (>0.06 m) and surface temperatures of 7.1-11.7°C were associated with absence of foraging (Fig. 3.4).

Partial autocorrelation plots of the raw residuals showed that residual temporal autocorrelation was present (Fig. 3.5A). An AR1 model applied to the residuals improved the GAM fit (Fig. 3.5B). Since raw residual plots are not very useful for binomial models (Carruthers et al., 2008), residuals were binned and plotted by fitted values with a 95% confidence interval (Fig. 3.5C), which indicated a good fit. A variogram showed no residual spatial autocorrelation (Fig. 3.5D), indicating that any spatial autocorrelation was sufficiently modeled in the GAM via the bathymetry main effect (this exhibited concurvity with location) and/or the AR1 model.

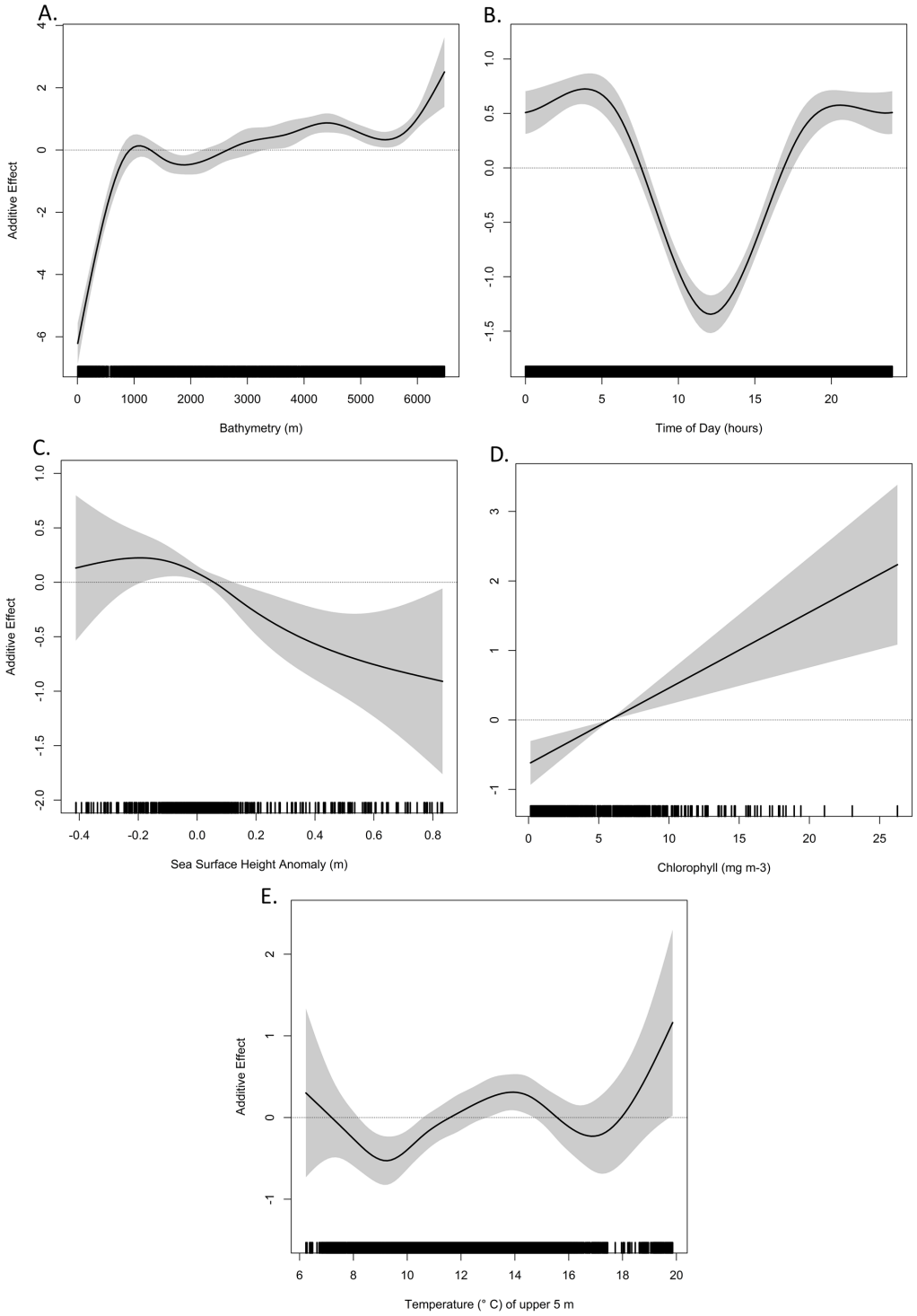

Figure 3.4. Smooth functions of explanatory variables from the final GAM with 95% shaded confidence interval with rug plots indicating distribution of data points. Values >0 indicate a positive additive effect (increased presence of foraging), while values <0 indicate a negative additive effect (reduced presence of foraging).

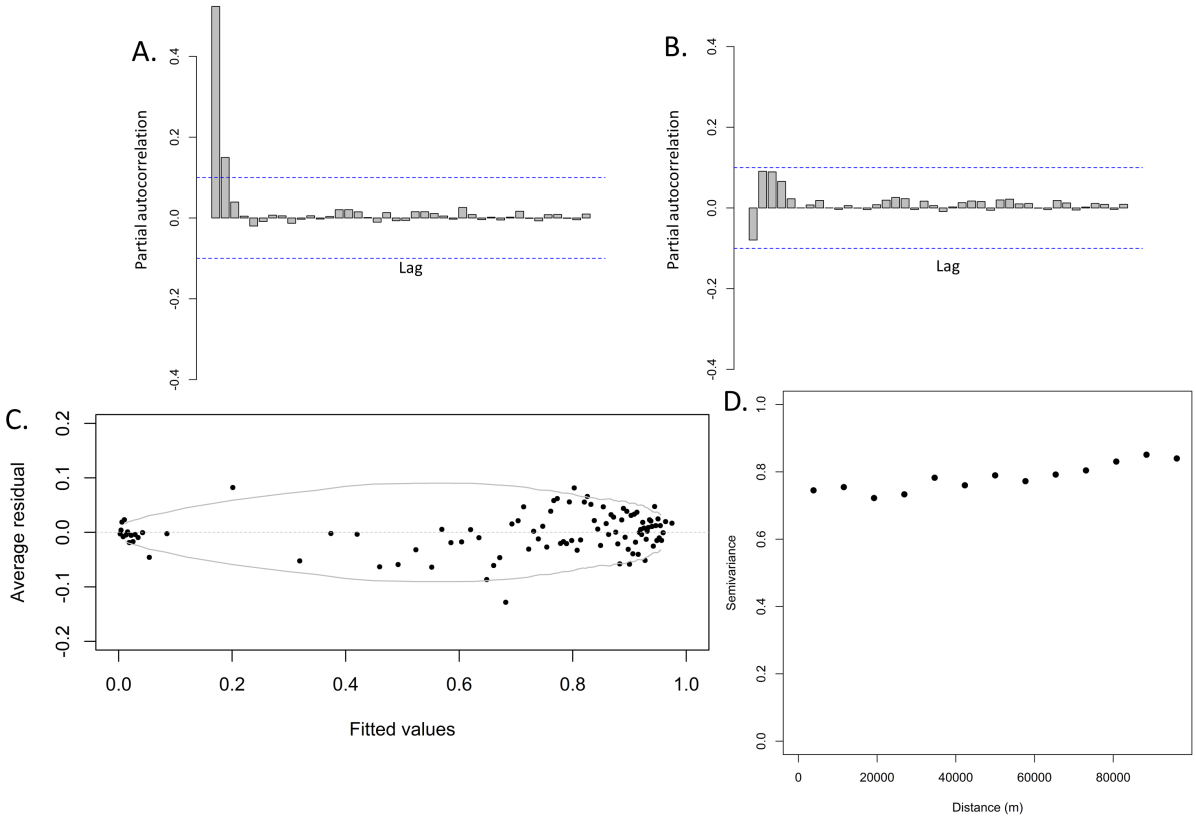

Figure 3.5. Residual plots for the final GAM. A. Partial autocorrelation plot of raw model residuals. Values above 0.1 indicate that temporal autocorrelation is present. B. Partial autocorrelation plot of standardized residuals after applying a first-order autoregressive model to the residuals. C. Binned plot of residuals by fitted values. D. Variogram. Sharply increasing values would indicate spatial autocorrelation.

3.3.2 Foraging habitat-associations at the surface

For foraging dives, the means and ranges over the slope and Argentine Basin were determined for sea surface salinity, surface chlorophyll-α concentration, sea surface height anomaly, and surface temperature (Figs. 3.6, 3.7, Table 3.2). Surface current direction ranged from -180° to 180° for dives over the slope and deep water (Fig. 3.8). Seals were present in cyclonic (cold-core) eddies for 20.6% of dives, in anticyclonic (warm-core) eddies for 4.9% of dives, and were not present in a detected eddy for 74.5% of dives (Fig. 3.9).

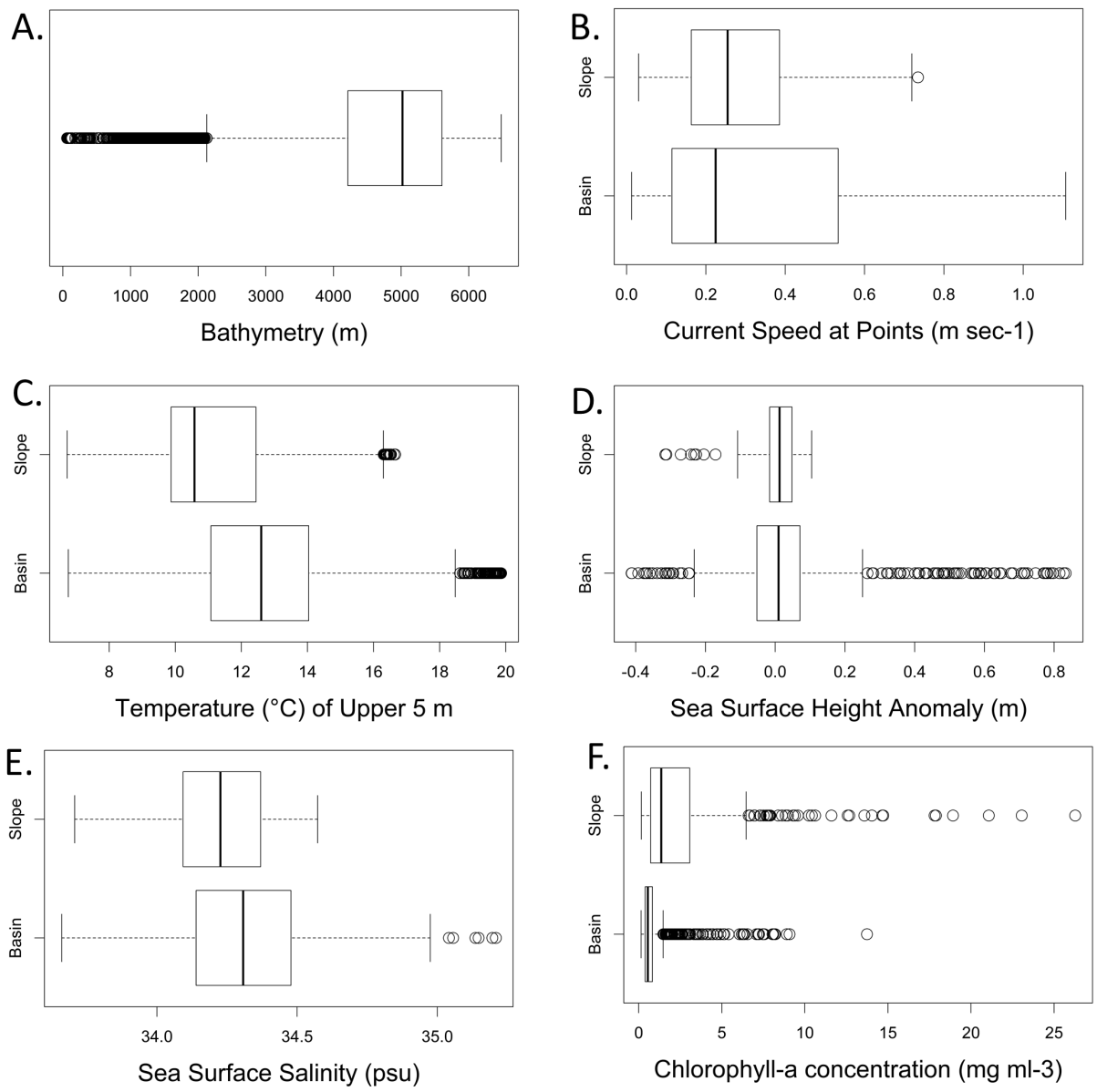

Figure 3.6. Boxplots of bathymetry and surface habitat variables for foraging dive locations over the slope (n = 1585) and Argentine Basin (n = 6589).

	All Foraging Dives	Slope Foraging Dives	Basin Foraging Dives
Bathymetry (m)	4516 ± 1525	1792 ± 807	5193 ± 633
Chl-α conc. (mg ml^{-3})	1.23 ± 2.12	2.89 ± 3.75	0.82 ± 1.05
Current speed (m sec^{-1})	0.32 ± 0.24	0.29 ± 0.15	0.33 ± 0.26
Surface temperature (°C)	12.32 ± 2.24	11.03 ± 2.16	12.64 ± 2.14
Sea surface height anomaly (m)	0.02 ± 0.18	-0.01 ± 0.1	0.03 ± 0.19
Sea surface salinity (psu)	34.29 ± 0.27	34.21 ± 0.19	34.32 ± 0.27

Table 3.2. Descriptive statistics for foraging dive surface environmental variables and bathymetry.

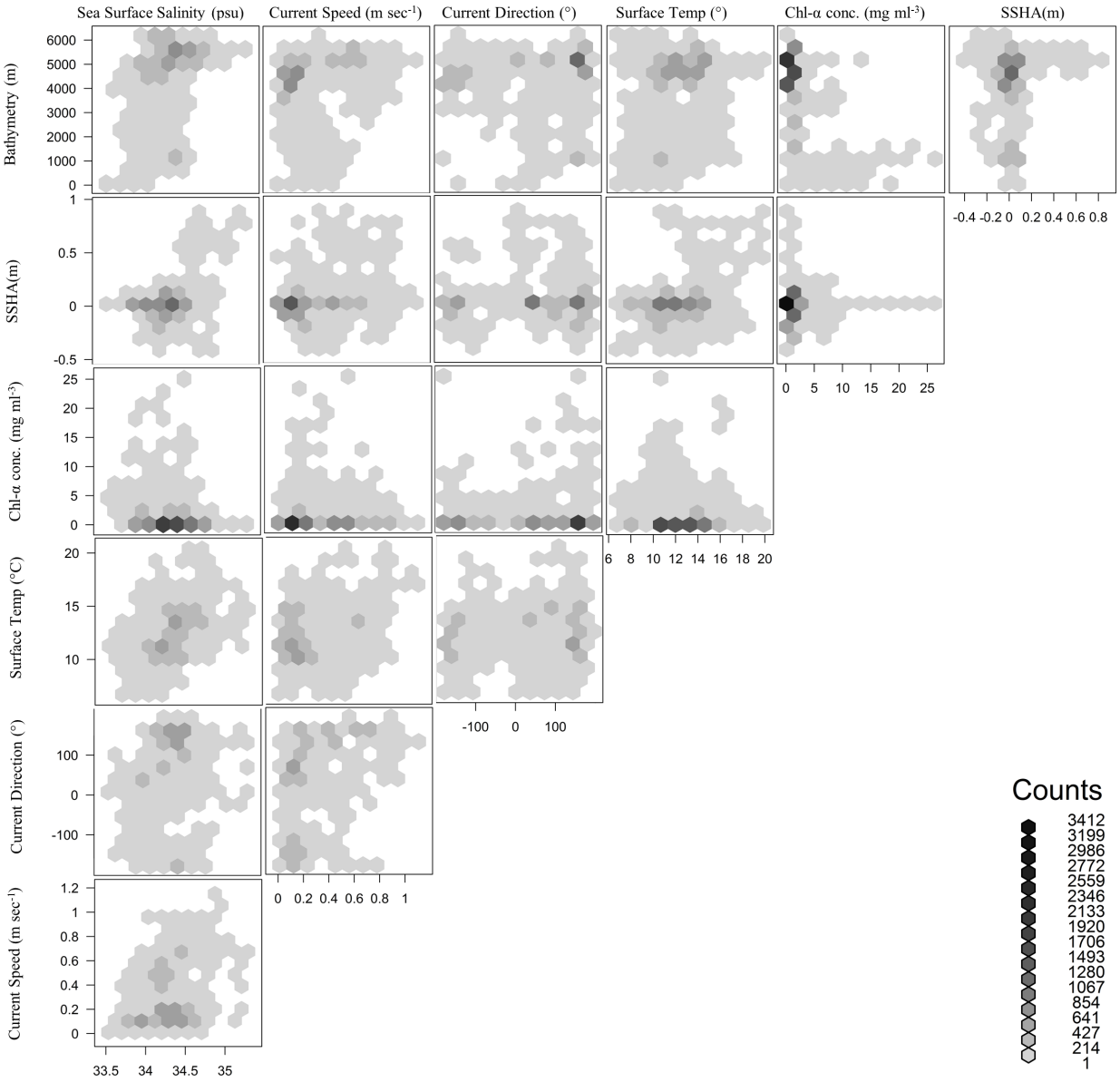

Figure 3.7. Binned shaded histograms depicting bivariate distributions of bathymetry and surface habitat variables for foraging dives (n=8206).

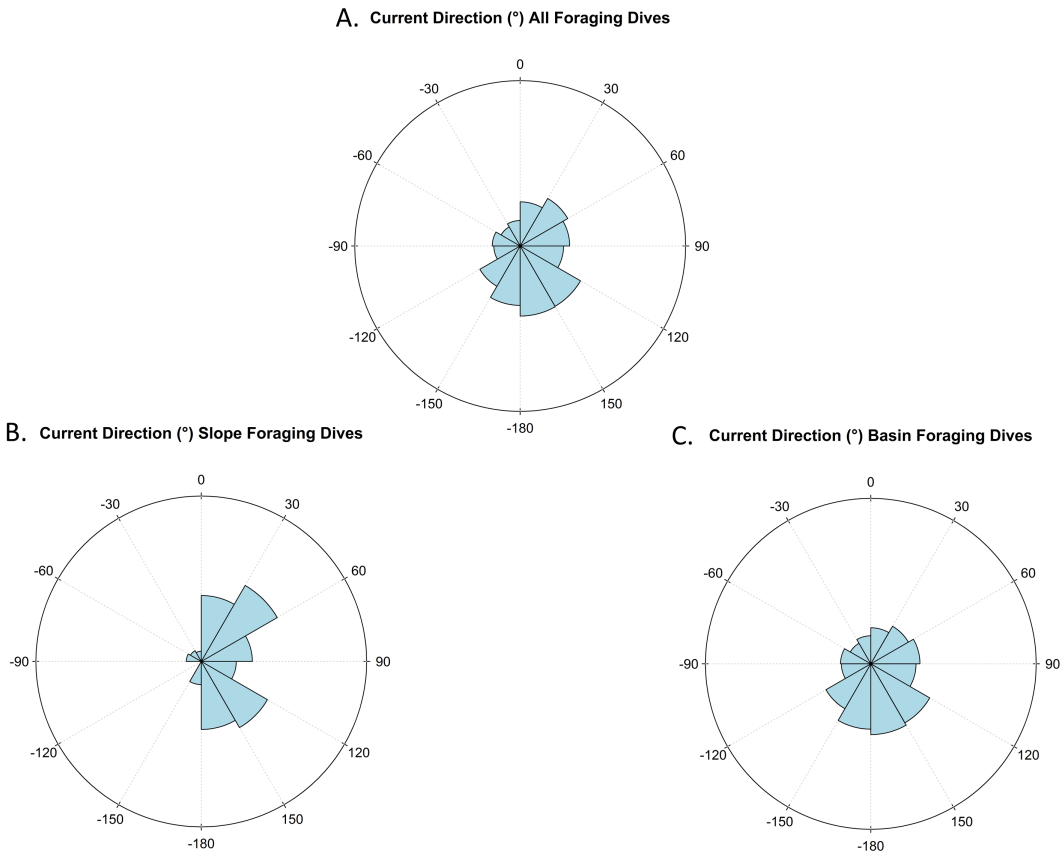

Figure 3.8. Circular histograms depicting distribution of current direction (°, binned into 30° segments) at foraging dives locations for A. all foraging dives (n=8206), B. slope foraging dives (n=1585), and C. deep water foraging dives (n=6589).

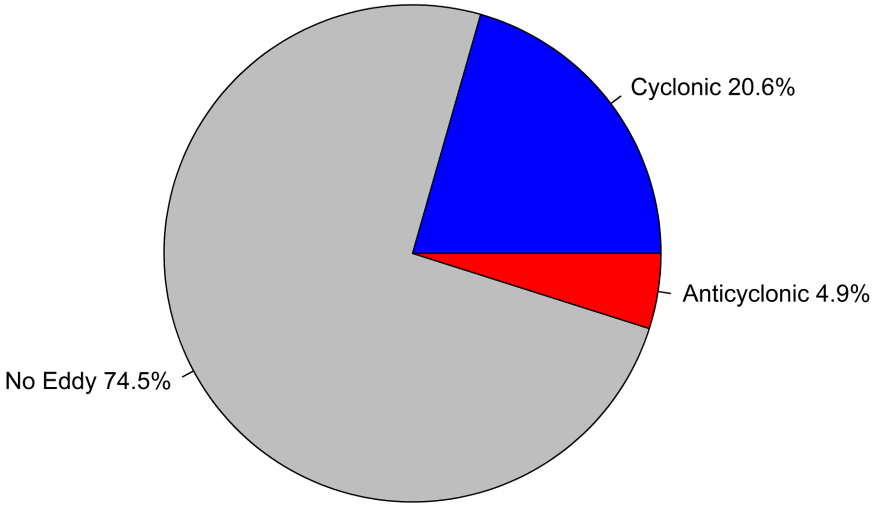

Figure 3.9. Pie chart depicting percent of foraging dives (n=8206) that occurred within and outside of cyclonic (cold-core) eddies, anticyclonic (warm-core) eddies, and in waters not within an eddy.

3.3.3 Foraging habitat-associations at depth

Maximum dive depth over the slope was 501 ± 234 s.d. m (range 2 to 1154 m) and 461 ± 283 s.d. m (range 2 to 1526 m) over deep water. Temperature at maximum depth was 3.73 ± 0.8 s.d. °C (range 2.36 - 9.43 °C) over the slope and 3.74 ± 1.27 °C (range 1.77 - 13 °C) over deep water. Salinity at maximum depth 33.56 ± 0.21 s.d. psu (range 33.21 - 34.37 psu) over the slope and 33.8 ± 0.41 s.d. psu (range 33.28 - 38.06 psu) over the Argentine Basin (Table 3.3, Fig. 3.10).

Seals encountered water masses with neutral densities ranging from 25.85 to 28.52 γ^n (Table 3.1, Fig. 3.3). Surface Water, Lower Circumpolar Deep Water, Weddell Sea Deep Water, and North Atlantic Deep Water were each encountered during < 1% of foraging dives (between 2-13 total dives each). In the majority of dives (70%), seals encountered Sub-Antarctic Mode Water at a mean maximum dive depth of 434 ± 250 s.d. m. Antarctic Intermediate Water was encountered in 17.4% of dives at a mean maximum dive depth of 540 ± 300 s.d. m, Upper Circumpolar Deep Water in 10.7% of dives at a mean maximum dive depth of 461 ± 257 s.d. m,, and Subtropical Mode Water in 1.7% of dives at a mean maximum dive depth 555 ± 250 s.d. m (Figs. 3.11, 3.12, 3.13). Upper Circumpolar Deep Water was encountered by one seal that foraged for a couple of weeks in waters at ~ 48°S (Fig. 3.13B), where this water mass is much more accessible, located at ~200 m from the surface as opposed to > 800 m from the surface near the Brazil-Malvinas Confluence (Jullion et al., 2010, Fig. 3.3).

	All Foraging Dives	Slope Foraging Dives	Basin Foraging Dives
Temp (°C) at max depth	3.74 ± 1.27	3.73 ± 0.8	3.73 ± 1.33
Salinity (psu) at max depth	33.84 ± 0.41	33.55 ± 0.21	33.95 ± 0.42
Maximum depth (m)	469 ± 275	501 ± 234	461 ± 284

Table 3.3. Descriptive statistics for foraging dive habitat at depth.

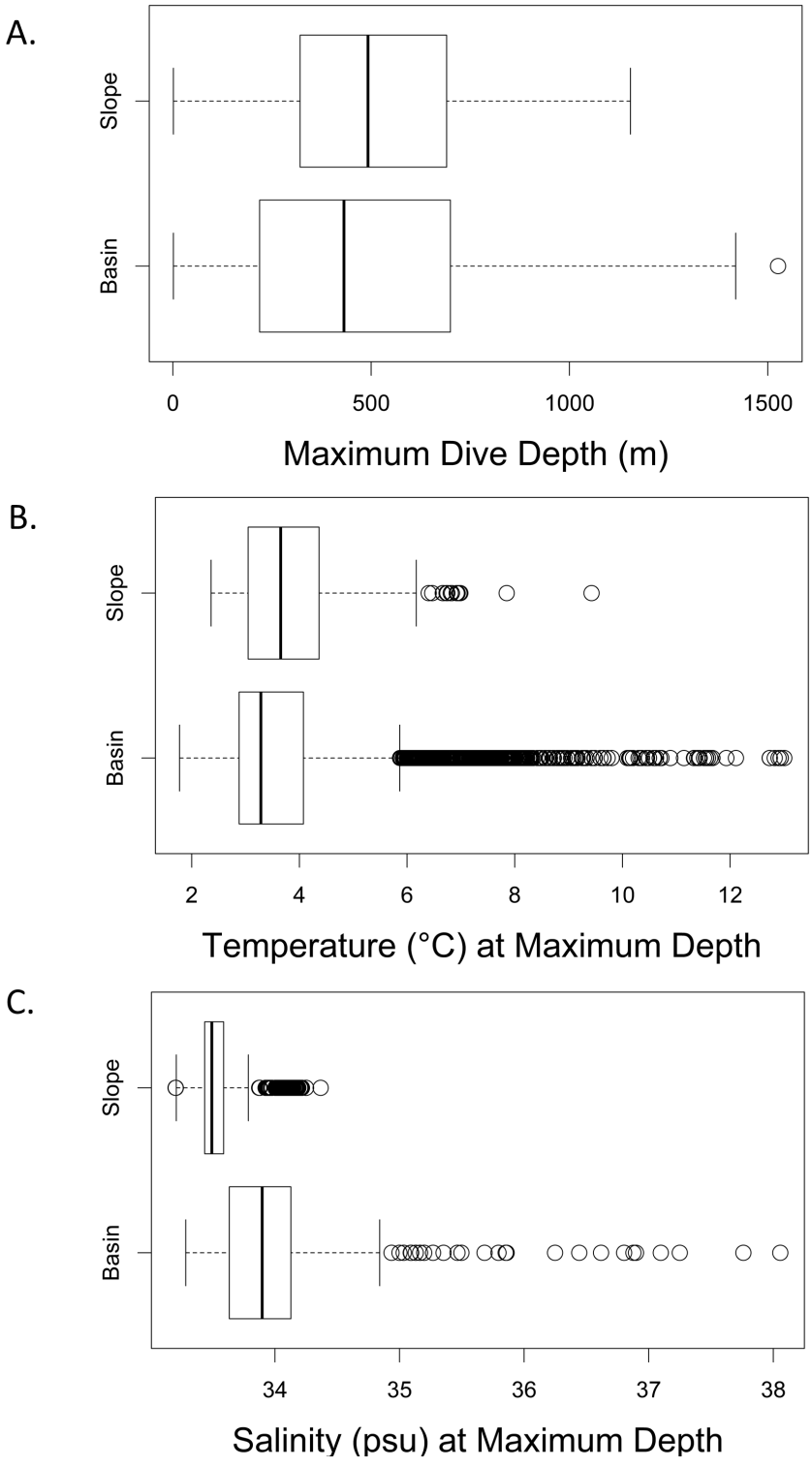

Figure 3.10. Boxplots for environmental variables at depth for foraging dives over the slope (n = 1585 for depth and temperature, n = 1087 for salinity) and over the Argentine Basin (n = 6589 for depth and temperature, n = 2908 for salinity).

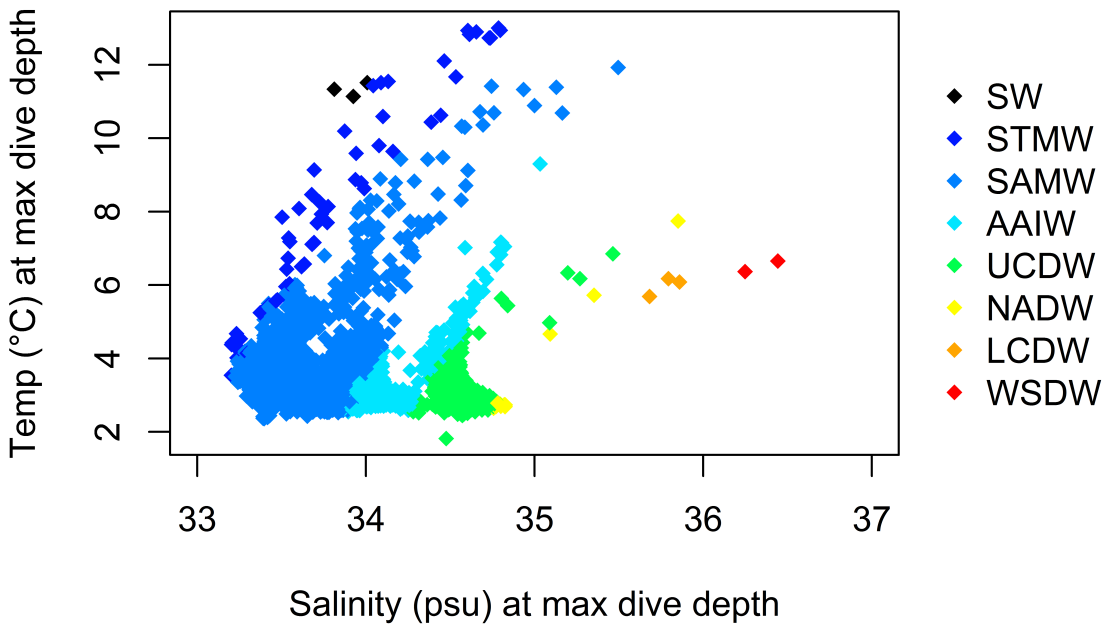

Figure 3.11. Plot of salinity and temperature at the bottom of foraging dives colored by water mass (n=3995). SW = Surface Water, STMW = Subtropical Mode Water, SAMW = Subantarctic Mode Water, AAIW = Antarctic Intermediate Water, UCDW = Upper Circumpolar Deep Water, NADW = North Atlantic Deep Water, LCDW = Lower Circumpolar Deep Water, WDSW = Weddell Sea Deep Water.

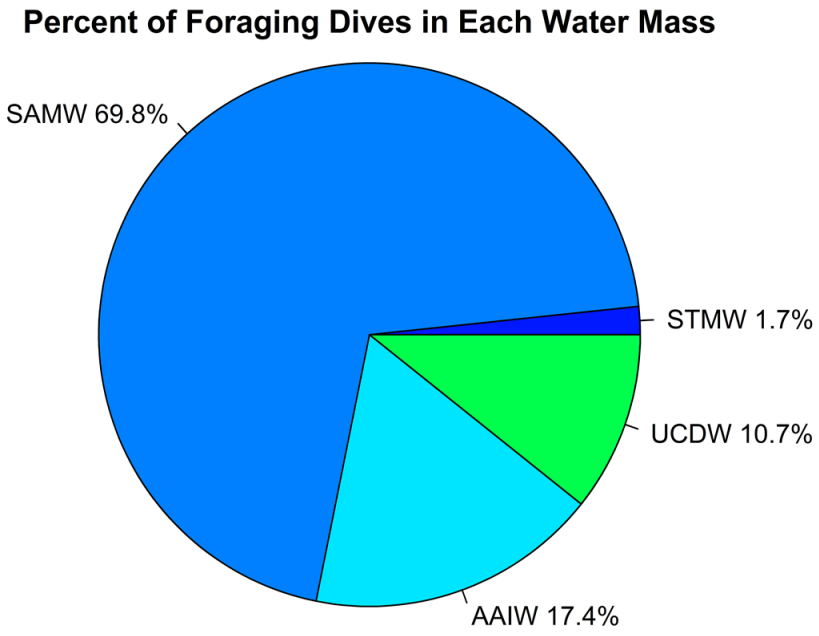

Figure 3.12. Pie chart depicting percentage of dives within each water mass. Water masses with < 1% of dives are not shown. STMW = Subtropical Mode Water, SAMW = Subantarctic Mode Water, AAIW = Antarctic Intermediate Water, UCDW = Upper Circumpolar Deep Water.

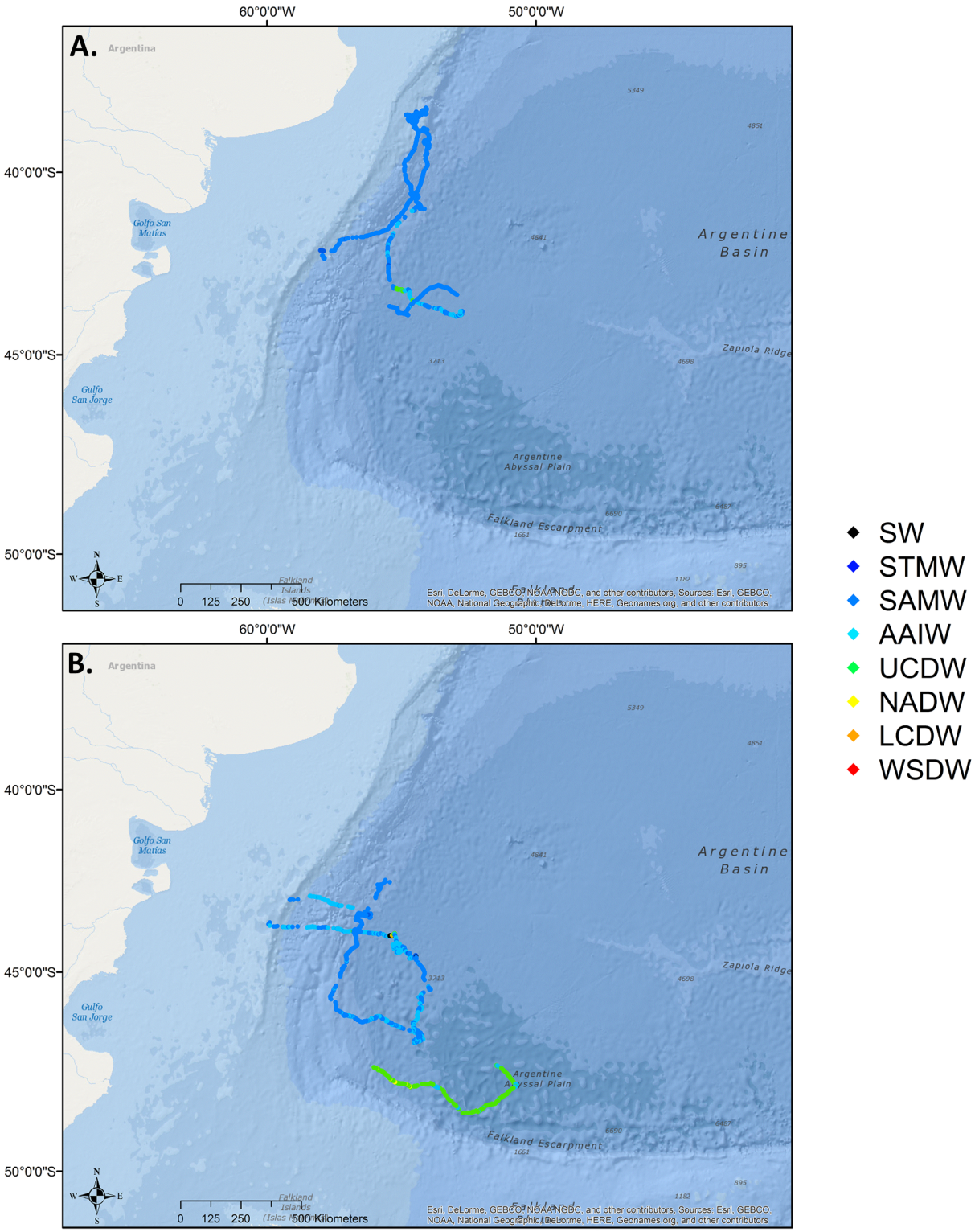

Figure 3.13. Map of foraging dives for which neutral density could be calculated (salinity measurements available at maximum dive depth) colored by water mass in A. 2013 (1 seal) and B. 2015 (two seals). SW = Surface Water, STMW = Subtropical Mode Water, SAMW = Subantarctic Mode Water, AAIW = Antarctic Intermediate Water, UCDW = Upper Circumpolar Deep Water, NADW = North Atlantic Deep Water, LCDW = Lower Circumpolar Deep Water, WDSW = Weddell Sea Deep Water.

3.4 Discussion

3.4.1 Bathymetry

Bathymetry was a significant explanatory variable in the final GAM, with increased likelihood of foraging occurring at bathymetries of greater than 3,000 m. This corresponds to the lower slope and Argentine Basin, further confirming that female seals do not forage on the continental shelf in this location (Campagna et al., 1995; Campagna et al., 1998).

3.4.2 Foraging habitat-associations at the surface

Although hydrographic features at the surface were significant in the GAM model, they represent habitat-associations that likely do not reflect the hydrographic conditions at depth (mean depth = 451 $\pm$ 280 s.d. m) where elephant seals forage. Surface water temperature was a significant explanatory variable, with increased likelihood of foraging associated with surface temperatures of 11.7 - 15.5°C likely associated with mixed surface waters in the confluence zone. Decreased likelihood of foraging was associated with surface temperatures of 7.1 - 11.7°C. These surface temperatures were typically encountered in low-salinity Shelf Waters, where the seals did not forage. The smooth function for surface temperature for values between 15.5 - 20°C occurred on either side of the zero additive effect line, and therefore interpretation of the smooth function for temperature should center on values outside of this range.

According to the respective GAM smooth function, likelihood of foraging decreased with increasing sea surface height anomaly likely associated with anticyclonic (warm-core) eddies and meanders of the Brazil Current. Likelihood of foraging increased with decreasing sea surface height anomaly (<0.06 m) likely associated with cyclonic (cold-core) eddies and meanders of the Malvinas Current. The confidence intervals for the smooth function for sea surface height

anomaly for values <0.2 m occurred on either side of the zero additive effect line, and therefore caution should be used when interpreting the smooth function for these values.

Over 20% of all foraging dives occurred in cyclonic eddies, while less than 5% occurred in anticyclonic (warm-core) eddies. Studies of juvenile foraging behavior from Península Valdés described associations with the outer edge of both cyclonic and anti-cyclonic eddies (Campagna et al., 2006). The meeting of the Brazil and Malvinas Currents gives rise to one of the most energetic eddy fields in the world ocean (Piola and Matano, 2001), which the seals in this study were in the midst of during their foraging trip (Fig. 3.14).

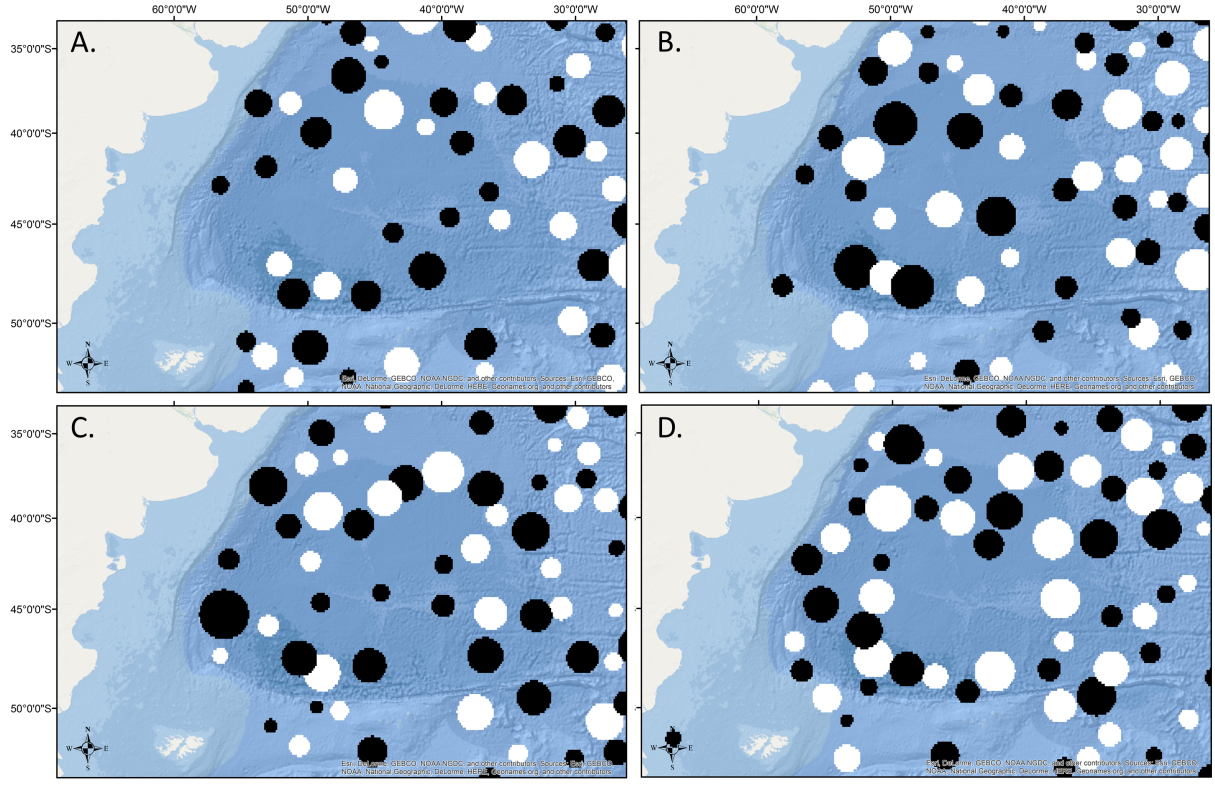

Figure 3.14. Map of study area with known eddies on A. Nov. 15, 2013. B. Dec. 15, 2013. C. Nov. 15, 2015. D. Dec. 15, 2015. Eddies represented in black are cyclonic (cold-core) eddies while eddies represented in white are anticyclonic (warm-core) eddies. This shows that the eddy field is very intense throughout the duration of the post-breeding foraging trip from year to year. Eddy track data downloaded from AVISO.

Surface chlorophyll-α concentration was also a significant explanatory variable in the final GAM. Chlorophyll-α concentrations were higher on the slope than in deep water, likely due to the shelf-break front where a seasonal chlorophyll bloom occurs in the spring and persists through the summer (Romero et al., 2006b).

Sea surface temperature gradient and sea surface salinity gradient were not included in the final GAM because they were insignificant. A recent study on the habitat use of southern elephant seals from each of the other major populations (Kerguelen Islands, Macquarie Island, South Georgia, and the Antarctic Peninsula) found that frontal areas were not focal foraging locations and that seals from these colonies were able to forage successfully both over the continental shelf and in the deep ocean away from fronts (Hindell et al., 2016). The same conclusion cannot be reached in this study, however, as both sea surface height anomaly and chlorophyll-α concentration were significant explanatory variables.

3.4.3 Foraging habitat-associations at depth

Seals made most foraging dives in Subantarctic Mode Water, followed by Antarctic Intermediate Water, Upper Circumpolar Deep Water, and Subtropical Mode Water. Sub-Antarctic Mode Water, Antarctic Intermediate Water, and Upper Circumpolar Deep Water are all transported by the Malvinas Current. Sub-Tropical Mode Water and recirculated Antarctic Intermediate Water (at depths of 700-1000 m) are transported by the Brazil Current (Charo and Martinez, 2000; Jullion et al., 2010; Matano et al., 2010; Palma et al., 2008). A study of the foraging migrations of southern elephant seals from the other major sub-Antarctic colonies and the Antarctic Peninsula indicated that post-breeding females spent the most time in Antarctic Surface Water, followed by Antarctic Intermediate Water and Circumpolar Deep Water (Hindell et al., 2016), meaning that two of the main water masses used by seals in this study are shared

with other populations of southern elephant seals. Some seals from other colonies do not travel far enough north to encounter Subantarctic Mode Water. A study of southern elephant seal distribution from South Georgia, the most proximal major colony to Península Valdés, indicated that the seals spent the majority of their time in Upper Circumpolar Deep Water and it's boundary with Antarctic Intermediate Water (Biuw et al., 2007). One seal in that study was associated with Sub-Antarctic Mode Water.

There is little information regarding the association of potential prey species with specific water masses in the southwest Atlantic. There is a fishery for *Ilex argentinus*, the Argentine short-fin squid, along the continental shelf-break. Although this squid is not a known prey species for southern elephant seals, *Martiala hyadensi,* a known prey species, is frequent bycatch in this fishery (Boyle and Rodhouse, 2008). Fish species that are known prey of southern elephant seals are also present over the Argentine continental slope and Argentine Basin. In one sampling study over the Argentine continental shelf and slope extending to ~48°W, 25 species of Southern Ocean fishes were recorded from 16 families, representing 15% of the ichthyofauna of the Southern Ocean (Cousseau et al., 2012). Of these 25 species identified, 9 are known prey species of southern elephant seals, including members of the families Bathylagidae, Gempylidae, Myctophidae, Nototheniidae, and Paralepididae. Another study that collected 47 species of fish from 23 families between 36°-56°S and 44°-62°W found that sub-Antarctic species were the most abundant (Figueroa et al., 1998). Of these 47 species identified, 10 are known prey species of southern elephant seals, including members of the families Bathylagidae, Centrolophidae, Gempylidae, Myctophidae, Paralepididae, and Photichthyidae. Information about temperature, salinity, or density of the water masses from which the fishes were sampled was not provided.

In summary, post-breeding female southern elephant seals from the Península Valdés, Argentina colony foraged away from the continental shelf over the continental slope and Argentine Basin in predominantly sub-Antarctic waters, in temperatures ranging from 1.8°C - 13°C and salinities ranging from 33.2 – 38.1 psu. The majority of dives were made in Sub-Antarctic Mode Water, followed by Antarctic Intermediate Water. One seal foraging near the southern rim of the Argentine Basin made a series of foraging dives in Upper Circumpolar Deep Water, which is closer to the surface at that latitude. A small percentage of dives (<2%) were made in Sub-Tropical Mode Water. Our hypotheses were upheld; seals foraged in association with areas of higher primary productivity as measured by chlorophyll-α concentration and in areas of negative sea surface height anomaly likely corresponding to meanders and anti-cyclonic eddies originating from the Malvinas Current; 21% of foraging dives were made within cyclonic eddies.

4. THE VIABILITY OF VIBRISSAE AS SENSORY STRUCTURES FOR PREY DETECTION AND CAPTURE IN ELEPHANT SEALS[1]

4.1 Introduction

Vibrissae are highly specialized hairs that are present at one or more developmental stages in the majority of therian taxa (Ahl, 1986). Pocock (1914) completed a comprehensive study of the arrangement of the vibrissae in a wide range of mammalian species and concluded that the architecture is evolutionarily highly conserved. While absent in prototherians, vibrissae are present in both eutherians and metatherians, indicating that they evolved before these two clades diverged (Pocock, 1914) over 160 MYA (Luo et al., 2011). Vibrissae consist of a hair follicle encircled by prominent blood sinuses and are therefore referred to as Follicle-Sinus Complexes (F-SCs) (Rice et al., 1986), each of which is encased in a dense connective tissue capsule (Patrizi and Munger, 1966). Surrounding the vibrissal hairshaft is the follicle proper, composed of the outer root sheath (ORS) and inner root sheath (IRS), and derived from the epidermis. Adjacent to the ORS is the glassy membrane (GM), contiguous with the basement membrane. Flanking the GM is the mesenchymal sheath (MS), derived from the dermis along with the dermal capsule (DC). Between the MS and the DC is the sinus cavity (Van Horn, 1970). In pinnipeds, the blood sinus cavity is split into three sections: the lower cavernous sinus (LCS), the ring sinus (RS), and the upper cavernous sinus (UCS). The ring sinus is separated from the UCS by the conical body (Marshall et al., 2006) and contains a collar-like projection of the MS referred to as the ringwulst (Ling, 1977). In general, vibrissal hairshafts are longer than pelage hairs and F-SCs are larger and more highly innervated than typical pelage hair follicles (Ahl, 1987; Reep et al., 2002). Each vibrissa acts as a biomechanical filter (Ginter, 2011; Sane and McHenry, 2009) that conveys

[1] The contents of this section are reprinted with permission from McGovern, K.A., Davis, R.W., Marshall, C.D., 2015. Are vibrissae viable sensory structures for prey capture in northern elephant seals, Mirounga angustirostris? Anat. Rec. 298, 750-760.

information regarding external stimulation to mechanoreceptors located in the lower part of the follicle (Ling, 1966; Yablokov and Klezeval, 1969).

There is a progressive increase in F-SC innervation with increased aquatic specialization. Semiaquatic and fully aquatic mammals generally have higher innervation than terrestrial mammals (Dehnhardt et al., 1999; Hyvärinen et al., 2009; Marshall et al., 2014a). In lieu of performance data, innervation can be used as a proxy for sensitivity (George and Holliday, 2013). Although there are few comparative data, the average number of axons per vibrissa in seals ranges from 1,000 to 1,600 (Hyvärinen et al., 2009; Marshall et al., 2006; Yablokov and Klezeval, 1969), 5- to 10-fold more than that of terrestrial mammals (Dehnhardt et al., 1999; Hyvärinen and Katajisto, 1984; Hyvärinen et al., 2009). We hypothesized that NES mystacial vibrissae were similar in microstructure to the vibrissae of other seals and that each F-SC was innervated by a minimum of 1,000 axons.

4.2 Materials and methods

Mystacial vibrissal pads were obtained from nine stranded NES (five weaned pups, two unweaned pups, and two yearlings) that died during rehabilitation efforts at the Marine Mammal Center in Sausalito, CA. Samples were fixed in phosphate buffered physiological formaldehyde. The number and distribution of vibrissal hairshafts were quantified and mapped for each mystacial mask. Measurements of length and width were made for individual vibrissal hairshafts using digital calipers. Since vibrissal hairshafts were oval in cross-section, two width measurements (maximum diameter and minimum diameter) were recorded. Larger F-SCs were dissected from the mystacial mask and sectioned at 35 to 40 µm on a Lipshaw 80A microtome fitted with a Physiotemp freezing stage. A total of 18 F-SCs were sectioned in the longitudinal plane and 15 F-SCs in cross-section. Sections were stained with either a modified Masson's

trichrome stain (Masson, 1929) or a modified Bodian silver stain (Bodian, 1936) following Reep et al. (2001) and Marshall et al. (2006). Longitudinal sections from the center of the F-SC and cross-sections from the center of the LCS that had been stained with trichrome and silver were used to characterize the microstructure of the F-SCs. All longitudinal measurements were made at the center of the F-SC. All cross-sectional morphometrics were made at the midlevel of the LCS (N = 12 for HS measurements; N = 14 for all other measurements). Silver stained cross-sections midway through the LCS were used to quantify axons. For each F-SC, all axons were counted for three consecutive cross-sections at the midlevel of the LCS. Axon counts from the three sections were then averaged for each F-SC. Micrographs were collected using a Nikon Eclipse microscope and SPOT Pursuit camera. Measurements were made using SPOT Advanced software. No adjustments were made to micrographs after photos were taken, with the exceptions of brightness and contrast enhancement, rotating, flipping, and the addition of scale bars to some images, as well as aligning of successive micrographs to reproduce the longitudinal sections.

To characterize NES F-SCs and to provide additional comparative data with other studies (e.g., Hyvärinen et al., 2009; Marshall et al., 2006), the following morphometric data were collected from histologically processed longitudinal sections: (1) maximum F-SC length, (2) maximum total sinus length, (3) maximum UCS length, (4) RS length, (5) maximum LCS length, (6) maximum RS width, (7) maximum DC thickness, and (8) maximum hair shaft (HS) diameter at the level of the RS. The following morphometrics were collected from histologically processed cross-sections at the level of the LCS: (1) mean maximum diameter of the F-SC, (2) mean maximum diameter of the LCS, (3) mean longitudinal axis of the HS, (4) mean perpendicular axis of the HS, (5) mean longitudinal axis of the ORS, (6) mean perpendicular axis of the ORS, and (7) DC thickness. All measurements are reported as means with standard

deviations. Separate linear regressions were conducted modeling F-SC size as a function of LCS diameter, F-SC length, animal body length, and animal body mass to see if any of these factors predict F-SC size.

4.3 Results

4.3.1 Vibrissal Hairshafts

The mean number of mystacial vibrissae was 100.4 ± 2.65 (range 97–105), and they were arranged in seven rows and 9 to 10 columns (Fig. 4.1). The vibrissal hair shafts were shortest at the rostrodorsal edge of the mystacial pad (range 7.54–20.11 mm) and successively increased in length approaching the caudoventral aspect (range 73.27–138.14 mm). They were oval in cross-section and exhibited beaded profiles. Maximum diameter ranged from 1.7 to 3.6 mm in rostrodorsal vibrissae to 10.9 to 16.6 mm in caudoventral vibrissae. Minimum diameters were 1.6 to 2.4 mm and 6.9 to 13.1 mm for rostrodorsal and caudoventral vibrissae, respectively. All axial diameters were measured at the hair-skin interface where the hair shaft exits the follicle.

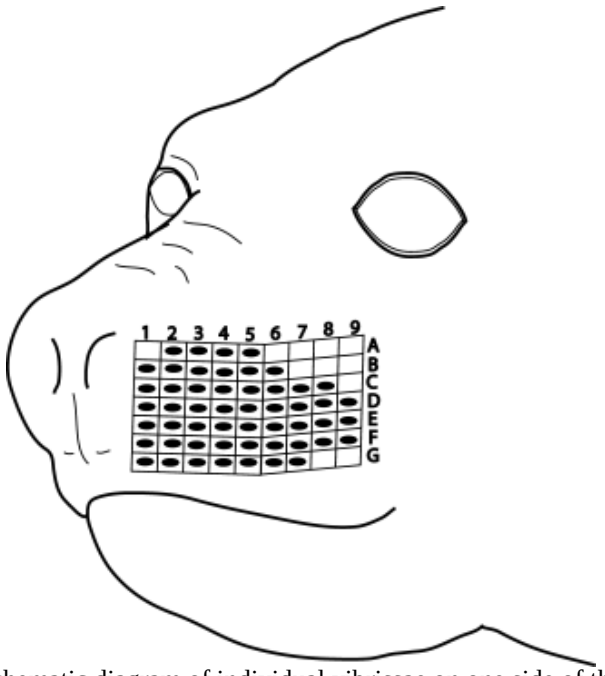

Figure 4.1. Representative schematic diagram of individual vibrissae on one side of the mystacial array.

4.3.2 F-SC Microstructure

The F-SCs had a tripartite sinus organization and were comprised of an UCS, RS, and LCS surrounded by a DC of dense connective tissue (Fig. 4.2). A small, asymmetrical ringwulst was present within the RS, and the RS and UCS were separated by a thick connective tissue band adjoining apical to the inner conical body (ICB) (Fig. 4.3). There were thick and robust connective tissue trabeculae traversing the UCS, while only very thin and delicate trabeculae were present in the LCS. The RS was devoid of any trabeculae. Longitudinal and cross-sectional morphometrics are detailed in Tables 4.1 and 4.2.

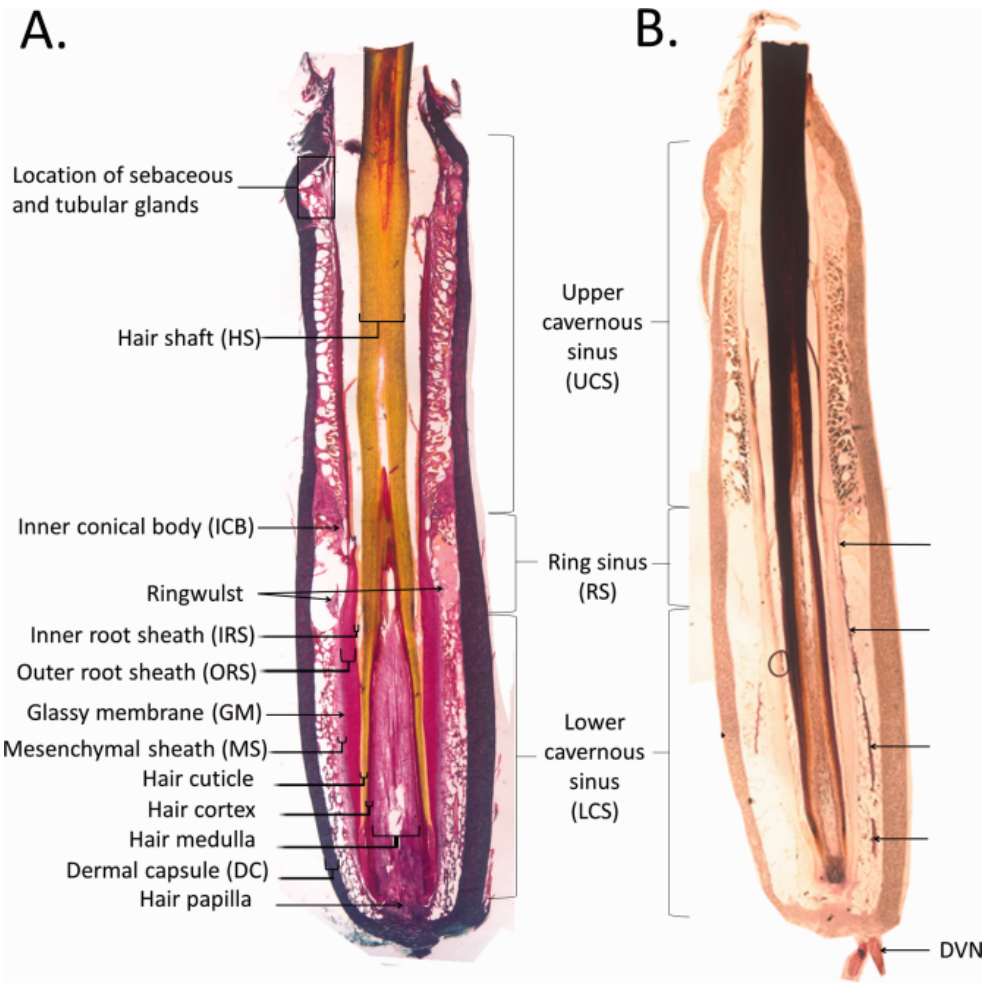

Figure 4.2. A. Longitudinal section. B. Longitudinal section; arrows point to the deep vibrissal nerve (DVN); A processed with a modified Masson's trichrome stain, B processed with a Bodian silver stain.

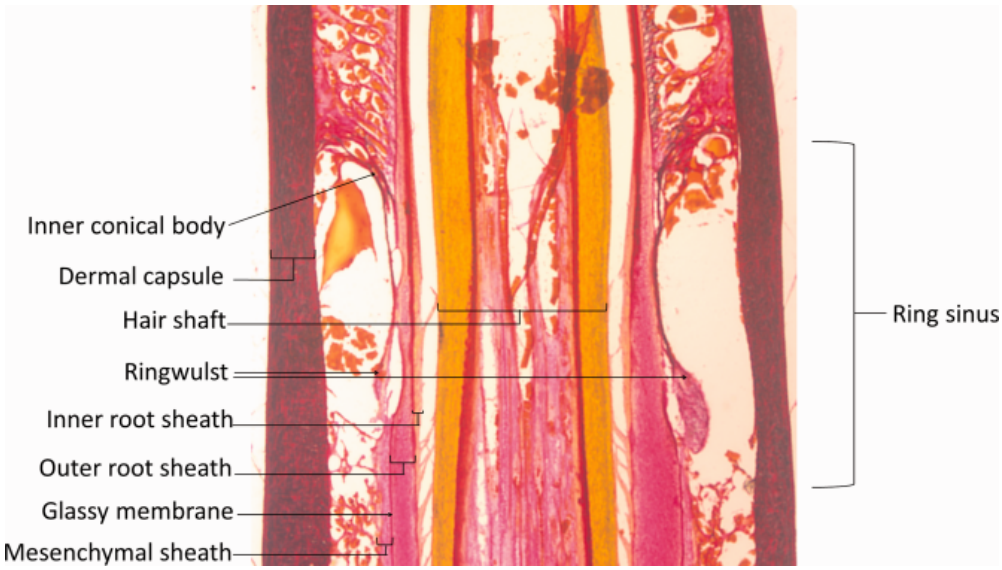

Figure 4.3. Ring sinus and asymmetrical ringwulst, processed with a modified Masson's trichrome stain.

	Mean	**S.D.**	**Minimum**	**Maximum**
F-SC length (mm)	19.99	1.65	15.32	21.85
Total sinus length (mm)	18.17	1.65	13.68	20.47
UCS length	8.62	1.07	6.08	10.36
% of total sinus length	47.3	2.5	43.8	50.7
RS length (mm)	2.53	0.38	1.85	2.95
% of total sinus length	13.9	1.6	11.8	16.2
LCS length (mm)	6.65	0.62	5.13	7.32
% of total sinus length	36.6	2.1	32.6	39.1
RS width (mm)	3.51	0.15	3.30	3.82
DC thickness at level of RS (mm)	0.46	0.04	0.37	0.53

Table 4.1. Longitudinal section F-SC morphometrics.

	Mean	S.D.	Minimum	Maximum
Max diameter of the F-SC (mm)	4.30	0.20	4.02	4.70
Max diameter of the LCS (mm)	3.44	0.19	3.16	3.84
Mean longitudinal axis of HS (mm)	1.38	0.15	1.15	1.66
Mean perpendicular axis of HS (mm)	1.02	0.11	0.87	1.22
Ratio HS diameter	0.74	0.05	0.67	0.81
Mean longitudinal axis of ORS (mm)	2.13	0.17	1.82	2.46
Mean perpendicular axis of ORS (mm)	1.67	0.18	1.42	2.06
Ratio ORS diameter	0.78	0.05	0.71	0.87

Table 4.2. Transverse section F-SC morphometrics.

Other structural features included the presence of a glandular network composed of sebaceous glands and tubular glands spanning the upper ~4 to 5 mm of the UCS (Fig. 4.4). The tubular glands had a myoepithelium and were putatively identified as apocrine sweat glands. Granules of an unknown substance ~1 µm in diameter were observed within the secretory portion of the apocrine sweat glands for some of the samples, which further supported the identification. There were four or more sebaceous glands and two or more apocrine sweat glands for each F-SC; secretions of each appeared to empty directly into the hair canal. The apocrine sweat glands were located along the periphery of the UCS in close proximity to the DC, while the sebaceous glands were more centrally located.

Blood vessels were observed to transect the DC and enter the F-SC at its base and at the mid-UCS. Putative nutritional blood vessels transected the DC in the upper UCS adjacent to the glandular network (Fig. 4.5).

4.3.3 F-SC Innervation

The deep vibrissal nerve (DVN) entered through the base of the DC and subdivided into smaller branches that coursed apically through the LCS (Fig. 4.2B). Branches extended through

the LCS, RS, and RW to the ICB, innervating structures along this path. Axons terminated on presumptive mechanoreceptors located along the junction of the GM and ORS in the LCS, RS, and ICB. No axons were observed in the UCS, indicating that a superficial vibrissal nerve (SVN) was not present.

The mean number of axons present at the level of the mid-LCS was 1,584.89 ± 281 (N = 15) (range 1,164–2,161) (Fig. 4.6) and was not highly correlated with LCS diameter, F-SC length, or animal length. There was a weak relationship ($R^2 = 0.65$) between the number of myelinated axons and body mass. Mechanoreceptors presumed to be Merkel-cell neurite complexes (MNCs) and lanceolate receptors were present along the junction of the GM and ORS in the LCS and RS (Fig. 4.7).

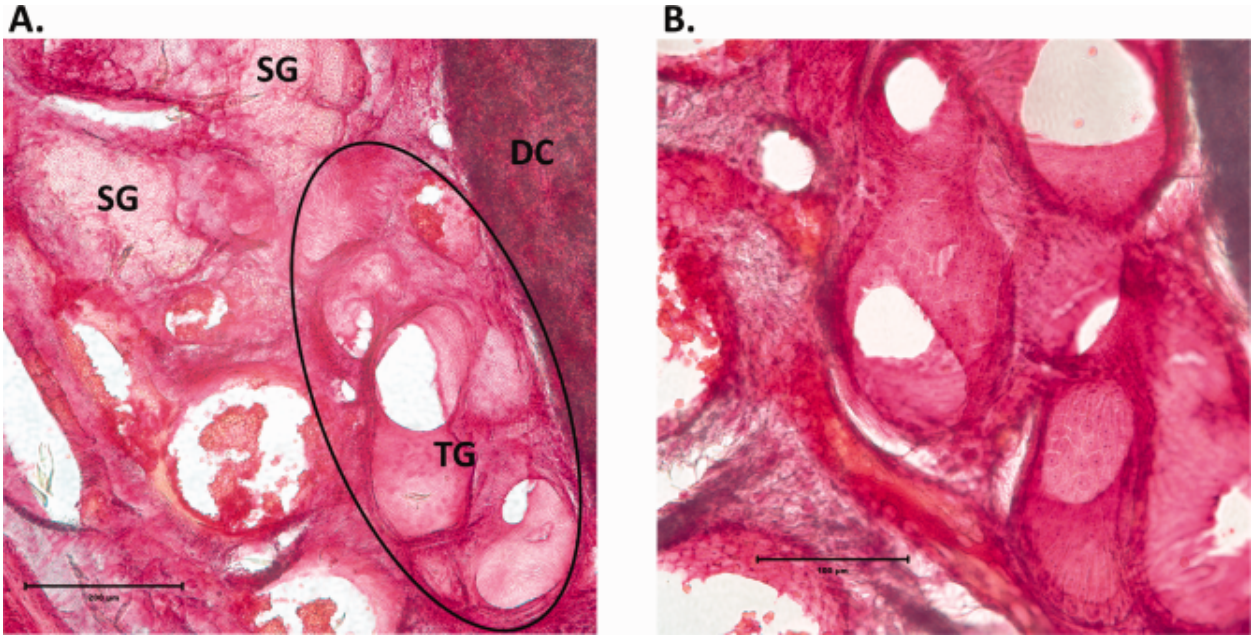

Figure 4.4. Sebaceous and tubular glands located within the glandular network of the UCS. A. The secretory portion of a tubular gland is circled (calibration mark is 200 µm). SG = sebaceous gland element, TG = tubular gland element. B. Tubular gland located within the glandular network of the UCS (calibration mark is 100 µm); A and B processed with a modified Masson's trichrome stain.

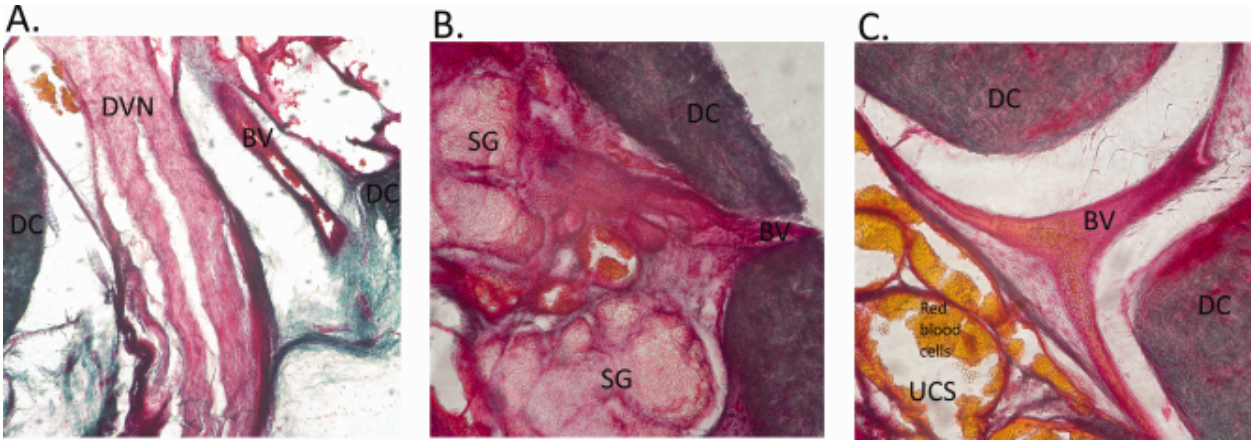

Figure 4.5. Blood vessels of the F-SC. A. Blood vessel entering through the DC at the base of the F-SC. BV = blood vessel. B. Putative nutritional blood vessel transecting the DC and entering the glandular network in the upper UCS. C. Blood vessel traversing the DC at the mid-UCS; A, B, and C processed with a modified Masson's trichrome stain.

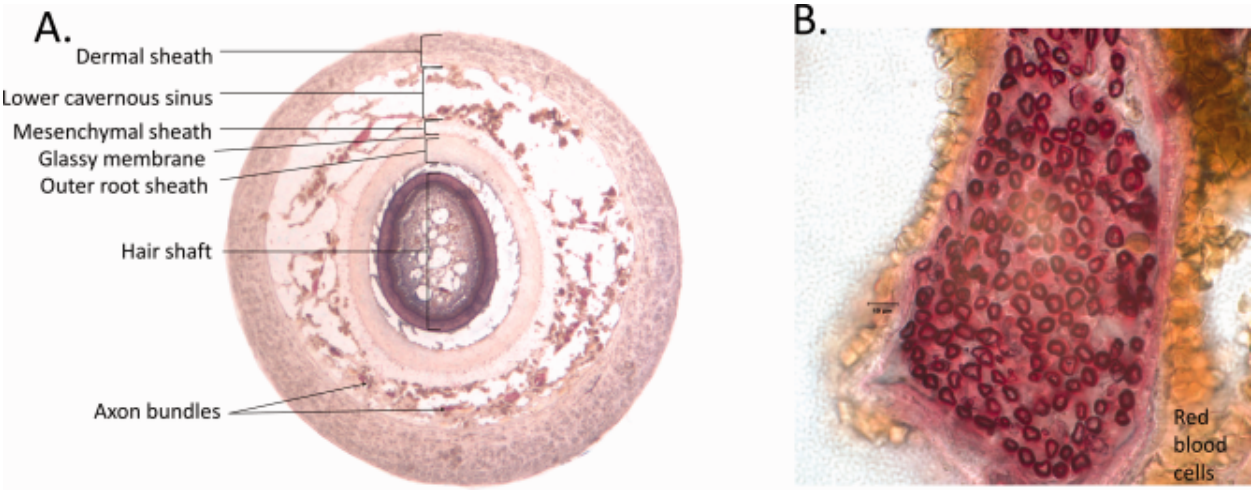

Figure 4.6. Axon bundles in the LCS. **A**. Cross-section at the level of the mid-LCS. **B**. Axon bundle (calibration mark is 10 µm). Myelinated sheaths of individual axons are stained red; A and B processed with a Bodian silver stain.

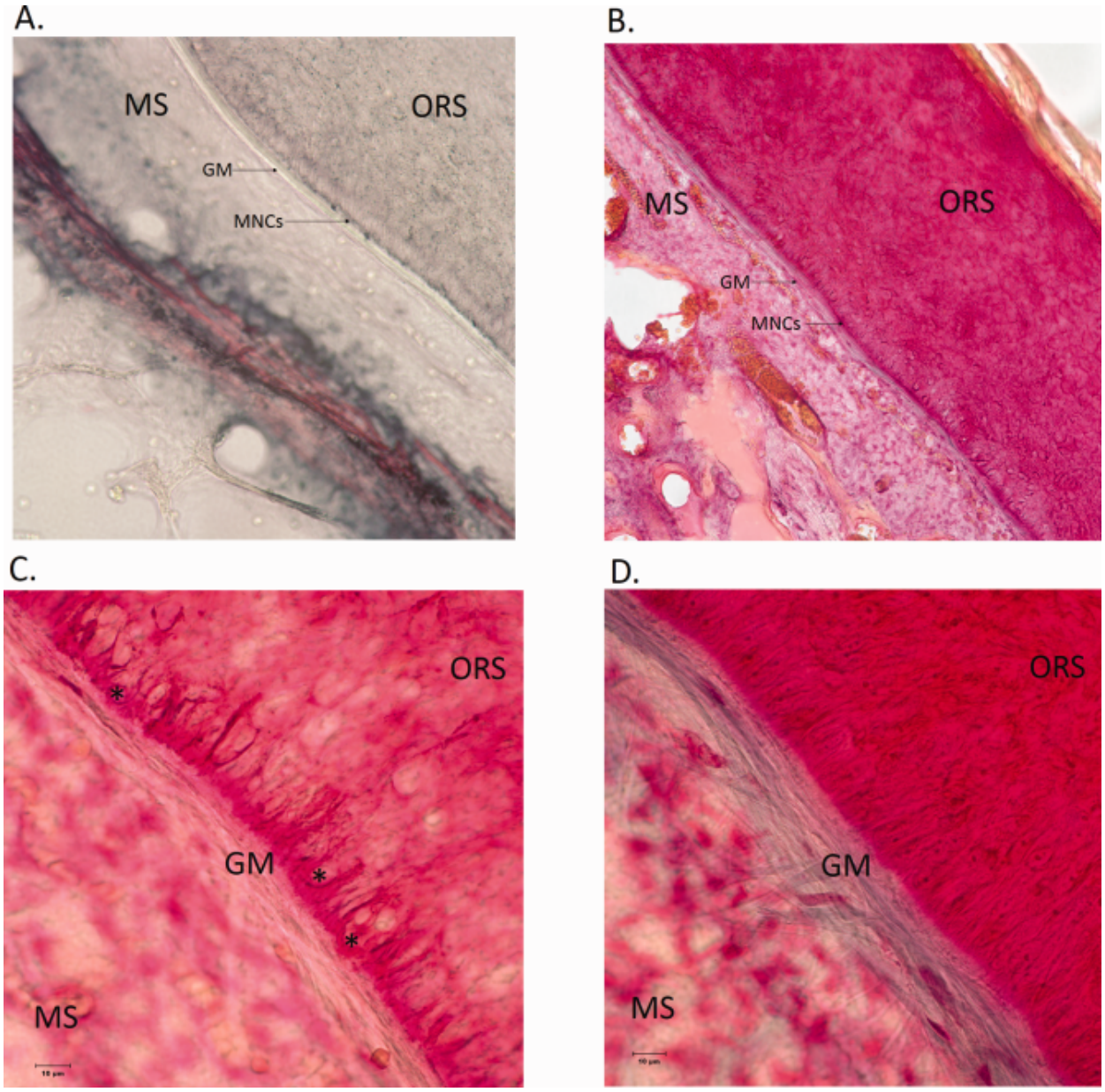

Figure 4.7. Mechanoreceptors in the LCS. A. Mechanoreceptors (MNCs) located at the junction of the GM and ORS in the upper LCS. B.Mechanoreceptors located along the junction of the GM and ORS in the upper LCS. C. Presumed Merkel cell-neurite complexes (MNCs, *) in the upper LCS (calibration mark is 10 µm) D. Nerve tufts (grayish streaks along GM) terminating on mechanoreceptors in the upper LCS (calibration mark is 10 µm); A processed with a Bodian silver stain; B, C, and D processed with a modified Massons's trichrome stain.

4.4 Discussion

4.4.1 Vibrissal Hairshafts

The number of vibrissae in the mystacial array of NES is similar to that of other phocids that forage pelagically (Dehnhardt and Kaminski, 1995; Ling, 1966, 1972; Ling, 1977; Marshall et al., 2006; Yablokov and Klezeval, 1969). The longest vibrissa measured in this study was 13.8 cm. The two yearlings in this study had longer vibrissae than the pups. It is probable that NES vibrissae attain even longer dimensions in adults. It is known that larger southern elephant seals (*Mirounga leonina*) have longer vibrissae than smaller animals, with lengths measuring up to 16 cm in large adults (Ling, 1966). Among other pinnipeds, maximum vibrissal lengths are 4 cm in the Ross seal (*Ommatophoca rossii*) (Ling, 1972), 22 cm in bearded seal (*Erignathus barbatus*) juveniles (Marshall et al., 2006), and 15 cm in northern fur seals (*Callorhinus ursinus*) (Ladygina et al., 1985), although these are approximations because over time vibrissae can sustain damage and wear, becoming abraded (Marshall et al., 2006).

The beaded profile in NES vibrissal hair shafts is a distinctive feature observed in most species of phocids (Ginter et al., 2012; Ginter et al., 2010; Hanke et al., 2013; Hyvärinen, 1995; Hyvärinen et al., 2009; Ling, 1966; Yablokov and Klezeval, 1969), with the known exceptions of monk seals (*Monachus* sp.), bearded seals, Ross seals, and leopard seals (*Hydrurga leptonyx*) (Berta et al., 2006; Ginter et al., 2012; Ginter et al., 2010; Ling, 1972; Marshall et al., 2006). This stands in contrast to the smooth vibrissal hair shafts of otariids and terrestrial mammals (Ginter et al., 2012; Hanke et al., 2013; Hyvärinen et al., 2009) and has functional significance in terms of sensory perception. The beaded profile of harbor seal vibrissae suppresses vortex shedding while the vibrissae are moving through water, resulting in a higher signal-to-noise ratio than that experienced by smooth vibrissae (Hanke et al., 2013; Hanke et al., 2010).

4.4.2 F-SC Microstructure

The average F-SC length of NES (20 mm) was similar to that observed in other pinnipeds, which include 18 mm in Ross seals (Ling, 1972), 19.1 mm in bearded seals (Marshall et al., 2006), and ~20 mm in ringed seals (Hyvärinen and Katajisto, 1984). In this study, the RS comprised 14% of the F-SC length in NES, which is lower than the roughly 20% reported in the southern elephant seal (Ling, 1966) but similar to the 13% reported in bearded seals (Marshall et al., 2006). Qualitatively, the ringwulst in NES mystacial F-SCs appears similar in size to that described in southern elephant seals (Ling, 1966), but appears much smaller than that observed in bearded and ringed seals (Hyvärinen, 1989, 1995; Marshall et al., 2006). The presence of an UCS is a distinctive feature of pinniped vibrissae (Hyvärinen, 1989; Hyvärinen et al., 2009; Marshall et al., 2006). The UCS comprised 47% of the F-SC length in NES, which is similar to about 40% in southern elephant seals (Ling, 1966) and ~60% in bearded seals (Marshall et al., 2006) and ringed seals (Hyvärinen, 1989). Dehnhardt et al. (2003) hypothesized that the long UCS functions to thermally protect the ICB, RS, LCS, and associated mechanoreceptors, thereby maintaining discriminatory capabilities when diving in cold water (Hyvärinen, 1989; Hyvärinen and Katajisto, 1984; Hyvärinen et al., 2009). Measurements of follicle temperature and thermal imaging of harbor seals have shown that F-SC temperature remains elevated above ambient and that vibrissae do not lose sensitivity in colder water (Dehnhardt et al., 1998; Erdsack et al., 2014). A similar outcome may be achieved by arteriovenous anastomoses thought to be present in the dermis surrounding the F-SCs in ringed seals and Florida manatees (*Trichechus manatus latirostris*) (Hyvärinen and Katajisto, 1984; Sarko et al., 2007) and by an extended neck area in the F-SC of Australian water rats *(Hydromys chrysogaster)* which comprises 20% of the total F-

SC length (Dehnhardt et al., 1999). An enlarged UCS in excess of 55% may be indicative of ice seals inhabiting very cold waters. Additional comparative data are needed to test this hypothesis.

Blood vessels were observed entering the F-SC at the base and transecting the DC at the level of the UCS. Vessels crossing the upper UCS appeared to intermingle with elements of the glandular network to supply nutrients to the glands. Vessels entering at the base or crossing the mid-UCS appeared to empty directly into the sinus. Blood vessels supplying the UCS in pinnipeds have not been previously described; blood vessels have been documented penetrating the F-SC solely at the base (Hyvärinen, 1989; Hyvärinen and Katajisto, 1984; Stephens et al., 1973; Yablokov and Klezeval, 1969). Blood vessels were not observed transecting the DC in the RS. Yablokov and Klezeval (1969) commented on the curious lack of blood vessels traversing the side of the follicle in the walrus, hooded seal, and Greenland seal, as they had observed that blood vessels bisected the DC in the F-SCs of mysticetes at numerous places along the side of the follicle. Cats, rats, and rhesus monkeys also have blood vessels that transect the DC on the side of the follicle (Ebara et al., 2002; Van Horn, 1970). This is the first evidence to suggest that blood supply to the LCS and UCS may be separate and distinct. It is possible that the thick connective tissue band between the UCS and RS effectively prevents blood flow between the UCS and the RS/LCS. This has implications regarding thermoregulation of the F-SC and associated mechanoreceptors and warrants further investigation.

Because blood is incompressible, even a slight deflection of the vibrissa will shift the fluid in the sinus (Japha, 1910). This suggests that the vibrissa could be rendered more or less sensitive by increasing or decreasing the blood pressure within the sinus. Recording of afferent neurons from the F-SCs of cats during stimulation of the vibrissae revealed that opening the follicle, and thereby decreasing blood pressure within the sinus complex, completely stopped or weakened

spike activity from certain slow-adapting receptors (Gottschaldt et al., 1973). The presence of blood vessels in the LCS and UCS of the northern elephant seal indicates the ability to regulate blood pressure, and thus sensitivity, within the F-SC.

Tubular glands were observed in the upper UCS of NES mystacial vibrissae. Similar structures were also described in southern elephant seals (Ling, 1966) and Ross seals (Ling, 1972); studies of the vibrissae of bearded seals and ringed seals did not report these structures (Hyvärinen and Katajisto, 1984; Hyvärinen et al., 2009; Marshall et al., 2006). The function of these glands in NES is unknown, but apocrine sweat glands are present to some degree in association with pelage hairs in all pinnipeds, albeit reduced in size from those of terrestrial mammals. Although there is a consensus that otariids have apocrine sweat glands associated with the majority of pelage hair follicles, there is less agreement about the pervasiveness of these glands in phocid seals. Some studies have reported their existence in most or all pelage hair follicles (Gray et al., 2006; Ling, 1968; Montagna and Harrison, 1957), while other studies have described a less frequent occurrence on specific parts of the body (Khamas et al., 2012). Apocrine sweat glands are more prominent in otariids than phocids and may even have some function in thermoregulation. While it is doubtful that there is any thermoregulatory benefit in phocids (Khamas et al., 2012; Ling, 1965, 1970), it is probable that the structures have some chemosensory function during haul-out behaviors. Studies of the development of pelage hairs in southern elephant seal fetuses showed that the apocrine sweat glands begin to form before the sebaceous glands, although the secretory tubular portion is slower to develop and is not complete until just before or shortly after birth (Ling and Thomas, 1967). We suggest that apocrine sweat glands may provide chemosensory information either for mom-pup recognition or sexual signaling. There is some evidence that enlarged apocrine sweat glands associated with pelage

follicles on the face are linked to sexual signaling in male gray seals (*Halichoerus grypus*) and male ringed seals (Hardy et al., 1991). Ahl (1986) suggested that movement of the vibrissae may function to disseminate pheromones.

4.4.3 F-SC Innervation

The DVN penetrated the DC of NES at the base rather than laterally as exhibited in terrestrial mammals. This entry location has also been reported in other pinnipeds and mysticete whales (Japha, 1910; Ling, 1966; Marshall et al., 2006; Stephens et al., 1973). Effort was spent searching for axons in the UCS since Ling (1966) reported observing axons in the UCS of southern elephant seal mystacial F-SCs. However, no axons were observed in the UCS nor other pinniped F-SCs for which data are available (Hyvärinen et al., 2009; Marshall et al., 2006). The F-SCs of all terrestrial mammals studied thus far, as well as the semiaquatic Australian water rat, are innervated by the SVN at the apical portion of the follicle and by the DVN near the follicular base (Dehnhardt et al., 1999; Dykes, 1975; Rice et al., 1986).

The average number of axons per vibrissa (1,584) was similar to that observed in other pinnipeds: bearded seals 1,314 (max 1,650) (Marshall et al., 2006), harp seals ~1,100 (Yablokov and Klezeval, 1969), and ringed seals 1,350 (Hyvärinen et al., 2009). Overall, innervation to the mystacial field is similar among most pinnipeds studied, with the exception of bearded seals, which have increased innervation to the mystacial field as a result of their greater number of vibrissae (122 per side compared with 50 per side in NES). This is likely due to differences in foraging location (benthic *vs*. pelagic) and use of vibrissae (active touch *vs*. of hydrodynamic sensation) (Marshall et al., 2006). The estimated mean number of axons innervating the mystacial array in NES is 159,097. This number is remarkably close to that reported for ringed seals and sea otters (Hyvärinen et al., 2009; Marshall et al., 2014a). The number of axons

innervating each F-SC in NES and other pinnipeds indicates that these are extremely sensitive sensory organs. Neurological recordings of the region of the somatosensory cortex that receives afferent fibers from mystacial vibrissae in northern fur seals provides further evidence for the sensitivity of these structures in pinnipeds; the vibrissal projections have their own dedicated region within the cortical region that represents the face (Ladygina et al., 1985).

The increased innervation to individual pinniped F-SCs relative to that of terrestrial and semiaquatic animals cannot be attributed solely to the increase in F-SC length that is also observed. Individual F-SCs in the humpback whale (*Megaptera novaeangliae*), which also average about 20 mm in length, are innervated by 300 to 450 axons (Japha, 1910). Likewise, F-SCs approaching similar lengths (10.7–18.5 mm) in the Florida manatee are innervated by 210 to 254 axons (Reep et al., 2001). In contrast, the caudal F-SCs of Australian water rats, which measure ~6.3 mm in length, are each innervated by an average of 560 axons (Dehnhardt et al., 1999). This information indicates that innervation cannot be predicted by F-SC size alone when making comparisons between taxa.

Within species, there is some evidence that larger F-SCs are innervated by a larger number of axons. Ringed seal caudoventral F-SCs are innervated by an average of 1,540 axons compared with 1,050 to 1,200 axons in smaller rostrodorsal F-SCs (Hyvärinen et al., 2009) There is a similar trend in Australian water rats, with 537 versus 363 axons in caudoventral and rostrodorsal F-SCS, respectively (Dehnhardt et al., 1999). The current study focused on caudoventral F-SCs of NES; further investigation is needed to determine whether axon counts scale to F-SC size in this species. For this reason, the projected mean number of axons innervating the mystacial array in NES predicted in this study should be regarded as a maximum estimate. In the present study, axon counts were conducted at the midlevel of the LCS. It is

undetermined if larger F-SCs are innervated by a greater number of axons or if there is greater branching of axons before DVN entry into larger F-SCs. Is it unknown to what extent (or indeed, whether) individual axons from the DVN branch as they ascend through the F-SC. Hyvärinen et al. (2009) conducted axon counts on the DVN just before entry into the F-SC in ringed seal vibrissae and obtained very similar numbers (1,540 axons per caudal F-SC compared with 1,584 in this study), so it seems unlikely that much branching of individual axons occurs between the base of the F-SC and the mid-LCS. Whether branching of individual axons occurs in the upper LCS or RS is unknown. Substantial branching of axons for an individual F-SC would have implications regarding the directionality of sensory information from individual vibrissae. It is worth noting that most individual F-SCs are represented by similarly sized cortical areas in the northern fur seal somatosensory cortex, with the exception of the first, generally smaller, row of vibrissae, which are each represented by reduced cortical areas (Ladygina et al., 1985).

4.4.4 Use of Vibrissae

The mystacial vibrissae of pinnipeds are highly mobile (Ahl, 1986; Hyvärinen, 1995) due to a lack of strong connective tissue attachments between the F-SCs and the surrounding dermis (Yablokov and Klezeval, 1969). Striated muscle fibers are attached to the bases of pinniped F-SCs (Hyvärinen, 1989; Ling, 1966; Marshall et al., 2006), demonstrating that they are under voluntary control (Dehnhardt et al., 2003). Mystacial vibrissae are protracted when seals use them for active touching (Dehnhardt, 1994; Dehnhardt and Dücker, 1996), investigating water movement (Wieskotten et al., 2011), or pursuing a hydrodynamic trail (Dehnhardt et al., 2001; Gläser et al., 2011; Schulte-Pelkum et al., 2007).

Mechanoreceptors of NES F-SCs characterized in this study deserve detailed follow-up with electron microscopy. However, based on our observations, we predict that mechanoreceptor

types and locations of NES are consistent with that of other pinnipeds. In general, F-SCs of pinnipeds feature a myriad of mechanoreceptor types also found in terrestrial species (Rice et al., 1986), including lanceolate endings, Merkel-cell neurite complexes (MNCs), and lamellated corpuscles (Dehnhardt and Dücker, 1996; Dykes, 1975; Hyvärinen, 1989; Hyvärinen and Katajisto, 1984; Marshall et al., 2006; Stephens et al., 1973). These mechanoreceptors are located along the junction of the GM and the ORS in the LCS and RS (Hyvärinen, 1995; Marshall et al., 2006). The LCS of southern elephant seals is reported to possess more delicate and elastic trabeculae than the UCS, and is thus exposed to the greatest amount of bending (Ling, 1966). Our observations confirm this distinction in NES. It has been hypothesized that F-SC mechanoreceptors are compressed on the leading side of the deflected shaft and stretched on the opposite side (Dehnhardt et al., 1999; Dykes, 1975; Gottschaldt et al., 1973). As in other seals, the hair shaft of NES is keratinized throughout its entire length, and the ORS maximum to minimum diameter ratio is practically identical to that of the HS so that forces should transmit effectively from the outer HS to the mechanoreceptors located in the GM.

NES likely use a combination of sensory modalities to locate prey underwater (Schulte-Pelkum et al., 2007), and there is increasing evidence that the vibrissae are an important sensory modality for foraging in all pinnipeds. Studies with captive harbor seals, California sea lions, and walruses have demonstrated that they are able to use their vibrissae to accurately discriminate between objects of different sizes and shapes with a high resolving capacity similar to that of a prehensile organ (Dehnhardt, 1990; Dehnhardt and Dücker, 1996; Dehnhardt and Kaminski, 1995; Kastelein and Van Gaalen, 1988). California sea lions and harbor seals are also able to use their vibrissae to follow abiotic and biotic trails in the water (Dehnhardt et al., 2001; Gläser et al., 2011; Schulte-Pelkum et al., 2007). Harbor seals, as a representative generalized phocid

species, have highly sensitive and directional vibrissae (Hanke et al., 2013; Hanke et al., 2012; Renouf, 1979) which enables them to determine directionality of water flow when approaching a hydrodynamic trail from a perpendicular angle, detect and follow turns in the trail (Dehnhardt et al., 2001), and discriminate between wakes created by objects of differing sizes and shapes (Wieskotten et al., 2011).

Our work adds to the growing body of evidence that phocids and perhaps all pinnipeds, which exhibit varying and divergent feeding niches, possess highly sensitive mystacial vibrissae that detect prey. This is supported by animal-borne video camera footage of southern elephant seals, Weddell seals (*Leptonychotes weddellii*), and Steller sea lions (*Eumetopias jubatus)* foraging that demonstrate the mystacial vibrissae are protracted during pursuit of prey (McGovern KA, Davis RW, Olivier P, personal observations). For NES, recent work by Naito et al. (2013), in which jaw accelerometers were deployed on NES, demonstrated jaw movements associated with feeding at depths ranging from 507 to 562 m. Still images revealed foraging on myctophids and bathylagids (Naito et al., 2013). In addition, the still images were partially occluded by the mystacial vibrissae (Naito et al., 2013), which could only occur if the seals' vibrissae were protracted at the time of the image. These data confirm that NES forage at depth (>500 m) on prey that are not bioluminescent (bathylagids) and confirms protraction of vibrissae before prey capture, signifying that these seals complement vision with vibrotactile cues for prey localization. The number of myelinated axons in individual NES vibrissae supports our hypothesis that NES vibrissae are highly sensitive and likely are an important sensory modality for prey capture.

5. SUMMARY

5.1 Summary

I used video and movement data obtained from animal-borne video and data recorders (VDRs) and histological data obtained from vibrissal pads of elephant seals to address the questions: when, where, how, and on what prey do female southern elephant seals forage? The annual cycle of southern elephant seals for breeding, molting, and foraging is well known. Females spend ca. ten months per year at sea divided into a two-month post-breeding trip and eight-month post-molting trip (Le Boeuf and Laws, 1994). They exhibit a diurnal dive pattern in deep water, diving to shallower depths at night than during the day, presumably while foraging in the deep-scattering layer (Campagna et al., 1998; Hindell et al., 2016; McIntyre et al., 2011; McIntyre et al., 2010; Vacquié-Garcia et al., 2015). However, there is little information about their foraging strategies, hunting tactics, habitat-associations and sensory biology at sea.

Female southern elephant seals from Península Valdés traversed the continental shelf in 3.7 days to forage in the deep waters of the Patagonian continental slope and Argentine Basin, where I identified three distinct dive types and their functions (foraging, resting and transiting). Compared to resting and transit dives, foraging dives were deeper and less linear with bursts of speed, steeper descent and ascent angles, longer two-dimensional and three-dimensional dive paths, and greater variation in speed, descent angle, and vertical head movements. Seals completed 48.2 foraging dives $\pm$ 10.3 s.d. per day at depths of 689 m $\pm$ 213 s.d. during daylight hours and 391 m $\pm$ 219 s.d. during the night. Prey species imaged on video over the continental slope included herring smelt (*Argentinidae*) and myctophids (*Myctophidae*). On average, there were 3.4 prey encounters $\pm$ 2.1 s.d. during a foraging dive, each lasting 28 seconds $\pm$ 19.3 s.d. in duration and possibly representing more than one prey capture or attempt. In total, 98% of all

foraging dives were part of a bout consisting of 14 dives ± 8.4 s.d. When the cumulative prey encounter duration as a function of dive duration was compared by time of day, daytime dives were found to be significantly less successful than dives during dawn, dusk, or night.

While at sea, females spent 3.9% of their time resting or possibly sleeping at depth. Resting dives included drift dives and dives in which the seals rested on the ocean floor over the continental shelf and slope. In resting dives over the deeper water of the continental slope and Argentine Basin, seals typically glided to 100-200 m before beginning the drift portion of the dive, which was 6.7 min ± 4.5 s.d. in duration. Compared to foraging and transit dives, resting dives were longer in duration with shorter two-dimensional dive paths, lower stroking rates and speeds, and greater variation in pitch and roll angle during descent.

While traversing the continental shelf at the beginning and end of the post-breeding foraging trip and when moving to new foraging areas, the females made transit dives instead of swimming at the surface. Seals glided to depth and then either stroked continuously or used a stroke-and-glide mode of locomotion. Transit dives were shallower and more linear with higher swim speeds and stroking rates, shorter durations, shallower ascent angles, and farther straight-line distances traveled.

I used first passage time analysis to quantify the spatial scale(s) at which search effort was concentrated along the foraging trip trajectory (Bailleul et al., 2008; Fauchald and Tveraa, 2003). Over the course of the foraging trip, horizontal area-restricted search occurred on a scale of 45 km. Over the course of an individual dive, three-dimensional area-restricted search occurred at a scale of 10 m, representing the scale at which seals search for, pursue, and handle prey.

I found evidence for a temporal pattern in dive type. Resting dives comprised a significantly larger percentage of dives during daylight hours, with the greatest frequency between the hours

of 0700-1300 local time over the slope and 0600-1300 local time over the basin. Over the Argentine Basin, foraging dives comprised a significantly higher percentage of dives during dusk and dawn, with greater frequency between the hours of 1400-0500 local time. According to optimal foraging theory, animals should minimize the cost of transport to their foraging locations (Crocker et al., 2001). Although these seals travel large horizontal distances over the course of their foraging trips (81 km per day), they rest preferentially during the daytime when prey are deeper, thus minimizing the energetic cost of accessing prey at depth.

Over the continental slope, seals foraged at depths of 501 m $\pm$ 234 s.d., temperatures of 3.73°C $\pm$ 0.8 s.d. and salinities of 33.55 psu $\pm$ 0.21 s.d. Over the deep waters of the Argentine Basin, seals foraged at depths of 461 m $\pm$ 284 s.d, temperatures of 3.73°C $\pm$ 1.33 s.d. and salinities of 33.95 psu $\pm$ 0.42 s.d. Foraging was predominantly associated with waters of Antarctic and Sub-Antarctic origin at depth, with 70% of foraging dives occurring in Sub-Antarctic Mode Water, 17% in Antarctic Intermediate Water, 11% in Upper Circumpolar Deep Water, and a mere 2% in Sub-Tropical Mode Water. The seals that foraged in Upper Circumpolar Deep Water traveled along the southwest rim of the Argentine Basin where the Upper Circumpolar Deep Water is closer to the surface. Seals foraged in similar water masses to southern elephant seal colonies located farther south and avoided foraging in subtropical waters that were just as accessible to them as the subantarctic waters. The seals in this study foraged in association with the northernmost excursion of the Antarctic Circumpolar Current, the Malvinas Current (Talley, 2011).

When considering sea surface hydrography and bathymetry, seals foraged in association with: 1) bathymetries >3,000 m; surface temperatures of 11.7-15.5°C likely corresponding to mixed surface waters in the confluence zone, 3) chlorophyll concentration (>5.8 mg ml-3), 4) the diel

period from late afternoon to dawn (1350-0439 local time). Seals showed decreased foraging in association with: 1) increased sea surface height anomaly (>0.06 m) likely corresponding to meanders and warm-core eddies shed from the Brazil Current, 2) surface temperatures of 7.1-11.7°C likely corresponding to waters on the continental shelf and slope, 3) daylight hours of 0439-1350 local time. Seals foraged mainly (74.5% of foraging dives) where there were no known eddies (aged at least 4 weeks), whereas 21% and 5% of foraging dives were located within cold-core and warm-core eddies, respectively.

Fish sampling studies indicate that at least 13 known prey species of southern elephant seals are found in the waters of the continental shelf, slope, and Argentine Basin (Appendix A, Table A.2) (Cousseau et al., 2012; Figueroa et al., 1998). In this study, southern elephant seal females from Península Valdés foraged on *Myctophidae* and *Argentinidae* over the continental slope. Known prey of southern elephant seals also includes a number of cephalopod species (Appendix A, Table A.2). Although seals were not observed foraging on cephalopods in this study, *Martiala hyadensi*, a known prey species, occurs at times in great abundance in waters over the continental slope. There is also a large fishery for Argentine shortfin squid, *Ilex argentinus*, over the continental slope (Boyle and Rodhouse, 2008), although there is no known evidence that they are exploited by southern elephant seals.

I found that elephant seal vibrissae have similar microstructure and innervation as other pinniped species. Northern elephant seals have 1,584 axons per vibrissae, similar to that found in bearded, harp, and ringed seals (Hyvärinen et al., 2009; Marshall et al., 2006; Yablokov and Klezeval, 1969). California sea lions and harbor seals are able to detect and track hydrodynamic trails using their vibrissae alone (Dehnhardt et al., 2001; Gläser et al., 2011; Schulte-Pelkum et al., 2007). Hydrodynamic trails left behind by swimming prey can persist on the order of

minutes and have particle velocities within the detection range of the vibrissae (Dehnhardt et al., 2003; Fish and Lauder, 2006; Hanke and Bleckmann, 2004; Hanke et al., 2000). Neurological recordings of the region of the somatosensory cortex that receives afferent fibers from mystacial vibrissae in northern fur seals shows that the vibrissal projections have their own dedicated region within the cortical region that represents the face (Ladygina et al., 1985), further indicating that the vibrissae are highly sensitive sensory structures. The video recordings in this study showed that the elephant seals' vibrissae were protracted during periods of foraging. Although elephant seals likely use a combination of sensory modalities to locate prey underwater, the evidence presented in this volume adds to the growing body of evidence that phocids, and perhaps all pinnipeds, possess highly sensitive vibrissae that are viable sensory structures for prey detection and capture.

In conclusion, female southern elephant seals from Península Valdés depart the coast after breeding and traverse the continental shelf in less than 4 days at an easterly heading en route to the deep waters of the Patagonian continental slope and Argentine Basin where they begin making foraging dives in deep, cold water originating in south polar regions. While at sea for 75 days, they travel an average horizontal distance of 6,080 km and make 2,815 foraging dives to an average depth of 469 m in water with a temperature of 3.7°C and a salinity of 33.8 psu. Their primary prey are small fish and possibly other prey that they detect and capture in total darkness using vision and the tactile sensory system in their vibrissae. Between bouts of foraging dives, they make transit dives to new foraging areas or rest and probably sleep while drifting to an average maximum depth of 375 m. Of the 18 species of seals in the family Phocidae, southern elephant seals are the deepest diving and most pelagic. Each year, females spend 10 months at sea and 89% of their time submerged while transiting, hunting and resting at depth.

5.2 Future research

Future research should include deploying VDRs on both female and male southern elephant seals from the Península Valdés colony during the post-breeding and post-molting season to compare foraging location and prey preference. This would help identify the trophic level(s) occupied by the seals, determine the range and differences of prey species exploited by females and males, and shed some light on whether males and/or females are generalist or specialist feeders. Future fisheries sampling research to determine the distribution of potential prey species and their association with hydrographic variables over the Argentine Basin would complement research on elephant seal foraging behavior.

REFERENCES

Acha, E.M., Mianzan, H.W., Guerrero, R.A., Favero, M., Bava, J., 2004. Marine fronts at the continental shelves of austral South America: Physical and ecological processes. J. Mar. Syst. 44, 83-105.

Adachi, T., Costa, D.P., Robinson, P.W., Peterson, S.H., Yamamichi, M., Naito, Y., Takahashi, A., 2017. Searching for prey in a three-dimensional environment: hierarchical movements enhance foraging success in northern elephant seals. Funct. Ecol. 31, 361-369.

Ahl, A.S., 1986. The role of vibrissae in behavior: a status review. Vet. Res. Commun. 10, 245-268.

Ahl, A.S., 1987. Relationship of vibrissal length and habits in the Sciuridae. J. Mammal. 68, 848-853.

AVISO, 2017. The Mesoscale Eddy Trajectory Atlas products were produced by SSALTO/DUACS and distributed by AVISO+ with support from CNES, in collaboration with Oregon State University with support from NASA.

Bailleul, F., Charrassin, J.B., Ezraty, R., Girard-Ardhuin, F., McMahon, C., Field, I., Guinet, C., 2007. Southern elephant seals from Kerguelen Islands confronted by Antarctic Sea ice. Changes in movements and in diving behaviour. Deep-Sea Res. (II Top. Stud. Oceanogr.) 54, 343-355.

Bailleul, F., Pinaud, D., Hindell, M., Charrassin, J.B.Î., Guinet, C., 2008. Assessment of scale dependent foraging behaviour in southern elephant seals incorporating the vertical dimension: a development of the First Passage Time method. J. Anim. Ecol. 77, 948-957.

Ballance, L.T., Pitman, R.L., Fiedler, P.C., 2006. Oceanographic influences on seabirds and cetaceans of the eastern tropical Pacific: a review. Prog. Oceanogr. 69, 360-390.

Berta, A., Sumich, J.L., Kovacs, K.M., 2006. Marine Mammals: Evolutionary Biology. Academic Press.

Biuw, M., Boehme, L., Guinet, C., Hindell, M., Costa, D., Charrassin, J., Roquet, F., Bailleul, F., Meredith, M., Thorpe, S., 2007. Variations in behavior and condition of a Southern Ocean top predator in relation to in situ oceanographic conditions. Proc. Natl. Acad. Sci. 104, 13705-13710.

Biuw, M., Nøst, O.A., Stien, A., Zhou, Q., Lydersen, C., Kovacs, K.M., 2010. Effects of Hydrographic Variability on the Spatial, Seasonal and Diel Diving Patterns of Southern Elephant Seals in the Eastern Weddell Sea. PLoS ONE 5, e13816.

Bivand, R., Lewin-Koh, N., 2013. maptools: Tools for reading and handling spatial objects. R package version 0.8 27.

Bivand, R., Rundel, C., 2013. rgeos: interface to geometry engine-open source (GEOS). R package version 0.3-2.

Bodian, D., 1936. A new method for staining nerve fibers and nerve endings in mounted paraffin sections. Anat. Rec. 65, 89-97.

Boyd, I., Arnbom, T., 1991. Diving behaviour in relation to water temperature in the southern elephant seal: foraging implications. Polar Biol. 11, 259-266.

Boyle, P., Rodhouse, P., 2008. Cephalopods: ecology and fisheries. John Wiley & Sons.

Bradshaw, C., Hindell, M., Best, N., Phillips, K., Wilson, G., Nichols, P., 2003. You are what you eat: describing the foraging ecology of southern elephant seals (Mirounga leonina) using blubber fatty acids. Proc. R. Soc. (B Biol. Sci.) 270, 1283-1292.

Brown, D.J., Boyd, I.L., Cripps, G.C., Butler, P.J., 1999. Fatty acid signature analysis from the milk of Antarctic fur seals and Southern elephant seals from South Georgia: implications for diet determination. Mar. Ecol. Prog. Ser. 187, 251-263.

Burns, Jennifer M., Williams, T.M., Secor, Stephen M., Owen-Smith, N., Bargmann, Naomi A., Castellini, Michael A., 2006. New Insights into the Physiology of Natural Foraging. Physiol. Biochem. Zool. 79, 242-249.

Burton, H., van den Hoff, J., 2002. Humans and the southern elephant seal Mirounga leonina. Aust. Mammal. 24, 127-139.

Campagna, C., Fedak, M., McConnell, B., 1999. Post-breeding distribution and diving behavior of adult male southern elephant seals from Patagonia. J. Mammal. 80, 1341-1352.

Campagna, C., Le Boeuf, B., Blackwell, S., Crocker, D., Quintana, F., 1995. Diving behaviour and foraging location of female southern elephant seals from Patagonia. J. Zool. 236, 55-71.

Campagna, C., Lewis, M., 1992. Growth and distribution of a southern elephant seal colony. Mar. Mamm. Sci. 8, 387-396.

Campagna, C., Lewis, M., Baldi, R., 1993. Breeding biology of southern elephant seals in Patagonia. Mar. Mamm. Sci. 9, 34-47.

Campagna, C., Piola, A.R., Marin, M.R., Lewis, M., Zajaczkovski, U., Fernández, T., 2007. Deep divers in shallow seas: Southern elephant seals on the Patagonian shelf. Deep-Sea Res. (1 Oceanogr. Res. Pap.) 54, 1792-1814.

Campagna, C., Piola, A.R., Rosa Marin, M., Lewis, M., Fernández, T., 2006. Southern elephant seal trajectories, fronts and eddies in the Brazil/Malvinas Confluence. Deep-Sea Res. (1 Oceanogr. Res. Pap.) 53, 1907-1924.

Campagna, C., Quintana, F., Le Boeuf, B., Blackwell, S., Crocker, D., 1998. Diving behaviour and foraging ecology of female southern elephant seals from Patagonia. Aquat. Mamm. 24, 1-12.

Campagna, C., Rivas, A., Marin, M., 2000. Temperature and depth profiles recorded during dives of elephant seals reflect distinct ocean environments. J. Mar. Syst. 24, 299-312.

Carrick, R., Csordas, S., Ingham, S.E., Keith, K., 1962. Studies on the southern elephant seal, Mirounga leonina (L.). III. The annual cycle in relation to age and sex. CSIRO Wildl. Res. 7, 119-160.

Carrick, R., Ingham, S.E., 1962. Studies on the southern elephant seal, Mirounga leonina (L.). V. Population dynamics and utilization. CSIRO Wildl. Res. 7, 198-206.

Carruthers, E., Lewis, K., McCue, T., Westley, P., 2008. Generalized linear models: model selection, diagnostics, and overdispersion. Memorial University of Newfoundland.

Charo, M., Martinez, C., 2000. Subtropical Shelf Front off eastern South America. J. Geophys. Res. 105, 6565-6578.

Cherel, Y., Ducatez, S., Fontaine, C., Richard, P., Guinet, C., 2008. Stable isotopes reveal the trophic position and mesopelagic fish diet of female southern elephant seals breeding on the Kerguelen Islands. Mar. Ecol. Prog. Ser. 370, 239-247.

Clarke, M., MacLeod, N., 1982. Cephalopods in the diet of elephant seals at Signy Island, South Orkney Islands. Brit. Antarct. Surv. B. 57, 27-31.

Corrigan, L., Fabiani, A., Chauke, L., McMahon, C., Bruyn, M., Bester, M., Bastos, A., Campagna, C., Muelbert, M., Hoelzel, A., 2016. Population differentiation in the context of Holocene climate change for a migratory marine species, the southern elephant seal. J. Evol. Biol. 29, 1667-1679.

Cotté, C., d'Ovidio, F., Dragon, A.-C., Guinet, C., Lévy, M., 2015. Flexible preference of southern elephant seals for distinct mesoscale features within the Antarctic Circumpolar Current. Prog. Oceanogr. 131, 46-58.

Cousseau, M.B., Barbini, S.A., Figueroa, D.E., 2012. The presence of southern fishes in the Argentinian continental shelf and adjacent areas. Mar. Biodivers. 42, 73-78.

Crocker, D.E., Le Boeuf, B.J., Naito, Y., Asaga, T., Costa, D.P., 1994. Swim speed and dive function in a female northern elephant seal, in: Le Boeuf, B. (Ed.), Elephant seals: Population ecology, behavior, and physiology, pp. 328-342.

Crocker, D.E., Williams, J.D., Costa, D.P., Le Boeuf, B.J., 2001. Maternal traits and reproductive effort in northern elephant seals. Ecology 82, 3541-3555.

Daneri, G., Carlini, A., Rodhouse, P., 2000. Cephalopod diet of the southern elephant seal, Mirounga leonina, at King George Island, South Shetland Islands. Antarct. Sci. 12, 16-19.

Davis, R., Weihs, D., 2007. Locomotion in diving elephant seals: physical and physiological constraints. Philos. Trans. R. Soc. Lond. B Biol. Sci 362, 2141.

Davis, R.W., Fuiman, L.A., Madden, K.M., Williams, T.M., 2013. Classification and behavior of free-ranging Weddell seal dives based on three-dimensional movements and video-recorded observations. Deep-Sea Res. (II Top. Stud. Oceanogr.) 88-89, 65-77.

Davis, R.W., Fuiman, L.A., Williams, T.M., Horning, M., Hagey, W., 2003. Classification of Weddell seal dives based on three-dimensional movements and video-recorded observations. Mar. Ecol. Prog. Ser. 264, 109-122.

De Bruyn, M., Hall, B.L., Chauke, L.F., Baroni, C., Koch, P.L., Hoelzel, A.R., 2009. Rapid response of a marine mammal species to Holocene climate and habitat change. PLoS genetics 5, e1000554.

Dehnhardt, G., 1990. Preliminary results from psychophysical studies on the tactile sensitivity in marine mammals. Sensory abilities of cetaceans. Plenum Press, New York, 435-446.

Dehnhardt, G., 1994. Tactile size discrimination by a California sea lion (Zalophus californianus) using its mystacial vibrissae. J. Comp. Phys. A. 175, 791-800.

Dehnhardt, G., Dücker, G., 1996. Tactual discrimination of size and shape by a California sea lion (Zalophus californianus). Anim. Learn. Behav. 24, 366-374.

Dehnhardt, G., Hyvärinen, H., Palviainen, A., Klauer, G., 1999. Structure and innervation of the vibrissal follicle-sinus complex in the Australian water rat, Hydromys chrysogaster. J. Comp. Neurol. 411, 550-562.

Dehnhardt, G., Kaminski, A., 1995. Sensitivity of the mystacial vibrissae of harbour seals (Phoca vitulina) for size differences of actively touched objects. J. Exp. Biol. 198, 2317-2323.

Dehnhardt, G., Mauck, B., Hanke, W., Bleckmann, H., 2001. Hydrodynamic trail-following in harbor seals (Phoca vitulina). Science 293, 102-104.

Dehnhardt, G., Mauck, B., Hyvärinen, H., 1998. Ambient temperature does not affect the tactile sensitivity of mystacial vibrissae in harbour seals. J. Exp. Biol. 201, 3023-3029.

Dehnhardt, G., Mauck, B., Hyvärinen, H., 2003. The Functional Significance of the Vibrissal System of Marine Mammals, The Merkel Cell. Springer, pp. 127-135.

Dogliotti, A.I., Lutz, V.A., Segura, V., 2014. Estimation of primary production in the southern Argentine continental shelf and shelf-break regions using field and remote sensing data. Remote Sens. Environ. 140, 497-508.

Ducatez, S., Dalloyau, S., Richard, P., Guinet, C., Cherel, Y., 2008. Stable isotopes document winter trophic ecology and maternal investment of adult female southern elephant seals (Mirounga leonina) breeding at the Kerguelen Islands. Mar. Biol. 155, 413-420.

Dykes, R.W., 1975. Afferent fibers from mystacial vibrissae of cats and seals. J. Neurophysiol. 38, 650-662.

Ebara, S., Kumamoto, K., Matsuura, T., Mazurkiewicz, J.E., Rice, F.L., 2002. Similarities and differences in the innervation of mystacial vibrissal follicle-sinus complexes in the rat and cat: A confocal microscopic study. J. Comp. Neurol. 449, 103-119.

Eder, E., Lewis, M., 2005. Proximate composition and energetic value of demersal and pelagic prey species from the SW Atlantic Ocean. Mar. Ecol. Prog. Ser. 291, 43-52.

Eder, E.B., Lewis, M.N., Campagna, C., Koch, P.L., 2010. Evidence of demersal foraging from stable isotope analysis of juvenile elephant seals from Patagonia. Mar. Mamm. Sci. 26, 430-442.

Ehrlich, M.D., Sánchez, R.P., de Ciechomski, J., Machinandiarena, L., Pájaro, M., 1999. Ichthyoplankton composition, distribution and abundance on the southern patagonian shelf and adjacent waters.

Erdsack, N., Dehnhardt, G., Hanke, W., 2014. Thermoregulation of the vibrissal system in harbor seals (Phoca vitulina) and Cape fur seals (Arctocephalus pusillus pusillus). J. Exp. Mar. Biol. Ecol. 452, 111-118.

ESR, 2009. (Earth & Space Research). OSCAR third degree resolution ocean surface currents. Ver. 1., in: Center, P.O.D.A.A. (Ed.), CA, USA.

Farrell, E., Fuiman, L., 2013. animalTrack: Animal track reconstruction for high frequency 2-dimensional (2D) or 3-dimensional (3D) movement data. R package version 1.0.0.

Fauchald, P., Tveraa, T., 2003. Using first-passage time in the analysis of area-restricted search and habitat selection. Ecology 84, 282-288.

Field, I., Bradshaw, C., van den Hoff, J., Burton, H., Hindell, M., 2007. Age-related shifts in the diet composition of southern elephant seals expand overall foraging niche. Mar. Biol. 150, 1441-1452.

Field, I., Hindell, M., Slip, D., Michael, K., 2001. Foraging strategies of southern elephant seals (Mirounga leonina) in relation to frontal zones and water masses. Antarct. Sci. 13, 371-379.

Field, I.C., Bradshaw, C.J.A., Burton, H.R., Hindell, M.A., 2004. Seasonal use of oceanographic and fisheries management zones by juvenile southern elephant seals (Mirounga leonina) from Macquarie Island. Polar Biol. 27, 432-440.

Field, I.C., Bradshaw, C.J.A., Burton, H.R., Sumner, M.D., Hindell, M.A., 2005. Resource partitioning through oceanic segregation of foraging juvenile southern elephant seals (Mirounga leonina). Oecologia 142, 127-135.

Figueroa, D.E., de Astarloa, J.M.D.a., Martos, P., 1998. Mesopelagic fish distribution in the southwest Atlantic in relation to water masses. Deep-Sea Res. (1 Oceanogr. Res. Pap.) 45, 317-332.

Fish, F., Lauder, G., 2006. Passive and active flow control by swimming fishes and mammals. Annu. Rev. Fluid Mech. 38, 193-224.

Florkowski, C.M., 2008. Sensitivity, specificity, receiver-operating characteristic (ROC) curves and likelihood ratios: communicating the performance of diagnostic tests. The Clinical Biochemist Reviews 29, S83-S87.

Freitas, C., 2010. argosfilter: Argos locations filter. R package version 0.62.

Gallon, S., Bailleul, F., Charrassin, J.B., Guinet, C., Bost, C.A., Handrich, Y., Hindell, M., 2013. Identifying foraging events in deep diving southern elephant seals, Mirounga leonina, using acceleration data loggers. Deep-Sea Res. (II Top. Stud. Oceanogr.) 88, 14-22.

George, I.D., Holliday, C.M., 2013. Trigeminal nerve morphology in Alligator mississippiensis and its significance for crocodyliform facial sensation and evolution. Anat. Rec. 296, 670-680.

Ginter, C.C., 2011. Comparative analysis of the morphology and material properties of pinniped vibrissae. Texas A&M University.

Ginter, C.C., DeWitt, T.J., Fish, F.E., Marshall, C.D., 2012. Fused traditional and geometric morphometrics demonstrate pinniped whisker diversity. PloS one 7, e34481.

Ginter, C.C., Fish, F.E., Marshall, C.D., 2010. Morphological analysis of the bumpy profile of phocid vibrissae. Mar. Mamm. Sci. 26, 733-743.

Gläser, N., Wieskotten, S., Otter, C., Dehnhardt, G., Hanke, W., 2011. Hydrodynamic trail following in a California sea lion (Zalophus californianus). J. Comp. Phys. A. 197, 141-151.

Gottschaldt, K.-M., Iggo, A., Young, D., 1973. Functional characteristics of mechanoreceptors in sinus hair follicles of the cat. J. Physiol. 235, 287-315.

Grant, R., Wieskotten, S., Wengst, N., Prescott, T., Dehnhardt, G., 2013. Vibrissal touch sensing in the harbor seal (Phoca vitulina): how do seals judge size? J. Comp. Physiol. A. 199, 521-533.

Gray, R., Canfield, P., Rogers, T., 2006. Histology of selected tissues of the leopard seal and implications for functional adaptations to an aquatic lifestyle. J. Anat. 209, 179-199.

Green, K., Burton, H., 1993. Comparison of the stomach contents of southern elephant seals, Mirounga leonina, at Macquarie and Heard Islands. Mar. Mamm. Sci. 9, 10-22.

Guinet, C., Vacquié-Garcia, J., Picard, B., Bessigneul, G., Lebras, Y., Dragon, A.C., Viviant, M., Arnould, J.P., Bailleul, F., 2014. Southern elephant seal foraging success in relation to temperature and light conditions: insight into prey distribution. Mar. Ecol. Prog. Ser. 499, 285-301.

Hall, B., Hoelzel, A., Baroni, C., Denton, G., Le Boeuf, B., Overturf, B., Töpf, A., 2006. Holocene elephant seal distribution implies warmer-than-present climate in the Ross Sea. Proc. Natl. Acad. Sci. 103, 10213.

Hanke, F.D., Hanke, W., Scholtyssek, C., Dehnhardt, G., 2009. Basic mechanisms in pinniped vision. Exp. Brain Res. 199, 299-311.

Hanke, W., Bleckmann, H., 2004. The hydrodynamic trails of Lepomis gibbosus (Centrarchidae), Colomesus psittacus (Tetraodontidae) and Thysochromis ansorgii (Cichlidae) investigated with scanning particle image velocimetry. J. Exp. Biol. 207, 1585-1596.

Hanke, W., Brücker, C., Bleckmann, H., 2000. The ageing of the low-frequency water disturbances caused by swimming goldfish and its possible relevance to prey detection. J. Exp. Biol. 203, 1193.

Hanke, W., Wieskotten, S., Marshall, C., Dehnhardt, G., 2013. Hydrodynamic perception in true seals (Phocidae) and eared seals (Otariidae). J. Comp. Physiol. A. 199, 421-440.

Hanke, W., Wieskotten, S., Niesterok, B., Miersch, L., Witte, M., Brede, M., Leder, A., Dehnhardt, G., 2012. Hydrodynamic perception in pinnipeds, Nature-Inspired Fluid Mechanics. Springer, pp. 255-270.

Hanke, W., Witte, M., Miersch, L., Brede, M., Oeffner, J., Michael, M., Hanke, F., Leder, A., Dehnhardt, G., 2010. Harbor seal vibrissa morphology suppresses vortex-induced vibrations. J. Exp. Biol. 213, 2665-2672.

Hardy, M.H., Roff, E., Smith, T.G., Ryg, M., 1991. Facial skin glands of ringed and grey seals, and their possible function as odoriferous organs. Can. J. Zool. 69, 189-200.

Hassrick, J.L., Crocker, D.E., Zeno, R.L., Blackwell, S.B., Costa, D.P., Le Boeuf, B.J., 2007. Swimming speed and foraging strategies of northern elephant seals. Deep-Sea Res. (II Top. Stud. Oceanogr.) 54, 369-383.

Hijmans, R.J., van Etten, J., 2014. raster: Geographic data analysis and modeling. R package version 2, 15.

Hindell, M., Perrin, W., 2008. Elephant seals, in: Perrin, W.F., Würsig, B.G., Thewissen, J. (Eds.), Encyclopedia of marine mammals. Academic Press.

Hindell, M., Slip, D., Burton, H., 1991. The diving behaviour of adult male and female southern elephant seals, Mirounga leonina (Pinnipedia: Phocidae). Aust. J. Zool 39, 595-619.

Hindell, M.A., McMahon, C.R., Bester, M.N., Boehme, L., Costa, D., Fedak, M.A., Guinet, C., Herraiz-Borreguero, L., Harcourt, R.G., Huckstadt, L., 2016. Circumpolar habitat use in the southern elephant seal: implications for foraging success and population trajectories. Ecosphere 7.

Hoelzel, A.R., Campagna, C., Arnbom, T., 2001. Genetic and morphometric differentiation between island and mainland southern elephant seal populations. Proc. R. Soc. (B Biol. Sci.) 268, 325.

Horsburgh, J., Morrice, M., Lea, M., Hindell, M., 2008. Determining feeding events and prey encounter rates in a southern elephant seal: a method using swim speed and stomach temperature. Mar. Mamm. Sci. 24, 207-217.

Hückstädt, L., Koch, P., McDonald, B., Goebel, M., Crocker, D., Costa, D., 2011. Stable isotope analyses reveal individual variability in the trophic ecology of a top marine predator, the southern elephant seal. Oecologia, 1-12.

Hyvärinen, H., 1989. Diving in darkness: whiskers as sense organs of the ringed seal (Phoca hispida saimensis). J. Zool. 218, 663-678.

Hyvärinen, H., 1995. Structure and function of the vibrissae of the ringed seal (Phoca hispida L.). Sensory Systems of Aquatic Mammals (ed. by RA Kastelein, JA Thomas and PE Nachtigall), De Spil Publishers, Woerden, The Netherlands, 429-445.

Hyvärinen, H., Katajisto, H., 1984. Functional structure of the vibrissae of the ringed seal (Phoca hispida Schr.). Acta Zool. Fenn. 171, 17-30.

Hyvärinen, H., Palviainen, A., Strandberg, U., Holopainen, I., 2009. Aquatic environment and differentiation of vibrissae: comparison of sinus hair systems of ringed seal, otter and pole cat. Brain Behav. Evolut. 74, 268-279.

IOC, I., 2003. Centenary edition of the GEBCO digital atlas, published on CD-ROM on behalf of the Intergovernmental Oceanographic Commission and the International Hydrographic Organization as part of the General Bathymetric Chart of the Oceans. British Oceanographic Data Centre.

Jackett, D.R., McDougall, T.J., 1997. A neutral density variable for the world's oceans. J. Phys. Oceanogr. 27, 237-263.

Japha, A., 1910. Die Haare der Waltiere, Lippert, p. 43

Jouma'a, J., Le Bras, Y., Richard, G., Vacquié-Garcia, J., Picard, B., El Ksabi, N., Guinet, C., 2016. Adjustment of diving behaviour with prey encounters and body condition in a deep diving predator: the Southern Elephant Seal. Funct. Ecol. 30, 636-648.

Jullion, L., Heywood, K.J., Naveira Garabato, A.C., Stevens, D.P., 2010. Circulation and water mass modification in the Brazil–Malvinas Confluence. J. Phys. Oceanogr. 40, 845-864.

Jurasinski, G., Koebsch, F., Hagemann, U., Günther, A., Beetz, S., 2014. flux: Flux rate calculation from dynamic closed chamber measurements. R package version 0.1-4.

Kastelein, R., Van Gaalen, M., 1988. The tactile sensitivity of the vibrissae of a Pacific walrus (Odobenus rosmarus divergem) Part I. Aquat. Mamm. 14, 123-133.

Kenyon, K.W., Rice, D.W., 1959. Life history of the Hawaiian monk seal. Pac. Sci. 13, 215-252.

Khamas, W.A., Smodlaka, H., Leach-Robinson, J., Palmer, L., 2012. Skin histology and its role in heat dissipation in three pinniped species. Acta Vet. Scand. 54, 46.

Kuhn, C.E., Costa, D.P., 2006. Identifying and quantifying prey consumption using stomach temperature change in pinnipeds. J. Exp. Biol. 209, 4524-4532.

Kuhn, M., Wing, J., Weston, S., Williams, A., Keefer, C., Engelhardt, A., Cooper, T., Mayer, Z., Kenkel, B., Team, R., 2014. caret: Classification and regression training. R package version 6.0–21. CRAN: Wien, Austria.

Labrousse, S., Vacquié-Garcia, J., Heerah, K., Guinet, C., Sallée, J.-B., Authier, M., Picard, B., Roquet, F., Bailleul, F., Hindell, M., 2015. Winter use of sea ice and ocean water mass habitat by southern elephant seals: The length and breadth of the mystery. Prog. Oceanogr. 137, 52-68.

Ladygina, T., Popov, V., Supin, A.Y., 1985. Topical organization of somatic projections in the fur seal cerebral cortex. Neurophysiology 17, 246-252.

Laws, R., 1956. The elephant seal (Mirounga leonina Linn.): II. General, social and reproductive behaviour, Falkland Islands Dependencies Survey Scientific Report British Antarctic Survey, London, p. 88.

Le Boeuf, B., Laws, R., 1994. Elephant seals: population ecology, behavior, and physiology. Univ of California Pr.

Le Boeuf, B.J., Crocker, D.E., Costa, D.P., Blackwell, S.B., Webb, P.M., Houser, D.S., 2000. Foraging ecology of northern elephant seals. Ecol. Monogr. 70, 353-382.

Lee, G.N., Fujita, H., 2007. K-means clustering for classifying unlabelled MRI data, 9th Biennial Conference of the Australian Pattern Recognition Society on Digital Image Computing Techniques and Applications. Institute of Electrical and Electronics Engineers (IEEE), pp. 92-98.

Legeckis, R., Gordon, A.L., 1982. Satellite observations of the Brazil and Falkland currents—1975 1976 and 1978. Deep Sea Research Part A. Oceanographic Research Papers 29, 375-401.

Levenson, D., Ponganis, P., Crognale, M., Deegan, J., Dizon, A., Jacobs, G., 2006. Visual pigments of marine carnivores: pinnipeds, polar bear, and sea otter. J. Comp. Phys. A. 192, 833-843.

Levenson, D.H., Schusterman, R.J., 1999. Dark adaptation and visual sensitivity in shallow and deep diving pinnipeds. Mar. Mamm. Sci. 15, 1303-1313.

Lewis, M., Campagna, C., Zavatti, J., 2004. Annual cycle and inter-annual variation in the haul-out pattern of an increasing southern elephant seal colony. Antarct. Sci. 16, 219-226.

Lewis, R., O'Connell, T.C., Lewis, M., Campagna, C., Hoelzel, A.R., 2006. Sex-specific foraging strategies and resource partitioning in the southern elephant seal (Mirounga leonina). Proc. R. Soc. (B Biol. Sci.) 273, 2901-2907.

Ling, J.K., 1965. Functional significance of sweat glands and sebaceous glands in seals. Nature 208, 560-562.

Ling, J.K., 1966. The skin and hair of the southern elephant seal, Mirounga leonina (Linn.) I. The facial vibrissae. Aust. J. Zool. 14, 855-866.

Ling, J.K., 1968. The skin and hair of the southern elephant seal, Mirounga leonina (Linn.) III. morphology of the adult integument. Aust. J. Zool. 16, 629-645.

Ling, J.K., 1970. Pelage and molting in wild mammals with special reference to aquatic forms. Q. Rev. Biol. 45, 16-54.

Ling, J.K., 1972. Vibrissa follicles of the Ross seal. Brit. Antarct. Surv. B. 27, 19-24.

Ling, J.K., 1977. Vibrissae of marine mammals, in: Harrison, R.J. (Ed.), Functional anatomy of marine mammals, pp. 387-415.

Ling, J.K., Thomas, C., 1967. The skin and hair of the southern elephant seal, Mirounga Leonina (Linn.) II. pre-natal and early post-natal development and moulting. Aust. J. Zool. 15, 349-365.

Luo, Z.-X., Yuan, C.-X., Meng, Q.-J., Ji, Q., 2011. A Jurassic eutherian mammal and divergence of marsupials and placentals. Nature 476, 442-445.

Marshall, C.D., Amin, H., Kovacs, K.M., Lydersen, C., 2006. Microstructure and innervation of the mystacial vibrissal follicle-sinus complex in bearded seals, Erignathus barbatus (Pinnipedia: Phocidae). Anat. Rec. 288A, 13-25.

Marshall, C.D., Kovacs, K.M., Lydersen, C., 2008. Feeding kinematics, suction and hydraulic jetting capabilities in bearded seals (Erignathus barbatus). J. Exp. Biol. 211, 699-708.

Marshall, C.D., Rosen, D., Trites, A.W., 2015. Feeding kinematics and performance of basal otariid pinnipeds, Steller sea lions (Eumetopias jubatus), and northern fur seals (Callorhinus ursinus): implications for the evolution of mammalian feeding. J. Exp. Biol. 218, 126573.

Marshall, C.D., Rozas, K., Kot, B., Gill, V.A., 2014a. Innervation patterns of sea otter (Enhydra lutris) mystacial follicle-sinus complexes. Front. Neuroanat. 8, 121.

Marshall, C.D., Wieskotten, S., Hanke, W., Hanke, F.D., Marsh, A., Kot, B., Dehnhardt, G., 2014b. Feeding kinematics, suction, and hydraulic jetting performance of harbor seals (Phoca vitulina). PLoS One 9, e86710.

Masson, P., 1929. Some histological methods. Trichrome stainings and their preliminary technique. Bull Int Assoc Med 12, 75-90.

Matano, R., Palma, E., Piola, A., 2010. The influence of the Brazil and Malvinas Currents on the southwestern Atlantic shelf circulation. Ocean Sci. Disc. 7, 837-871.

Matthews, L.H., 1929. The Natural History of the Elephant Seal: With Notes on Other Seals Found at South Georgia. National Institute of Oceanography.

Mattson, E.E., Marshall, C.D., 2016. Follicle microstructure and innervation vary between pinniped micro-and macrovibrissae. Brain Behav. Evol. 88, 43-58.

McConnell, B., Chambers, C., Fedak, M., 1992. Foraging ecology of southern elephant seals in relation to the bathymetry and productivity of the Southern Ocean. Antarct. Sci. 4, 393-398.

McGovern, K.A., Davis, R.W., Marshall, C.D., 2015. Are vibrissae viable sensory structures for prey capture in northern elephant seals, Mirounga angustirostris? Anat. Rec. 298, 750-760.

McIntyre, T., Bornemann, H., Plötz, J., Tosh, C.A., Bester, M.N., 2011. Water column use and forage strategies of female southern elephant seals from Marion Island. Mar. Biol. 158, 2125-2139.

Mcintyre, T., Bornemann, H., Plötz, J., Tosh, C.A., Bester, M.N., 2012. Deep divers in even deeper seas: habitat use of male southern elephant seals from Marion Island. Antarct. Sci. 24, 561-570.

McIntyre, T., de Bruyn, P.J.N., Ansorge, I., Bester, M., Bornemann, H., Plötz, J., Tosh, C., 2010. A lifetime at depth: vertical distribution of southern elephant seals in the water column. Polar Biol. 33, 1037-1038.

McMahon, C., Bester, M., Burton, H., Hindell, M., Bradshaw, C., 2005. Population status, trends and a re-examination of the hypotheses explaining the recent declines of the southern elephant seal Mirounga leonina. Mammal. Rev. 35, 82-100.

Montagna, W., Harrison, R.J., 1957. Specializations in the skin of the seal (Phoca vitulina). American Journal of Anatomy 100, 81-113.

Muelbert, M., Souza, R., Lewis, M., Hindell, M.A., 2013. Foraging habitats of southern elephant seals, Mirounga leonina, from the Northern Antarctic Peninsula. Deep-Sea Res. (II Top. Stud. Oceanogr.) 88, 47-60.

Murphy, R.C., 1914. Notes on the sea elephant, Mirounga leonina (Linné). Bulletin of the AMNH; v. 33, article 2.

Naito, Y., Costa, D.P., Adachi, T., Robinson, P.W., Fowler, M., Takahashi, A., 2013. Unravelling the mysteries of a mesopelagic diet: a large apex predator specializes on small prey. Funct. Ecol. 27, 710-717.

Naito, Y., Costa, D.P., Adachi, T., Robinson, P.W., Peterson, S.H., Mitani, Y., Takahashi, A., 2017. Oxygen minimum zone: An important oceanographic habitat for deep-diving northern elephant seals, Mirounga angustirostris. Ecology and Evolution 7, 6259-6270.

NASA Goddard Space Flight Center, O.E.L., Ocean Biology Processing Group, 2014. Moderate-resolution Imaging Spectroradiometer (MODIS) Aqua Chlorophyll Data; 2014 Reprocessing. , in: OB.DAAC, N. (Ed.). doi: 10.5067/AQUA/MODIS/L3B/CHL/2014., Greenbelt, MD, USA.

Newland, C., Field, I., Nichols, P., Bradshaw, C., Hindell, M., 2009. Blubber fatty acid profiles indicate dietary resource partitioning between adult and juvenile southern elephant seals. Mar. Ecol. Prog. Ser. 384, 303-312.

O'Toole, M., Hindell, M.A., Charrassin, J.-B., Guinet, C., 2014. Foraging behaviour of southern elephant seals over the Kerguelen Plateau. Mar. Ecol. Prog. Ser. 502, 281-294.

Orsi, A.H., Whitworth III, T., Nowlin Jr, W.D., 1995. On the meridional extent and fronts of the Antarctic Circumpolar Current. Deep-Sea Res. (1 Oceanogr. Res. Pap.) 42, 641-673.

Palma, E.D., Matano, R.P., Piola, A.R., 2008. A numerical study of the Southwestern Atlantic Shelf circulation: Stratified ocean response to local and offshore forcing. J. Geophys. Res. 113, C11010.

Patrizi, G., Munger, B., 1966. The ultrastructure and innervation of rat vibrissae. J. Comp. Neurol. 126, 423-435.

Piatkowski, U., Vergani, D., Stanganelli, Z., 2002. Changes in the cephalopod diet of southern elephant seal females at King George Island, during El Niño-La Niña events. J. Mar. Bio. Ass. UK 82, 913-916.

Piatkowski, U., Vergani, D.F., 2000. The cephalopod prey of southern elephant seals (Mirounga leonina) from Stranger Point, King George Island, Antarctica, CIAC Symposium Cephalopod Biomass and Production, University of Aberdeen, Scotland, pp. 3-7.

Piola, A.R., Matano, R.P., 2001. Brazil And Falklands (Malvinas) Currents, in: Steele, J. (Ed.), Encyclopedia of Ocean Sciences. Academic Press, Oxford, pp. 340-349.

Pocock, R., 1914. On the Facial Vibrissæ of Mammalia. Proc. Zool. Soc. Lond. 84, 889-912.

R Core Team, 2013. R: a language and environment for statistical computing. Version 3.1. 3. Vienna, Austria: R Foundation for Statistical Computing; 2015.

Reep, R.L., Marshall, C.D., Stoll, M.L., 2002. Tactile hairs on the postcranial body in Florida manatees: A mammalian lateral line? Brain Behav. Evolut. 59, 141-154.

Reep, R.L., Stoll, M.L., Marshall, C.D., Homer, B.L., Samuelson, D.A., 2001. Microanatomy of facial vibrissae in the Florida manatee: the basis for specialized sensory function and oripulation. Brain Behav. Evolut. 58, 1-14.

Renouf, D., 1979. Preliminary measurements of the sensitivity of the vibrissae of harbour seals (Phoca vitulina) to low frequency vibrations. J. Zool. 188, 443-450.

Rice, F.L., Mance, A., Munger, B.L., 1986. A comparative light microscopic analysis of the sensory innervation of the mystacial pad. I. Innervation of vibrissal follicle-sinus complexes. J. Comp. Neurol. 252, 154-174.

Richards, W.J., 2005. Early stages of Atlantic fishes: an identification guide for the western central north Atlantic, Two Volume Set. CRC Press.

Robin, X., Turck, N., Hainard, A., Tiberti, N., Lisacek, F., Sanchez, J.-C., Müller, M., 2011. pROC: an open-source package for R and S+ to analyze and compare ROC curves. BMC Bioinformatics 12, 77.

Rodhouse, P., Arnbom, T., Fedak, M., Yeatman, J., Murray, A., 1992. Cephalopod prey of the southern elephant seal, Mirounga leonina L. Can. J. Zool. 70, 1007-1015.

Romero, S., Piola, A., Charo, M., Garcia, C., 2006a. Seasonal to interannual variability along the Patagonia shelf and shelf-break based on satellite ocean color data. J. Geophys. Res. 111, C05021.

Romero, S.I., Piola, A.R., Charo, M., Garcia, C.A.E., 2006b. Chlorophyll-a variability off Patagonia based on SeaWiFS data. J. Geophys. Res. 111, C05021.

Ryan, J.A., 2013. Quantmod: Quantitative financial modelling framework. r package version 0.4-0. CRAN: Wien, Austria.

Sánchez, R., Ciechomski, J., 1995. Spawning and nursery grounds of pelagic fish species in the sea-shelf off Argentina and adjacent areas. Sci. Mar 59, 455-478.

Sane, S.P., McHenry, M.J., 2009. The biomechanics of sensory organs. Integr. Comp. Biol. 49, i8-i23.

Saraceno, M., Provost, C., Piola, A., Bava, J., Gagliardini, A., 2004. Brazil Malvinas Frontal System as seen from 9 years of advanced very high resolution radiometer data. J. Geophys. Res. 109, C05027.

Sarko, D.K., Reep, R.L., Mazurkiewicz, J.E., Rice, F.L., 2007. Adaptations in the structure and innervation of follicle-sinus complexes to an aquatic environment as seen in the Florida manatee (Trichechus manatus latirostris). J. Comp. Neurol. 504, 217-237.

Schreer, J.F., Testa, J.W., 1996. Classification of Weddell seal diving behavior. Mar. Mamm. Sci. 12, 227-250.

Schulte-Pelkum, N., Wieskotten, S., Hanke, W., Dehnhardt, G., Mauck, B., 2007. Tracking of biogenic hydrodynamic trails in harbour seals (Phoca vitulina). J. Exp. Biol. 210, 781-787.

Simmons, S., Crocker, D., Kudela, R., Costa, D., 2007. Linking foraging behaviour of the northern elephant seal with oceanography and bathymetry at mesoscales. Mar. Ecol. Prog. Ser. 346, 265-275.

Skinner, J.P., Mitani, Y., Burkanov, V.N., Andrews, R.D., 2014. Proxies of food intake and energy expenditure for estimating the time–energy budgets of lactating northern fur seals Callorhinus ursinus. J. Exp. Mar. Biol. Ecol. 461, 107-115.

Slade, R.W., Moritz, C., Hoelzel, A.R., Burton, H.R., 1998. Molecular population genetics of the southern elephant seal Mirounga leonina. Genetics 149, 1945.

Slip, D.J., 1995. The diet of southern elephant seals (Mirounga leonina) from Heard Island. Can. J. Zool. 73, 1519-1528.

Sprowls, C., 2017. Innervation patterns of mystacial vibrissae support active touch behaviors in California sea lions (*Zalophus californianus*), Department of Marine Biology. Texas A&M University.

Stephens, R., Beebe, I., Poulter, T., 1973. Innervation of the vibrissae of the California sea lion, Zalophus californianus. Anat. Rec. 176, 421-441.

Stewart, R.H., 2008. Introduction to physical oceanography. Robert H. Stewart.

Talley, L.D., 2011. Descriptive physical oceanography: an introduction. Academic press.

Vacquié-Garcia, J., Guinet, C., Laurent, C., Bailleul, F., 2015. Delineation of the southern elephant seal′ s main foraging environments defined by temperature and light conditions. Deep-Sea Res. (II Top. Stud. Oceanogr.) 113, 145-153.

van den Hoff, J., 2004. A comparative study of the cephalopod prey of Patagonian toothfish (Dissostichus eleginoides) and southern elephant seals (Mirounga leonina) near Macquarie Island. Polar Biol. 27, 604-612.

van den Hoff, J., Burton, H., Davies, R., 2003. Diet of male southern elephant seals (Mirounga leonina L.) hauled out at Vincennes Bay, East Antarctica. Polar Biol. 26, 27-31.

Van Horn, R., 1970. Vibrissae structure in the rhesus monkey. Folia Primatol. 13, 241-285.

Violante, R.A., Paterlini, C.M., Costa, I.P., Hernández-Molina, F.J., Segovia, L.M., Cavallotto, J.L., Marcolini, S., Bozzano, G., Laprida, C., García Chapori, N., 2010. Sismoestratigrafia y evolución geomorfológica del talud continental adyacente al litoral del este bonaerense, Argentina. Latin American Journal of Sedimentology and Basin Analysis 17, 33-62.

Viviant, M., Trites, A.W., Rosen, D.A., Monestiez, P., Guinet, C., 2010. Prey capture attempts can be detected in Steller sea lions and other marine predators using accelerometers. Polar Biol. 33, 713-719.

Volpov, B.L., Rosen, D.A., Hoskins, A.J., Lourie, H.J., Dorville, N., Baylis, A.M., Wheatley, K.E., Marshall, G., Abernathy, K., Semmens, J., 2016. Dive characteristics can predict foraging success in Australian fur seals (Arctocephalus pusillus doriferus) as validated by animal-borne video. Biol. open. 5, 262-271.

Wainer, I., Gent, P., Goni, G., 2000. Annual cycle of the Brazil-Malvinas Confluence region in the National Center for Atmospheric Research climate system model. J. Geophys. Res. 105, 26167-26177.

Whitehead, H., MacLeod, C.D., Rodhouse, P., 2003. Differences in niche breadth among some teuthivorous mesopelagic marine mammals. Mar. Mamm. Sci. 19, 400-406.

Wieskotten, S., Mauck, B., Miersch, L., Dehnhardt, G., Hanke, W., 2011. Hydrodynamic discrimination of wakes caused by objects of different size or shape in a harbour seal (Phoca vitulina). J. Exp. Biol. 214, 1922-1930.

Wood, S.N., 2008. Fast stable direct fitting and smoothness selection for generalized additive models. J. R. Stat. Soc. Series B. Stat. Methodol. 70, 495-518.

Yablokov, A., Klezeval, G., 1969. Whiskers of whales and seals and their distribution, structure and significance. Translation Bureau, Foreign Languages Division, Department of the Secretary of State of Canada Fisheries Research Board of Canada, Arctic Biological Station: Ste. Anne de Bellevue, Quebec. Translated from: *Vibrissy kitoobraznykh i làstonogikh, ikh raspredelenie, stroenie i znachenie.* In: Morfologicheskie osobennosti vodnikh mlekopitayushchikh. Ed. S.E. Kleinenberg: 48-81, 1962: Izdatel'stvo, Naukall, Moscow.

Zhang, Y., 2016. Binned level-3 Sea Surface Salinity from the European Space Agency Soil Moisture Ocean Salinity (SMOS) in support of the National Centers for Environmental Information (NCEI) data quality monitoring system (DQMS) from 2010-06-01 to 2016-05-31 (NCEI Accession 0151732), in: Information., N.N.C.f.E. (Ed.).

Zlotnicki, V.Q., Zheng; Willis, Joshua., 2016. JPL MEaSUREs Gridded Sea Surface Height Anomalies Version 1609. , in: PO.DAAC (Ed.), CA, USA.

APPENDIX A. KNOWN PREY SPECIES OF SOUTHERN ELEPHANT SEALS

Class	Order	Species	South Georgia	Macquarie Island	Heard Island	South Shetland	E. Antarctica	Signey Island	Pen. Valdés
Cephalopoda	Teuthida	Alluroteuthis unidentified sp.		SL[1]	SL[1]			SL[8]	
		Alluroteuthis antarcticus	SL[2]	SL[3, 4]	SL[5]	SL[6, 9]	SL[7]		
		Batoteuthis skolops	SL[2]						
		Brachioteuthis unidentified sp.		SL[1, 4]	SL[1, 5]				
		Brachioteuthis linkovskyi		SL[3]					
		Brachioteuthis picta	SL[2]			SL[6] 9			
		Chiroteuthis unidentified sp.	SL[2]	SL[1]	SL[1, 5]				
		Chiroteuthis veranyl				SL[6]			
		Galiteuthis unidentified sp.		SL[1]	SL[1]			SL[8]	
		Galiteuthis glacialis	SL[2]	SL[3, 4]	SL[5]	SL[9]			
		Gonatus antarcticus	SL[2]	SL[1, 3]	SL[5, 4]	SL[6, 9]		SL[8]	
		Histioteuthis unidentified sp.	SL[2]	SL[3]					
		Histioteuthis atlantica		SL[4]					
		Histioteuthis eltaninae		SL[1, 3]	SL[1, 4, 5]				
		Liocranchia unidentified sp.			SL[5]				
		Lycoteuthis lorigera		SL[3]					
		Kondokavia longimana	SL[2]	SL[1, 3, 4]	SL[1, 5]	SL[6, 9]		SL[8]	SI[11]
		Martiala unidentified sp.		SL[1]					
		Martiala hyadensi	SL[2]	SL[3, 4]	SL[5]				SI[11]
		Mastigoteuthis unidentified sp.		SL[1]	SL[1, 5]				
		Mastigoteuthis psychrophilia	SL[2]						
		Mesonychoteuthis hamiltoni	SL[2]						
		Moroteuthis unidentified sp.		SL[4]					
		Moroteuthis ingens		SL[1, 3, 4]	SL[1, 5]				
		Moroteuthis knipovitchi	SL[2]	SL[1, 3, 4]	SL[1, 5]	SL[6]		SL[8]	
		Pholidoteuthis unidentified sp.			SL[1]				
		Pholidoteuthis boschmai		SL[3, 4]					
		Psychroteuthis unidentified sp.						SL[8]	
		Psychroteuthis glacialis	SL[2]	SL[3, 4]	SL[5]	SL[6, 9]	SL[7]		
		Taonius unidentified sp.		SL[1]	SL[1]				
		Taonius pavo		SL[4]	SL[5]				
		Todarodes unidentified sp.		SL[1]	SL[1]				
		Todarodes filippovae		SL[3]	SL[5]				
		Unid cranchid		SL[3]					
		Slosarczykovia circumantartica		SL[3, 4]					
		Vampyroteuthis		SL[1]					
	Octopoda	Grimpoteuthis glacialis				SL[9]			
		Pareledone charcoti	SL[2]			SL[6, 9]			
		Pareledone polymorpha	SL[2]			SL[6]			
		Pareledone turqueti				SL[6]			
		Unidentified genus and species						SL[8]	

Table A.1. Known cephalopod prey of southern elephant seals. SL: stomach lavage, SI: stable isotope, FA: fatty acid signature, DO: direct observation. Sources are numbered (see legend for Table A2).

Family	Species	South Georgia	Macquarie Island	Heard Island	Peninsula Valdés
Bathylagidae	Bathylagus sp.		SL[1, 4]		
Centrolophidae	Icichthys australis		SL[4]		
Channichthyidae	Unidentified genus and species			SL[1]	
	Champsocephalus gunnari			SL[1]	
	Channichthys rhinoceratus			SL[1]	
Gempylidae	Paradiplosinus gracilis		SL[4]		
Myctophidae	Electrona unidentified species		SL[1]		
	Electrona antarctica			SL[1, 5]	
	Electrona carlsbergi		SL[1, 4]	SL[1, 5]	
	Electrona subaspara		SL[1, 4]		
	Gymnoscopelus unidentified sp.		SL[1]		
	Gymnoscopelus bolini		SL[4]		
	Gymnoscopelus braueri		SL[4]	SL[1]	
	Gymnoscopelus nicholsi	FA[12]	SL[1, 4]	SL[1, 5]	
	Gymnoscopelus piabilis		SL[4]		
	Krefftichthys anderssoni		SL[4]		
	Protomyctophum choriodon		SL[4]		
	Protomyctophum normani		SL[4]		
	Unidentified genus and species			SL[1]	
Nototheniidae	Dissostichus eleginoides	FA[12], DO[13]	SL[4]	SL[5]	SI[11]
	Notothenia acuta			SL[1]	
	Notothenia coriceps	SL[10]			
	Notothenia squamifrons			SL[1]	
	Nototheniops mizops			SL[1]	
	Unidentified genus and species		SL [4]		
Paralepididae	Magnisudis prionosa		SL[4]		
Photichthyidae	Photichthys argenteus		SL[4]		

Table A2. Known fish prey of southern elephant seals. SL: stomach lavage, SI: stable isotope, FA: fatty acid signature, DO: direct observation. Sources are numbered. Species highlighted in blue were observed in the fisheries sampling study described by Figueroa et al. (1998), dives highlighted in yellow were observed in the fisheries sampling study observed by Cousseau et al. (2012), and dives highlighted in green were observed in both.

1.Green, K. and H. Burton, *Comparison of the stomach contents of southern elephant seals, Mirounga leonina, at Macquarie and Heard Islands.* Marine Mammal Science, 1993. **9**(1): p. 10-22.
2.Rodhouse, P., et al., *Cephalopod prey of the southern elephant seal, Mirounga leonina L.* Canadian Journal of Zoology/Revue Canadienne de Zoologie, 1992. **70**(5): p. 1007-1015.
3.van den Hoff, J., *A comparative study of the cephalopod prey of Patagonian toothfish (Dissostichus eleginoides) and southern elephant seals (Mirounga leonina) near Macquarie Island.* Polar Biology, 2004. **27**(10): p. 604-612.
4.Field, I., et al., *Age-related shifts in the diet composition of southern elephant seals expand overall foraging niche.* Marine Biology, 2007. **150**(6): p. 941-952.
5.Slip, D.J., *The diet of southern elephant seals (Mirounga leonina) from Heard Island.* detail (e. g., Rodhouse et al. 1992a; Green and Burton 1993), 1995. **1960**: p. 1977.
6.Daneri, G., A. Carlini, and P. Rodhouse, *Cephalopod diet of the southern elephant seal, Mirounga leonina, at King George Island, South Shetland Islands.* Antarctic Science, 2000. **12**(01): p. 16-19.
7.van den Hoff, J., H. Burton, and R. Davies, *Diet of male southern elephant seals (Mirounga leonina L.) hauled out at Vincennes Bay, East Antarctica.* Polar Biology, 2003. **26**(1): p. 27-31.
8.Clarke, M. and N. MacLeod, *Cephalopods in the diet of elephant seals at Signy Island, South Orkney Islands.* British Antarctic Survey Bulletin, 1982. **5**: p. 27-31.
9.Piatkowski, U. and D.F. Vergani. *The cephalopod prey of southern elephant seals (Mirounga leonina) from Stranger Point, King George Island, Antarctica*. 2000.
10.Laws, R. and F.I.D. Survey, *The elephant seal (Mirounga leonina Linn.): II. General, social and reproductive behaviour*. 1956: Falkland Islands Dependencies Survey.
11. Eder, E. B., et al. (2010). "Evidence of demersal foraging from stable isotope analysis of juvenile elephant seals from Patagonia." Marine Mammal Science **26**(2): 430-442.
12.Brown, D. J., et al. (1999). "Fatty acid signature analysis from the milk of Antarctic fur seals and Southern elephant seals from South Georgia: implications for diet determination." Marine Ecology Progress Series **187**: 251-263.
13.Reid, K. and Nevitt, G.A. (1998). "Observation of southern elephant seal, Mirounga leonina, feeding at sea near South Georgia." Marine Mammal Science **14**(3): 637-640.

APPENDIX B. MODEL DEVELOPMENT

Descriptor (R)	Descriptor full name	A	B	D	F	S	W
Depthvar	Depth variance	+	+	+	+	+	+
Diveduration	Dive duration (min)						+
headingROC	Mean heading rate of change	+	+	+	+	+	+
Headingvar	Heading variance	+	+	+	+	+	+
Horzpathlinearity	Horizontal path linearity				+	+	+
Maxconsectimeatzero	Maximum consecutive number of seconds speed =0 m/sec						+
maxconsectimeunderpt3	Maximum consecutive number of seconds speed <0.3 m/sec						+
maxconsectimeunderpt5	Maximum consecutive number of seconds speed <0.5 m sec^{-1}						+
Maxdepth	Maximum depth (m)	+	+	+	+	+	+
Maxspeed	Maximum speed (m sec^{-1})	+	+	+	+	+	+
Maxspeedh	Maximum horizontal speed (m sec^{-1})	+	+	+	+	+	+
Maxstrokingrate	Maximum stroking rate (strokes sec^{-1})	+	+	+	+	+	+
Meanpitchangle	Mean pitch angle (°)	+		+			
Meanrollangle	Mean roll angle (°)	+		+			
Meanspeed	Mean speed (m sec^{-1})	+	+	+	+	+	+
Meanspeedh	Mean horizontal speed (m sec^{-1})	+	+	+	+	+	+
Meanstrokingrate	Mean stroking rate (strokes sec^{-1})	+	+	+	+	+	+
Meanvectorlength	Mean vector length (measure of angular dispersion; 0=uniform , 1=none)	+	+	+	+	+	+
Meanverticalspeed	Mean vertical speed (m sec^{-1})	+		+			
Minspeedh	Minimum horizontal speed (m sec^{-1})	+	+	+	+	+	+
numsecshighROCzaxis	Number of seconds normalized rate of change in z-axis accelerometer >0.2						+
numsecslowspeedpt3	Number of seconds speed <0.3 m sec^{-1}						+
numsecslowspeedpt5	Number of seconds speed <0.5 m sec^{-1}						+
numsecslowspeedzero	Number of seconds speed =0 m sec^{-1}						+
Pathlinearity	Path linearity (3D)				+	+	+
proportiondiveconsectimeatzero	maxconsectimeatzero diveduration^{-1}						+
proportiondiveconsectimeunderpt3	maxconsectimeunderpt3 diveduration^{-1}						+
proportiondiveconsectimeunderpt5	maxconsectimeunderpt5 diveduration^{-1}						+
proportiontimehighROCzaxis	numsecshighROCzaxis diveduration^{-1}						+
proportiontimelowspeedpt3	numsecslowspeedpt3 diveduration^{-1}						+
proportiontimelowspeedpt5	numsecslowspeedpt5 diveduration^{-1}						+
proportiontimelowspeedzero	numsecslowspeedzero diveduration^{-1}						+
speedcalcROC_4	Mean speed (4 Hz) rate of change	+	+	+	+	+	+
speedcalcvar_4	Speed (4 Hz) variance	+	+	+	+	+	+
Speedhvar	Horizontal speed variance	+	+	+	+	+	+
speedROC	Mean speed rate of change	+	+	+	+	+	+
Speedvar	Speed variance	+	+	+	+	+	+
Straightlinehorzdist	Straight-line horizontal distance (m)				+	+	+
strokingROC	Mean stroking rate rate of change	+	+	+	+	+	+
totaldist3D	Total 3D distance (m)				+	+	+
Totalhorzdist	Total horizontal distance (m)				+	+	+
Varpitchangle	Pitch angle variance	+		+			
Varrollangle	Roll angle variance	+		+			
Varstrokingrate	Stroking rate variance	+	+	+	+	+	+
Varverticalspeed	Vertical speed variance	+		+			
Vertpathlinearity	Vertical path linearity				+	+	+
Xaccelvar	X-axis accelerometer variance	+	+	+	+	+	+
xaccelvar_16	X-axis accelerometer (16 Hz) variance	+	+	+	+	+	+
yaccelROC_16	Mean y-axis accelerometer (16 Hz) rate of change	+	+	+	+	+	+
Yaccelvar	Y-axis accelerometer variance	+	+	+	+	+	+
yaccelvar_16	Y-axis accelerometer (16 Hz) variance	+	+	+	+	+	+
zaccelROC	Mean z-axis accelerometer rate of change	+	+	+	+	+	+
zaccelROC_16	Mean z-axis accelerometer (16 Hz) rate of change	+	+	+	+	+	+
Zaccelvar	Z-axis accelerometer variance	+	+	+	+	+	+
zaccelvar_16	Z-axis accelerometer (16 Hz) variance	+	+	+	+	+	+

Table B.1. Dive descriptors. + indicates that the descriptor was calculated for the corresponding portion of the dive. A=ascent, B=bottom, D=descent, F=first half, S=second half, W=whole). Descriptors are calculated based on 1 Hz data unless otherwise specified. All distances were estimated using corrected (course made good) coordinates. Rate of change (ROC) is calculated per second unless otherwise indicated.

To select the initial variables to use in LDA and QDA, several transformations (cubed, squared, log, square root, exponent, third) for each descriptor were computed, standardized, and added to the predictor matrix. This was done to increase the potential for variables to be included in the model, as both LDA and QDA assume multivariate normality, and transformations can sometimes render non-normal data normal. The Shapiro-Wilks test in R was used to select variables that had a normal distribution (p-value > 0.05) for each of the three classes. These multivariate normal data were then entered into an initial feature selection process for use in QDA. LDA makes an additional assumption of equal covariance matrices between classes. The Bartlett test was used in R to select variables that met this assumption (p-value > 0.05). The resulting data was input into an initial feature selection process for use in LDA. RF makes no assumptions regarding multivariate normality or equal covariance, so the original predictors were entered into the initial feature selection process for use in RF.

The initial feature selection process was identical for each of the supervised classification models. A loop was written that incorporated the recursive feature elimination function from the caret package in R, which selected the predictors that contributed most to the separation between classes using 10-fold cross-validation. This function produced a list of predictors from most influential to least influential, according to how much each predictor contributed to variance between classes. During the first iteration of the loop, the most significant predictor was selected and all collinear variables were eliminated from the dataset. During each successive iteration of the loop, the next most significant predictor was selected and all collinear variables were eliminated. This process was repeated until there were no collinear variables present in the dataset. This process was completed for each dataset (original dataset for RF, multivariate

normal dataset for QDA, multivariate normal with equal covariance dataset for LDA) before training all classifiers.

To develop the LDA and QDA classifiers, the corresponding selected predictors were entered into a stepwise discriminant analysis (direction = both) using the stepclass function in the klaR package in R (Weihs, Ligges, Luebke, & Raabe, 2005) to determine the optimal predictors to include in each model. LDA or QDA was specified in the function input. The selected predictors for each were then used to develop the corresponding classifier using the MASS package in R (Venables & Ripley, 2013). The LDA was also fit in SPSS (IBM Corp, 2016) to calculate the eigenvalues and standardized canonical coefficients and to test the discriminant functions.

To develop the RF classifier, the rfe function in the caret package in R was used to determine the optimum number of predictors, ranging from sizes 1:30. The outer resampling method used was repeated (10 repeats) 10-fold cross-validation. The number of predictors chosen for use in the classifier was determined based on Accuracy and the Kappa statistic. To tune the values for mtry (number of predictors sampled at each node split) and ntree (number of trees in forest), 150 random forest models were fit to the data using the randomforest package in R (Liaw & Wiener, 2002) with mtry = 1:15 and ntree = 50, 100, 200, 300, 400, 500, 1000, 1500, 2000, and 2500. To avoid overfitting the classifier to the training data, each tree in each forest was fit with 13 (equal to 70% of the dives in the training set for the class with the smallest sample size) randomly selected and bootstrapped samples from each class. The out-of-bag (OOB) error estimate was calculated for each model by using each tree in the forest to predict dive class for the dives that were not used to train that particular tree, then averaging the prediction error across all of the trees in the forest. The OOB error rate was subtracted from 1 to obtain an OOB correct classification rate.

The kmeans cluster analysis was completed using the kmeans function in R. The elbow method and silhouette method were both used to determine the optimal number of clusters. The input variables used for the random forest model were used for the kmeans analysis, as kmeans also does not make any assumptions based on normality or equality of covariance matrices. The resulting clusters were labeled as “foraging”, “resting”, or “transit” based on the primary class of video dives occurring in each cluster.

APPENDIX C. INDIVIDUAL MODEL RESULTS

C.1 Linear discriminant analysis

Five predictors were selected by the stepclass function to develop the LDA classifier. The predictors chosen were transformations of 1) speed variance during the first half of the dive (in 4 Hz, speedcalcsmoothvar_4firsthalf), 2) stroking rate variance during the first half of the dive (varstrokingratefirsthalf), 3) rate of change in the y-axis accelerometer at the bottom of the dive (in 16 Hz, yaccelROC_16bottom), 4) variance in the x-axis accelerometer during the first half of the dive (in 16 Hz, xaccelvar_16firsthalf), and stroking rate variance during the second half of the dive (varstrokingratesecondhalf) (Table C.1). The coefficients of the linear discriminants are listed in Table C.2. Fig. C.1 depicts the decision boundaries for the resulting LDA classifier. The classifier correctly classified 76.9% of the training data (89.8%, 58.8%, and 57.1% of foraging, resting, and transit dives, respectively) (Table C.3). The eigenvalues of the first and second discriminant functions were 0.421 and 0.298, respectively (Table C.4). The proportion of the trace explained by the first and second discriminant functions was 58.5% and 41.5%, respectively. Chi-square tests for the first and second discriminant functions together and the second discriminant function solo were both significant at the $p<0.001$ significance level (χ^2 statistic of 86.9 and 37, respectively) (Table C.5). A plot of the canonical discriminant function coefficients standardized from 0 to 1 showed that varstrokingratefirsthalf contributed the most to the separation of classes on discriminant axis 1, and that yaccelROC_16bottom contributed most to the separation of classes on discriminant axis 2 (Fig. C.2). The LDA classifier was tested on the test dataset with an overall accuracy of 0.803 (95% CI: 0.687, 0.891) and a Kappa statistic of 0.638 (Table C.1). The classification had an overall accuracy significantly better than the no

information rate (NIR) at the 0.01 level with a p-value of 0.0002. Balanced accuracy was 0.825, 0.804, and 0.805 for foraging, transit, and resting, respectively (Table C.3).

	Foraging	Resting	Transit
sqrt(varstrokingratefirsthalf)	0.13 ± 0.68	-0.92 ± 0.99	-0.05 ± 0.79
third(xaccelvar_16firsthalf)	0.02 ± 0.64	-0.20 ± 0.63	-0.60 ± 0.63
log(yaccelROC_16bottom)	0.35 ± 0.79	-0.59 ± 0.87	-0.26 ± 0.71
third(speedcalcvar_4firsthalf)	0.17 ± 0.99	0.74 ± 0.61	-0.52 ± 0.86
third(varstrokingratesecondhalf)	0.31 ± 0.89	-0.12 ± 0.71	0.29 ± 1.02

Table C.1. Group means for LDA variables.

	LD1	LD2
sqrt(varstrokingratefirsthalf)	-1.32	0.26
third(xaccelvar_16firsthalf)	0.90	0.29
log(yaccelROC_16bottom)	0.71	1.03
third(speedcalcsmoothvar_4firsthalf)	0.65	-0.25
third(varstrokingratesecondhalf)	0.36	0.38

Table C.2. Coefficients of linear discriminants for LDA variables.

	Prediction			
Reference	Foraging	Resting	Transit	Correctly classified
Foraging	79	0	9	0.898
Resting	5	10	2	0.588
Transit	18	0	24	0.571

Table C.3. LDA classification performance on training dataset.

Function	Eigenvalue	% of Variance	Cumulative %	Canonical Correlation
1	.421a	58.5	58.5	0.544
2	.298a	41.5	100	0.479

Table C.4. Eigenvalues and % variance of first two linear discriminant functions.

Test of Function(s)	Wilks' Lambda	Chi-square	df	Sig.
1 through 2	0.542	86.911	10	0
2	0.77	37.04	4	0

Table C.5. Test of linear discriminant functions.

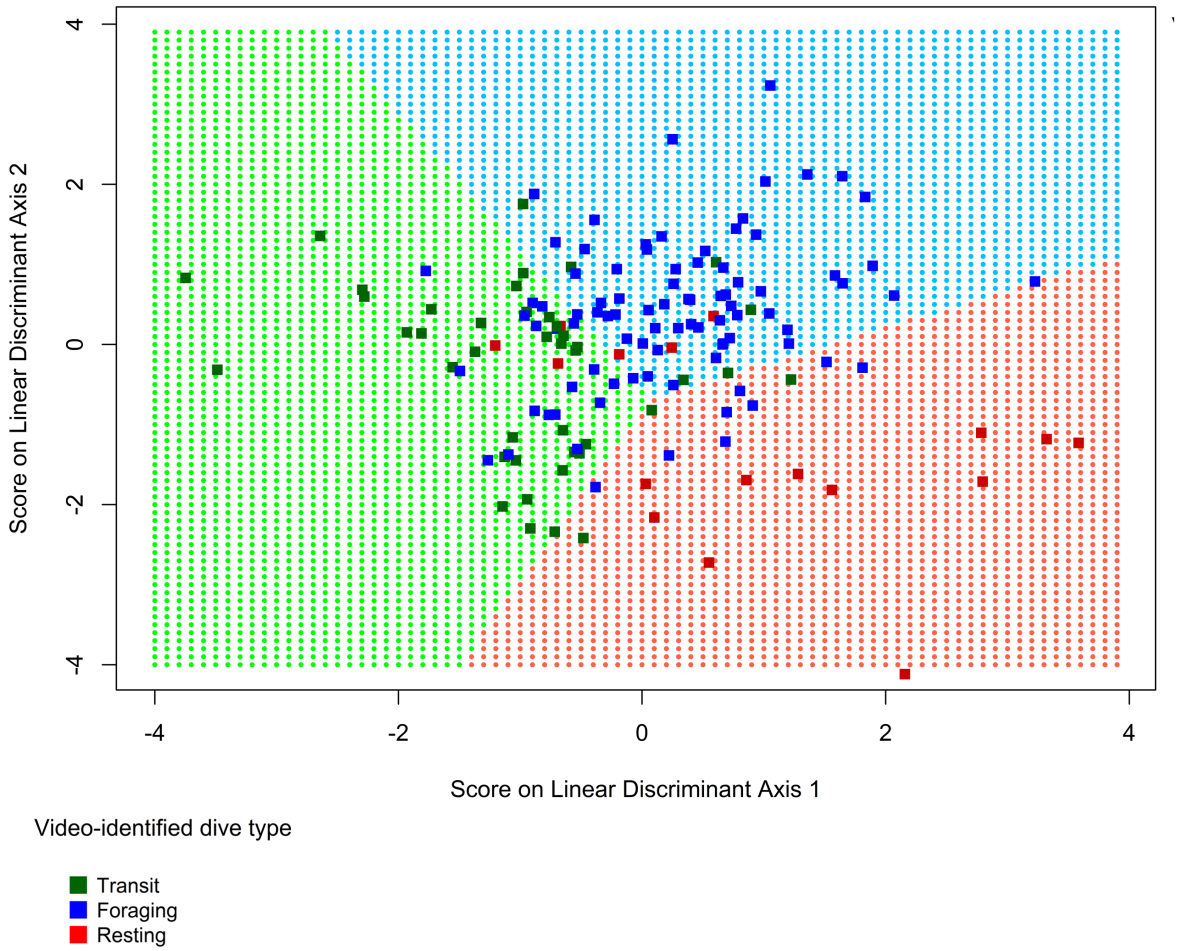

Figure C.1. Decision boundaries for LDA classifier, overlaid with training dataset color coded by known dive type. Correctly classified dives are located in the same color region (e.g. red on red for resting dives).

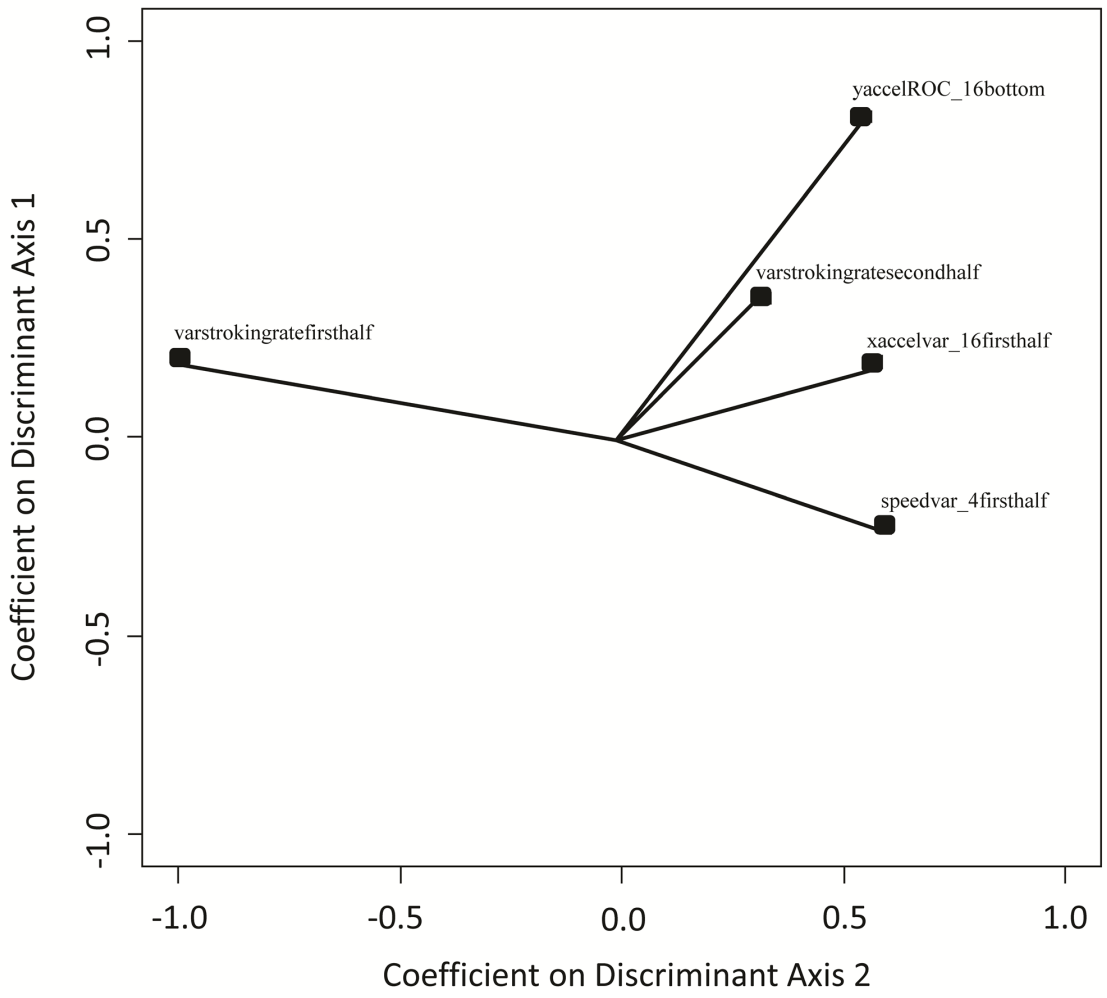

Figure C.2. Plot of standardized canonical linear discriminant function coefficients.

C.2 Quadratic discriminant analysis

Three predictors were selected by the stepclass function to train the QDA classifier. The predictors chosen were transformations of: 1) variance in the x-axis accelerometer during the bottom phase of the dive (in 16 Hz, xaccelvar_16bottom), 2) variance in the y-axis accelerometer (in 16 Hz, yaccelvar_16), and 3) rate of change in the z-axis accelerometer (in 1 Hz, zaccelROC). Group means for each of the predictors are listed in Table C.6. The classifier correctly classified 87% of the training data (95.5%, 65.5%, and 78.6% of foraging, resting, and

transit dives, respectively (Table C.7). Fig. C.3 depicts the QDA classification as a 3D plot of the three predictor variables. The 3D plot is shown as three biplots to better visualize the decision boundaries of the classifier. The larger spheres are the video-identified dives used to train the classifier. The smaller spheres are the remainder of the dataset, colored by predicted dive type as classified by the QDA classifier. The QDA classifier was tested on the test dataset with an overall accuracy of 0.864 (95% CI: 0.757, 0.936) and a Kappa statistic of 0.755 (Table 2.1). The classification had an overall accuracy significantly better than the NIR at the 0.01 level with a p-value of 1.4e-06. Balanced accuracy was 0.906, 0.92, and 0.826 for foraging, transit, and resting, respectively (Table 2.3).

	Foraging	Resting	Transit
log(xaccelvar_16bottom)	0.32	-0.80	-0.54
log(zaccelROC)	0.20	-0.55	-1.05
third(yaccelvar_16)	0.09	0.66	-0.65

Table C.6. Group means for QDA variables.

	Prediction			
Reference	Foraging	Resting	Transit	Correctly classified
Foraging	84	0	4	0.955
Resting	1	11	5	0.647
Transit	9	0	33	0.786

Table C.7. Performance of QDA on training dataset.

	Prediction			
Reference	Foraging	Resting	Transit	Correctly classified (OOB)
Foraging	82	0	6	0.93
Resting	0	16	1	0.94
Transit	5	0	37	0.88

Table C.8. Performance of random forest model on training set (OOB).

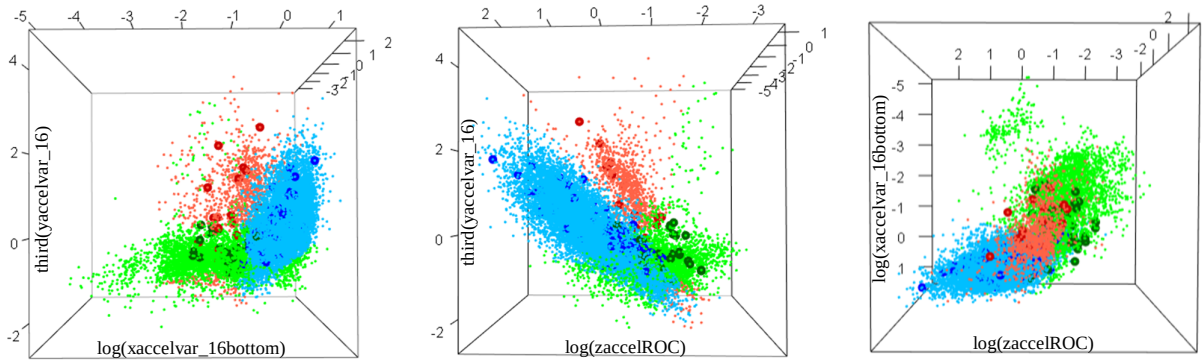

Figure C.3. 3D plot of QDA classification with all three predictors, viewed as three biplots. Large spheres are video-identified dives used to train the model; smaller spheres are the remainder of the dives, colored according to QDA classifier-predicted dive type.

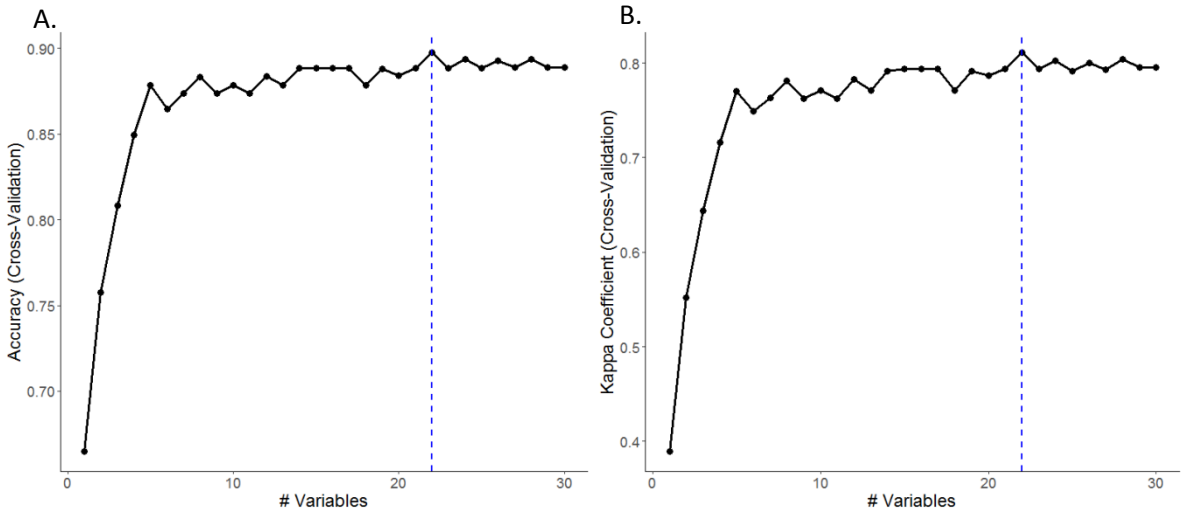

Figure C.4. Plot of A. Accuracy and B. Kappa coefficient by number of predictors in random forest model. Blue line indicates optimal number of predictors for each metric.

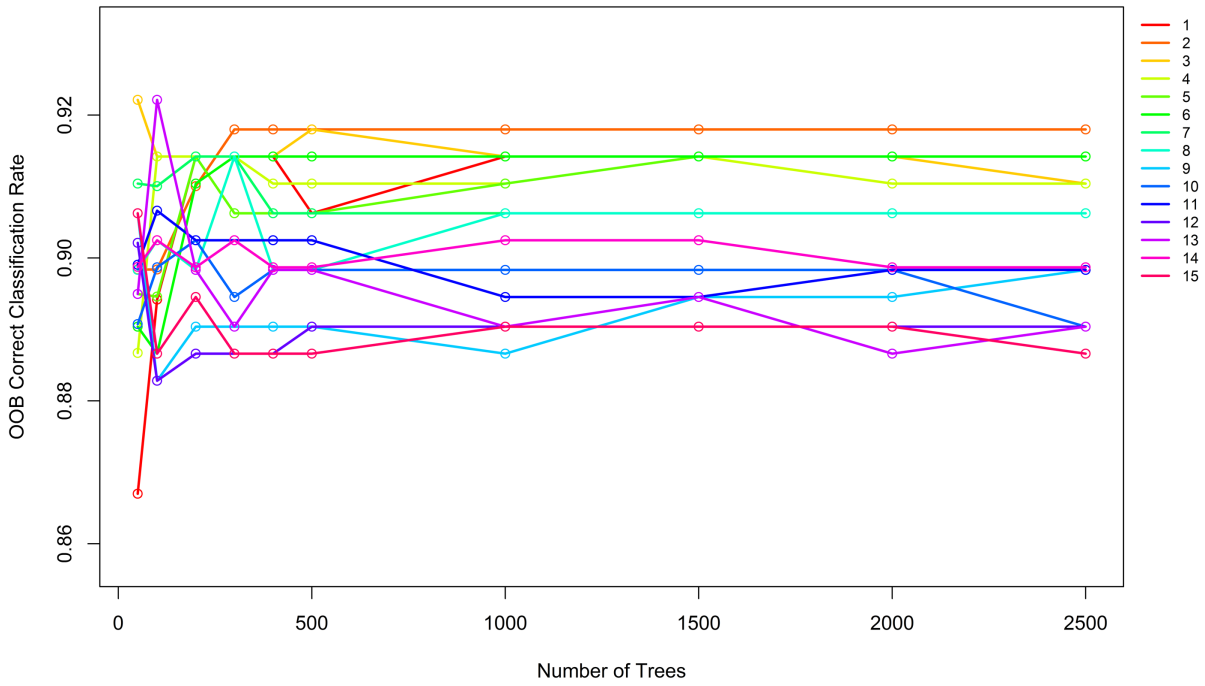

Figure C.5. Out of Bag Correct Classification Rate for varying values of ntree and mtry for use in tuning the random forest model.

C.3 Random forest classification

22 predictors were chosen for use in the classifier based on Accuracy and the Kappa statistic (Fig. C.4). An mtry of 2 performed consistently well across ntree values of 400:2500, with an OOB correct classification rate of 0.918 (Fig. C.5). An mtry of 2 and ntree of 1500 (mid-range of well-performing values) were selected for use in the final model. The selected 22 variables were input into the randomforest package in R with these parameters to train the RF classifier. The OOB estimate of error rate for the training set in the random forest classification model was 8.16%. The OOB error rate by class was 0.068, 0.059, and 0.119 for foraging, resting, and transit, respectively (Table C.8). The 22 variables included in the random forest model are listed from most important to least important in Fig. C.6 according to the mean decrease in the Gini coefficient. The random forest model was tested on the test dataset with an overall accuracy of

0.909 (95% CI: 0.813, 0.966) and a Kappa statistic of 0.842 (Table 2.1). The random forest classification had an overall accuracy significantly better than the NIR at the 0.01 level with a p-value of 9.7e-09. Balanced accuracy was 0.94 for each of the three classes (Table 2.3).

C.4 KMeans cluster Analysis

Fig. C.7 depicts the results of the kmeans cluster analysis plotted on the first two principal components overlaid with the training set dives. The elbow and silhouette method both indicated that the optimal number of clusters for kmeans cluster analysis was k=3 (Figs. C.8, C.9). The first two principal components explain 52.6% of the point variability (Fig. C.10). Based on the percent of known dive classes that were assigned to each cluster, the cluster classes were defined as “transit”, “foraging”, and “resting”, for clusters 1, 2, and 3, respectively. Classification was tested using all of the video dives with an overall accuracy of 0.812 (95% CI: 0.753, 0.862) and a Kappa statistic of 0.667 (Table 2.1). The kmeans cluster analysis assigned clusters had an overall accuracy significantly better than the NIR at the 0.01 level with a p-value of 1.9e-06. Balanced accuracy was 0.871, 0.74, and 0.864 for foraging, resting, and transit, respectively (Table 2.3).

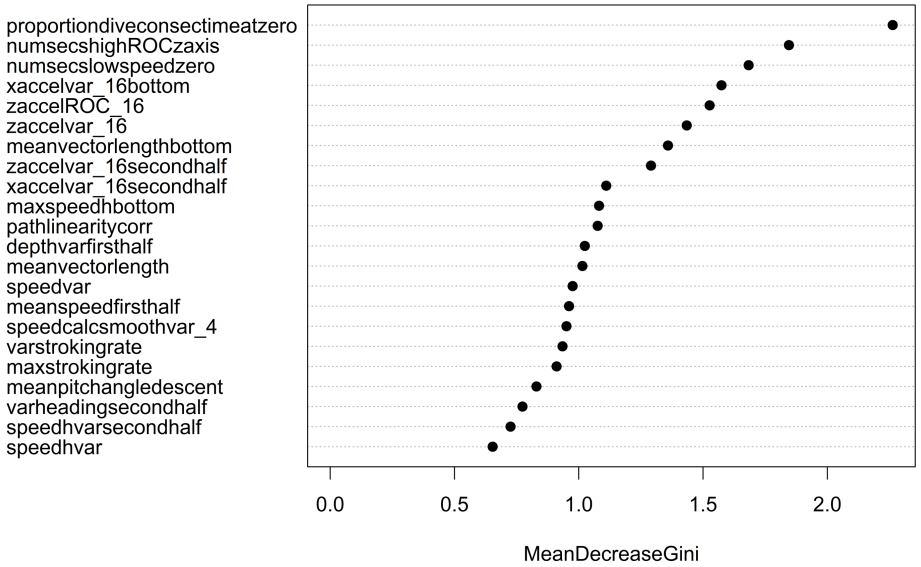

Figure C.6. Mean decrease in the Gini coefficient (a relative measure of how great of a role a predictor plays in separating the data into classes) for predictors in the random forest model.

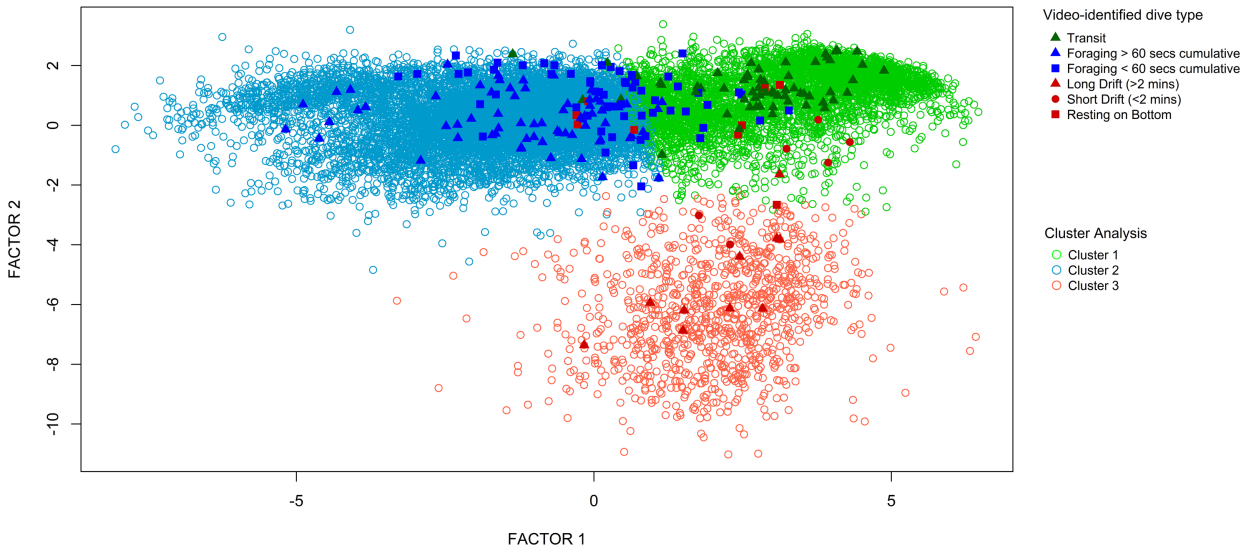

Figure C.7. KMeans cluster analysis results plotted on principal components 1 and 2, overlaid with known video-recorded dive types.

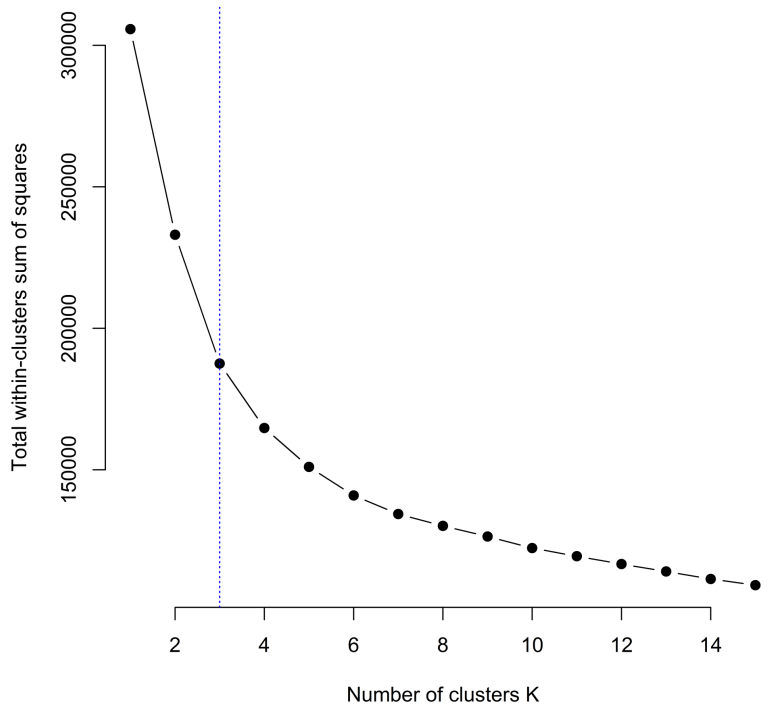

Figure C.8. Elbow plot for kmeans analysis. Blue line demarcates optimal number of clusters.

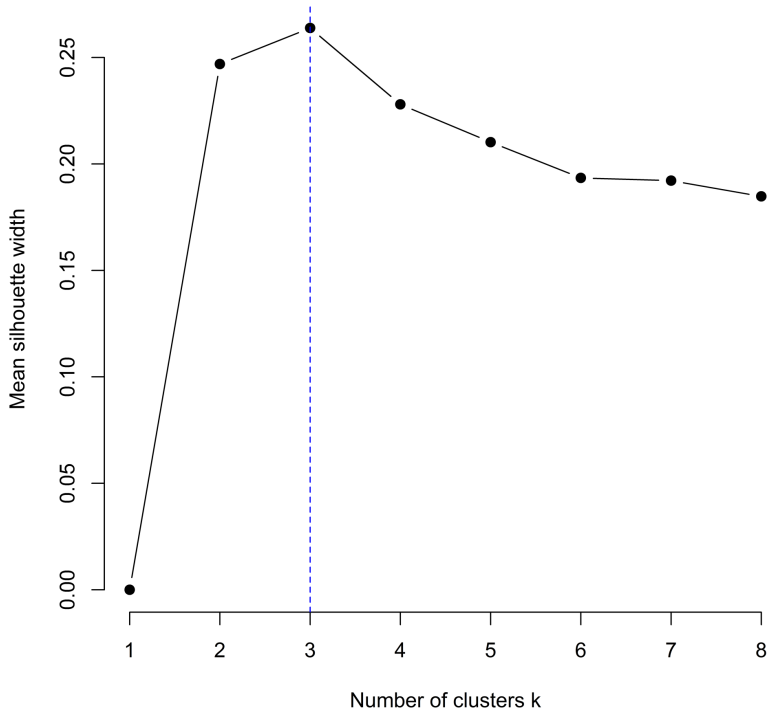

Figure C.9. Silhouette width plot for kmeans analysis. Blue line demarcates optimal number of clusters.

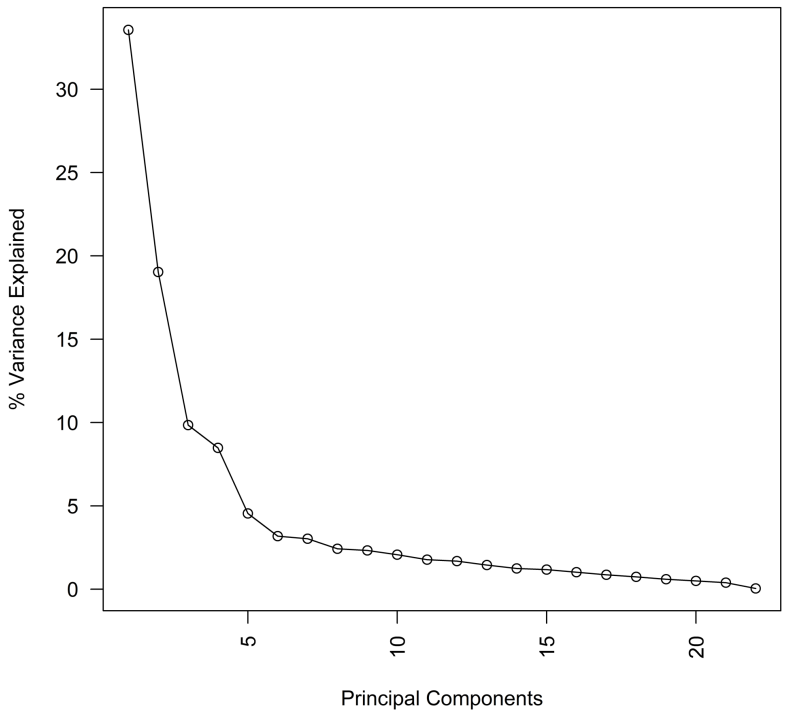

Figure C.10. Contribution of principal components to point variability.